FLUORESCENCE IN THE STUDY OF STEROID METABOLISM

Licentiate Thesis

University of Jyväskylä

Department of Chemistry

25.1.2020

Jari Petteri Ahonen

ABSTRACT

This thesis begins with a literature review that presents the basics of the fluorescence phenomenon and fluorescence microscopy. The literature on cellular cholesterol composition and cholesterol transport mechanisms is extensively studied. Thereafter, the fluorescent steroid-based molecules designed to identify cholesterol and cholesteryl esters suitable for use in living cells are covered. The literature review ends an overview of other applications for the use of fluorescent probes, for example in cell biology.

The aim of the experimental part was to optimize the synthesis pathway for producing fluorescent biocompatible bile acid-based molecules designed for the detection of cholesterol and cholesteryl esters. Preliminary cholesterol-binding assays were also performed for the prepared cholesterol probes by NMR titration, diffusion NMR-experiments, and mass spectrometry.

PREFACE

I started my postgraduate studies in the spring of 2017. This thesis has been compiled between spring 2017 and spring 2019. The experimental work was carried out at the Department of Chemistry, University of Jyväskylä. The work involved one and half month research visit to Prague in 2019.

The material was collected using the Google Scholar search engine and the SciFinder database. The keywords were: fluorescence microscopy, fluorescence, fluorophore, fluorescent probe, lipids and their function, cholesterol synthesis, intracellular cholesterol study, steroid probes, and bile acid probes.

My Licentiate Thesis supervisor was University Lecturer, Docent Elina Sievänen who I thank for the interesting topic. I am grateful for all the advice, support, and research ideas. I would also like to thank professor Vladimir Král for hosting, and Bc. Lenka Vosátková for practical arrangements concerning my research visit in Prague.

Professor Zdeněk Wimmer (Institute of Experimental Botany, The Czech Academy of Sciences, Czech Republic) and Dr. Petri Turhanen (University of Eastern Finland, Finland) are gratefully acknowledged for their detailed evaluation with valuable and constructive comments of the present thesis.

I would also like to thank Magnus Ehrnrooth Foundation for awarding me a grant for graduate studies (23 000 €) and Kemian Päivien Säätiö for post-graduate scholarship (2 000 €) for the research visit to University of Chemistry and Technology in Prague.

Finally, I would like to thank my mom and dad for their warmth and sense of humor, but mostly for their genes. I also want to thank my cousin and her husband for offering me a place to stay during the laboratory period in Jyväskylä. Furthermore, I like to thank my friends in Jyväskylä and Helsinki for all the support and adventures.

CONTENTS

ABBREVIATIONS

DCBC	3,5-Dichlorobenzoyl chloride
DCM	Dichloromethane
DIPEA	*N,N*-Diisopropylethylamine
DMAP	4-Dimethylaminopyridine
DMF	*N,N*-Dimethylformamide
EDC-HCl	*N*-(3-Dimethylaminopropyl)-*N*′-ethylcarbodiimide hydrochloride
ER	Endoplasmic reticulum
HATU	1-[Bis(dimethylamino)methylene]-1*H*-1,2,3-triazolo[4,5-*b*]pyridinium 3-oxid hexafluorophosphate
HBTU	*N,N,N′,N′*-Tetramethyl-*O*-(1*H*-benzotriazol-1-yl)uronium hexafluorophosphate
HMG-CoAR	3-Hydroxy-3-methylglutarylcoenzyme-A-reductase
INISG	Insulin-induced gene
LRX	Liver X receptors
MRI	Magnetic resonance imaging
PET	Positron-emission tomography
SCAP	Sterol regulatory element binding protein cleavage-activating protein
SREBP	Sterol regulating element binding proteins
StAR	Steroidogenic acute regulatory protein
OXYMA	Ethyl (hydroxyimino)cyanoacetate

1 INTRODUCTION

Fluorescence microscopy is based on the use of fluorescent chemical compounds, which can be used to locate the desired target material. Fluorescence microscopy provides a highly sensitive signaling mechanism to study events at the molecular level in chemistry, cell biology, and environmental sciences. Since most of the biomolecules to be studied are not fluorescent, various small-molecule fluorophores and small-molecule fluorescent probes are required.[1,2]

Organic fluorophores can be classified according to the increase of their absorption capacity and emission wavelength from near-ultraviolet to 500 nm and from 500 nm to near-IR. For example, boron-dipyrromethene (BODIPY) belong to the latter category. BODIPY conjugates are widely studies as potential sensors and for labeling.[3]

Lipids are a diverse class of compounds ranging from simple fatty acids to complex sterols and phospholipids. Cholesterol belongs to the class of sterols and is a crucial component of cellular membranes. Knowledge of its intracellular dynamics is, however scarce. Cholesterol metabolism disorders have shown to affect the development of many neurobiological diseases. Tools for visualizing cholesterol organization and dynamics in cells and tissues cannot be emphasized enough. For this purpose, effective fluorescent probes capable of recognizing cholesterol are needed.[2]

Many studies utilize fluorescent cholesterol derivatives. Dehydroergosterol is an example of intrinsically fluorescent cholesterol analog, whereas BOBIDY-tagged cholesterol represents an extrinsically fluorescent cholesterol analog. The fluorescent probe may also be a combination of these. An alternative approach is to use cholesterol-binding fluorescent molecules.[4]

2 INTRODUCTION TO FLUORESCENCE MICROSCOPY

Fluorescence microscopy is one of the major tools when monitoring cell physiology.[1] The fluorescence phenomenon was first discovered by an English mathematician and astronomer Sir John Fredrick William Herschel around the year 1825,[5] when he found, that blue light was emitted from the surface of quinine solution. In fluorescence microscopy, chemical compounds called fluorophores, are used for example for locating desired objects in the material being studied. In structural biology, examples of such objects may be cellular organisms, such as mitochondria or the Golgi apparatus.[1,5]

2.1 FLUORESCENCE

Fluorophores absorb invisible UV radiation and emit part of their energy as longer, visible light wavelengths.[6] Part of the absorbed energy is consumed in molecular vibrations, rotations, and heat, which is why the energy of the resulting emitted photon is smaller, and the wavelength of the irradiation longer. This phenomenon is called fluorescence, and it is described in detail by a Jablonski diagram (Figure 1), which illustrates the states of electrons in the molecule and the transitions between the states. For example, the Jablonski diagram in Figure 1 illustrates the absorption of a photon from the ground state ^1A into the excited state $^1A^*$, the internal transition to the excited state ^3A, and the fluorescence as well as the phosphorescence.[6,7,8]

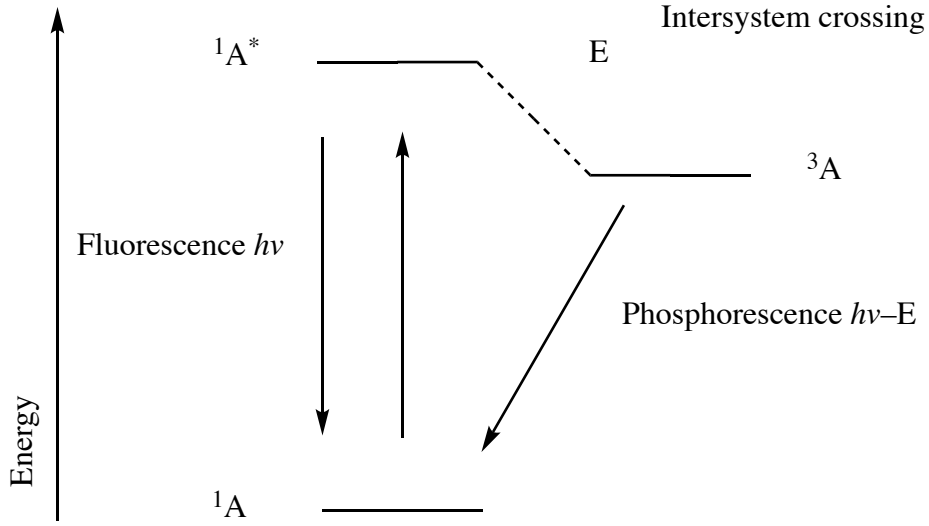

Figure 1: A Jablonski diagram showing the excitation of photon ^1A to its singlet excited state $^1A^*$ followed by an intersystem crossing to the triplet state ^3A that relaxes to the ground state by phosphorescence. In fluorescence, the electron relaxes to its ground state ^1A by emitting energy from an excited singlet state $^1A^*$.[6]

The key parameters that describe the fluorescence process of a system are the absorption maximum (λ_{max}) and the extinction coefficient at λ_{max} (ε). During the excitation, some energy is lost, and a rapid relaxation from the singlet excited state to the triplet excited state may occur. The triplet excited state may relax via a non-radiative mechanism, in which bond rotations are observed. If the relaxation takes place via a radiative mechanism, the process is called phosphorescence. Fluorescence, for one, takes place when the singlet excited state is relaxed back to the ground state followed by emission of energy. Phosphorescence differs from fluorescence by longer lifetimes of the states. Unlike in fluorescence, in phosphorescence, radiation is emitted even after the excitation is over.[6,7]

A consistent sequence of events leads to fluorescent emission of fluorophores and gives them their general properties. Every fluorophore has a typical emission maximum (λ_{em}). The maximal emission wavelength (λ_{em}) may be longer than the absorption maximum (λ_{max}). This is due to the loss of energy when the excited state is relaxed, and the solvent molecules around the fluorophore reorganized.[7]

The difference between the absorbance maximum (λ_{max}) and the emission maximum wavelength (λ_{em}) is called the Stokes shift (Figure 2).[6,9] Fluorophores with small Stokes shifts are capable of self-quenching *via* energy transfer mechanisms. This feature limits the number of fluorophores, that can be attached to the biomolecules. The typical lifetime of the excited state can range from 0.1 ns to 100 ns. Lifetime is one of the important parameters for the time-resolved measurements and fluorescence polarization applications, which are widely used in high throughput screening in drug discovery.[10,11] Another important parameter is the quantum yield, which describes the ratio of photons fluoresced to those absorbed.[9]

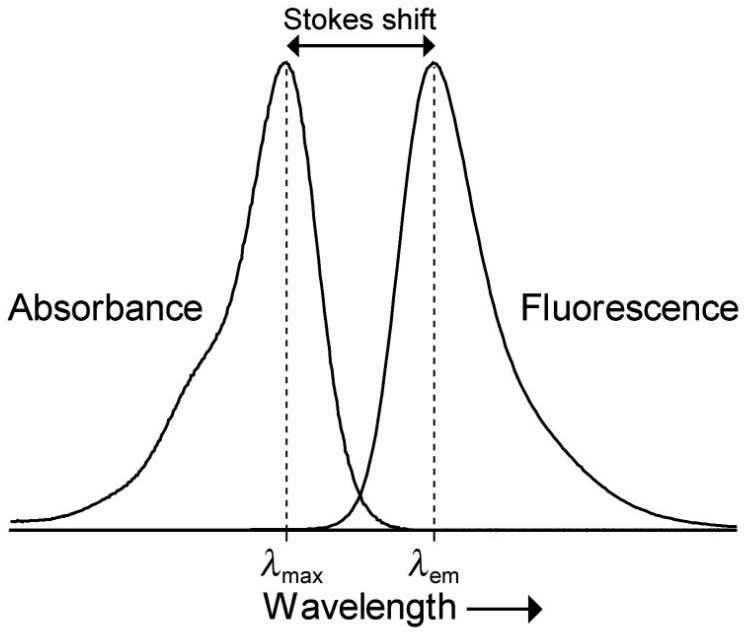

Figure 2: General absorption and emission spectra.[9]

The fluorophores can be modified synthetically in order to achieved advantages in terms of biological imaging. For example, a longer exciting wavelength that allows deeper penetration into the tissue can be obtained.[7,12]

2.2 FLUORESCENCE MICROSCOPY

Fluorescence microscopy has developed a lot over the past 20 years.[5] It is the only method that can be used in the study of living cells. The traditional light microscope has a resolution of about 200 nm. However, several interesting components in cell biology, such as proteins and viruses, are much smaller. Fluorescence microscopy reaches a few tens of nanometers. The equipment (Figure 3) consists of a lamp, a sample tray, some lenses, a digital camera, a light source, and filters. The monochromatic light is targeted to a sample containing the fluorophores that excite and emit light on the wavelength of the visible light. The excited light is reflected in the sample with two colored mirrors. These special mirrors are positioned so that the light is selectively reflected at certain wavelengths. The light with the longer wavelength is not reflected by the mirror but goes directly through it. Two-color mirrors are chosen based on the desired exciting wavelenght.[1,5,13,14]

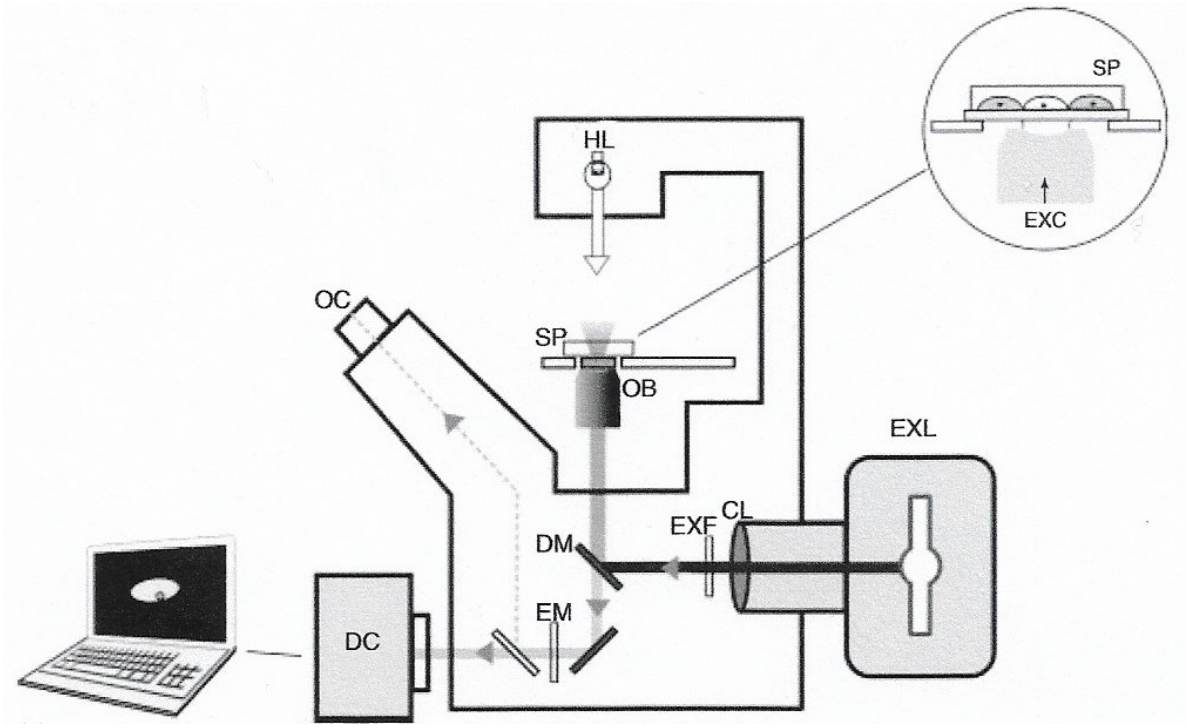

Figure 3: Schematic picture of a fluorescence microscope: HL = halogen lamp, SP = specimen, OB = objective lens, OC = ocular (eyepiece), DC = digital camera, EXL = exciting light source, CL = collector lens, EXF = excitation filter, DM = dichroic mirror, EM = emission filter, EXC = exciting light incident on the specimen.[5]

(Adapted from Ref.[5] with permission from John Wiley and Sons.)

Fluorescence microscopy distinguishes between the fading light and the bright light used for excitation. Fluorescence indicators with high Stokes shifts are advantageous in this task. Different filters are used to separate the emission light from the excitation light. A good filter cuts sharply and steeply the different wavelengths. There are three types of filters: 1) long-pass filters, which pass long wavelengths and stop short, 2) short-pass filters, which pass short wavelengths and stop long, and 3) bandpass filters, which pass only a certain wavelength or wavelength range. Filters are generally made of metal films or various polymer-based materials.[1,5,14]

The fluorescence microscope typically has two light sources.[2] The first lamp is often a halogen lamp used for the sample preview. The second lamp is used to excite the sample molecule for the following fluorescence. In a fluorescence microscope, laser or various lamps, such as mercury lamp, xenon bulb, metal halide lamp, halogen lamp, or led lamp, can be used. It is important that the light source contains only one wavelength. Gas lasers are effective. In a fluorescence microscope, the laser emits light between two mutually opposite mirrors, one of

which releases light from the formed laser beam. The laser can be guided through media, such as various gases or toners. Led lamps are semiconductor components that radiate light when conducting electrical current passing through them. Led has the advantage of a long lifetime and quick lamp ignition and exhaustion. The led does not need to cool, but for example, the laser demands a cooling system.[1,5,14]

The limitations of fluorescence microscopy can be classified into three principal issues: 1) photobleaching, 2) toxicity and 3) phototoxicity of fluorescent probes.[2] Earlier the resolution was one of the limiting factors, but the problem was solved by the development of new technologies. Photobleaching is a process where the fluorescence output intensity gradually decreases. This is caused by an interaction between the excited light and the labeled compound. In photobleaching, the molecules labeled with fluorescent dyes are photochemically destroyed. The problem can be solved by new applications, such as cutting-edge microscopy.[5,15]

Living cells that are fluorescently labeled and exposed to exciting light are sensitive to the photodynamic effects. This can result in damage when photosensitizers and molecular oxygen are present. A fluorescent dye, which interacts with the cell organelles during imaging of living cells, behaves as a photosensitizer and can cause various types of damage to the cell such as photo-oxidation of DNA bases leading to DNA breakdown. Such damage may lead to cell death, but it may not necessarily be observed immediately after the imaging experiment. It is, however, important to remember that light-induced damage to living cells can lead to physiological changes in them.[5]

In most of the fluorescent microscopy applications, images are stored. Often images need to be processed, analyzed, and archived within a short time period. Current fluorescence microscopes are equipped with suitable systems for detecting emitted light as well as digitizing and recording the images. The most commonly used light detectors in modern fluorescence microscopes are a charge-coupled device (CCD), intensified charge-coupled device (ICCD), and electron-multiplying charge coupled device (EMCCD), as well as, avalanche photodiode (APD) cameras.[5]

2.3. SMALL-MOLECULE FLUOROPHORES

As mentioned above, fluorescence microscopy is widely used in cell biology. Regrettably, most of the biomolecules are not fluorescent. Small-fluorescent molecules are commonly used for biomolecular labeling. Compared to the absorbance-based dye or radioactive labeling, fluorescent labeling is more sensitive. The amount of small-molecule fluorophores either commercially available or by *de novo* design and synthesis is countless. Fluorescent dyes can be attached to biomolecules either by covalent or noncovalent linkages or by using antibodies. The biomolecules that can be visualized by fluorescent labeling are typically amino acids, peptides, proteins, and DNA.[2,9]

One of the most widely used small-molecule fluorophores is the well-known xanthene dye fluorescein **1**, which was first synthesized by Bayer in 1871.[5] In aqueous solutions, fluorescein can occur in seven different prototrophic forms. The most important biological forms are the monoanion and the dianion. The interchange occurs with a $pK_a \approx 6.4$. Fluorescein is capable of absorbing blue light at one wavelength and blue-green light at another wavelength. Moreover, its structure can be modified further to tune its properties, for example, the wavelength and pK_a. 2,7-Difluorofluorescein is less basic than fluorescein **1** but maintains fluorescein-like wavelength. It exhibits increased photostability relative to fluorescein. Fluorescein exists in equilibrium between a closed lactone **1** and open quinoid form **2** (Figure 4). In an aqueous environment, acylation or alkylation of the phenolic groups locks the molecule into the nonfluorescent lactone form. The lactone form serves as a basis for many substrates, such as esterases and other enzymes.[9,16]

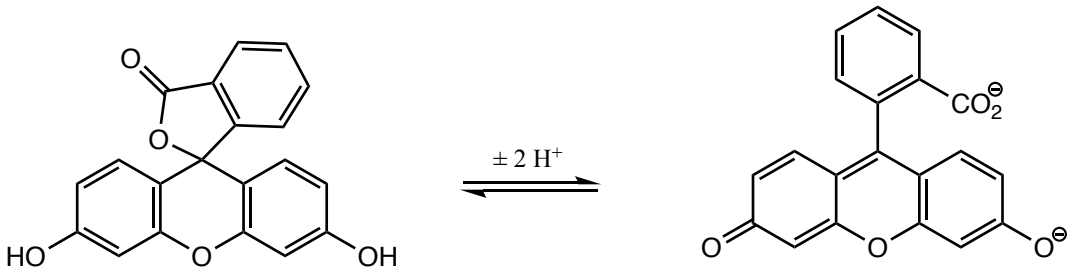

1 **2**

Figure 4: The closed lactone form **1** and the open quinoid form **2** of fluorescein.[9]

Polycyclic aromatic compounds represent another class of commonly used subset of fluorescent dyes. Naphthalene derivatives belong to this category. One example of naphthalene derivatives is the amino derivative 5-(dimethylamino)naphthalene-1-sulfonyl chloride **3**, which is also known as dansyl chloride **3** (Figure 5). Coumarin **4** and its derivatives represent a wide range of natural products, pharmaceuticals and, above all, fluorophores. Heteroatom substitution at position 7 of coumarin is responsible for the fluorescence property. The fluorescent properties of coumarin may be altered by adding different functional groups to the 3- or 4-positions. The coumarins can also act as enzyme substrates. Quinones represent yet another group of small fluorescent molecules. The simplest quinone is quinoline **5**. Several quinolinium compounds can be used as indicators for chloride ion.[17] Hydroxyquinoline derivatives, for example, 2-methyl-8-nitroquinoline, can be used as fluorescent Ca^{2+}-ion indicators.[9,18]

Isologues of fluorescein, such as the rhodamine **6** and its derivatives are widely used as fluorophores. The typical properties of this group are low pH sensitivity and tunable spectral properties. The spectral characteristics of rhodamines can be modified by different *N*-alkyl substitutions. Hybrid structures between fluorescein and rhodamines are termed rhodols. The properties of the rhodol fluorophores enable their use as ion indicators.[9,19]

The boron difluoride dipyrromethene, also known as BODIPY **7** (Figure 6), has been widely used as a building block for various fluorescent dyes and probes. The main features of this dye class are the sensitivity of the spectral properties to the environment, the small Stokes shift, and the general lipophilicity of the dye. The wavelengths of the BODIPY dyes and their derivatives can be tuned through appropriate substitution. They can also serve as surrogates for traditional dyes, such as fluorescein **1**. The BODIPY probes are mainly designed for fluorescence labeling. On the other hand, they have also been developed to identify ions. For example, V. V. Martin *et al.*[20] have studied BODIPY-based fluorescence indicators for intracellular sodium ions.[9]

Organic fluorophores can be classified according to the increase in absorption capacity and emission wavelength. Fluorescent labeling compounds from the near-ultraviolet to 500 nm include dansyl chloride **3**, oxobenzopyrans (for example coumarin **4**), and quinones (for example quinoline **5** (Figure 5)). Naphtofurans and benzooxodiazoles belong to organic fluorophores absorbing also at near-UV to 500 nm.[2,21]

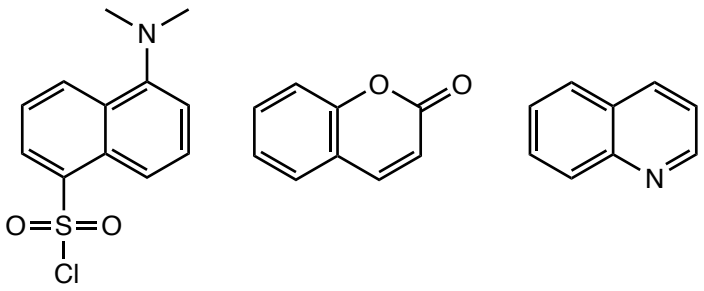

3 **4** **5**

Figure 5: Examples of fluorescent labeling compounds from the near-ultraviolet to 500 nm: dansyl chloride **3**, coumarin **4**, and quinoline **5**.[2,21]

Examples of compounds emitting from 500 nm to near-infrared include fluorescein **1**, squaraines, and cyanines. Rhodamine **6** and BODIPY **7** (Figure 6) belong to the class emitting from 500 nm to near-IR.[2,21]

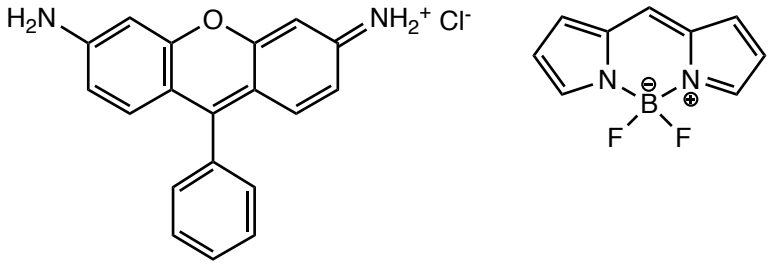

6 **7**

Figure 6: Examples of fluorescent labeling compounds emitting from 500 nm to near-infrared are rhodamine **6** and BODIPY **7**.[2,21]

2.4 SMALL-MOLECULE FLUORESCENT PROBES

Fluorescent probes consist of the receptor that recognizes the analyte, and the fluorophore that is responsible for signaling the recognition event. Upon recognition, the photophysical properties of the fluorophores are changed. Examples of such changes are emission intensity, excitation wavelength, and emission wavelength with concomitant environmental changes around the fluorophore through a binding event.[2,22]

There are three main classes of fluorescent molecular indicators for chemical sensing in solutions. The first group covers intrinsic fluorescent probes such as fluorescent molecules where the mechanism for signal transduction involves the interaction of the analyte with a ligand that is part of the π-system of the fluorophore. The second group includes external fluorescent probes, in which the receptor and the fluorophore are covalently linked. The third group covers chemosensing ensembles, where the receptor-fluorophore ensemble is selectively dissociated by the addition of a suitably competing analyte that is able to interact with the receptor. This results in a detectable response of the fluorophore.[2,22]

Fluorescent bioimaging is very sensitive and target-specific compared to, for example, magnetic resonance imaging (MRI) or positron-emission tomography (PET).[23] Fluorescent bioimaging technology enables the visualization of very low concentration of small biomolecules. Fluorescent probes for different analytes, for example, metal cations[24] and amino acids[25], can be prepared. Furthermore, Xinqi *et. al.*[26] have investigated rhodamine B-based fluorescent probes for hypochlorite anions. Fluorescent probes for toxic metals[27] and pH-monitoring[28] have also been synthesized.[2]

Fluorescent bioimaging enables visualization of physiological and pathophysiological changes in cells. The properties of fluorescent probes can be modified by using synthetic chemistry. For example, longer wavelengths, brightness, non-toxicity, cell membrane permeability, stability, water solubility, and photostability are properties that can be improved. Several small-molecule fluorophores, such as fluorescein **1** and BODIPY **7**, can be modified by using target-specific receptors.[2]

3 LIPIDS AND THEIR FUNCTIONS AND FEATURES

Lipids are one of the largest classes of biomolecules. They are macromolecules, but not polymers. The most important feature of lipids is their hydrophobicity. They can be classified according to their shape and function. The biologically most important lipids are fatty acids, phospholipids, and steroids. Lipids have three general tasks. The most important of them is probably the energy storage, that can take place by, for example, lipid droplets, which contain triacylglycerol and steryl esters. Furthermore, the cell membrane matrix consists of lipids. Lipids can also act as the first and second transmitters in signal transduction and molecular identification processes.[29,30,31]

Lipids are amphipathic molecules meaning that they have a hydrophobic tail and a hydrophilic head. Lipid bilayers are spontaneously formed of individual lipid molecules in water. Lipid molecules are organized in the forming layer so that the hydrophobic tails appear inside of the membrane to avoid interaction with water molecules, whereas, for the opposite reason, hydrophilic ends lie on the outer surfaces of the membrane. Due to the hydrophobic intermediate portion of the lipid membrane, nonpolar molecules can be easily diffused through the cell membrane. Polar molecules are not capable of doing it. Polar molecules must pass through the cell membrane via active transport. This fundamental principle of amphipathic lipids is a chemical property that allowed first cells to separate their internal components from the external environment.[30,32]

3.1 LIPIDS OF THE BIOLOGICAL MEMBRANES

The major structural lipids of eukaryotic membranes are glycerophospholipids. This group of lipids includes phosphatidylcholine **8**, phosphatidylethanolamine **9**, phosphatidylserine **10**, phosphatidylinositol **11** esters, and phosphatidic acid **12** (Figure 7). Their hydrophobic part consists diacylglycerol of saturated or cis-unsaturated fatty acids with varying lengths. The hydrophilic head consists phosphate group or its modifications such as choline, ethanolamine or serine moiety. In most eukaryotic membranes, phosphatidylcholine accounts for more than 50 % of phospholipids. It arranges itself spontaneously as a planar double layer with the lipid tails facing each other inside the membrane. The polar ends are deposited in the aqueous phase on the outer surface of the membrane. Phosphatidylcholine molecules have one cis-unsaturated fatty acid chain, which makes them liquid at room temperature.[30,33]

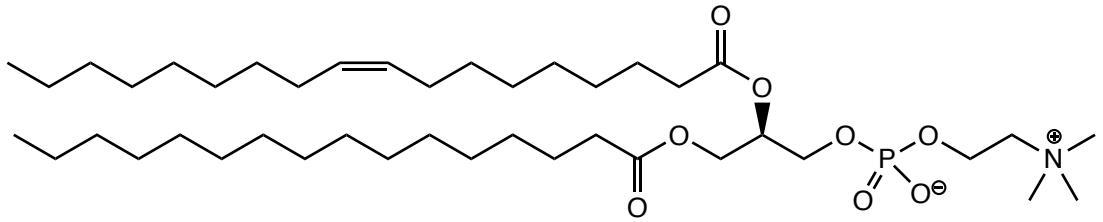

8

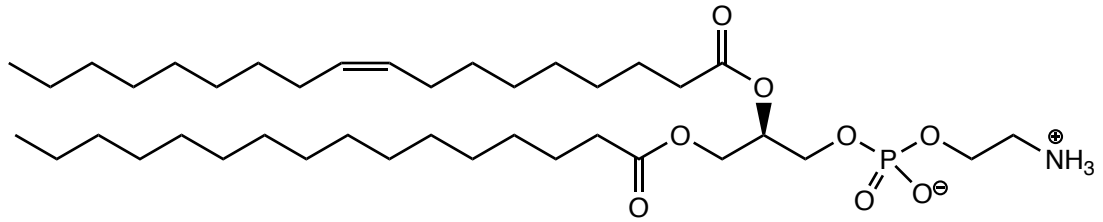

9

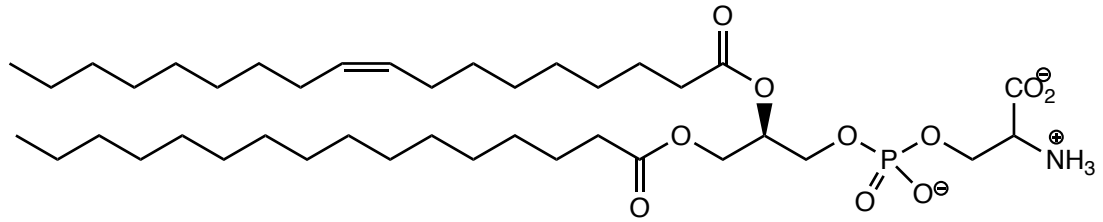

10

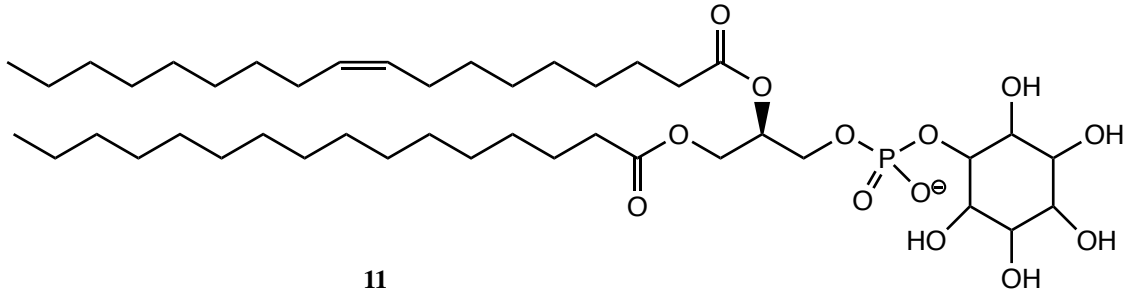

11

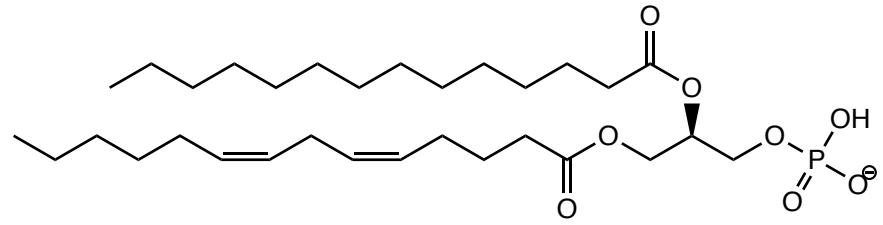

12

Figure 7: The major structural lipids of eukaryotic membranes are phosphatidylcholine **8**, phosphatidylethanolamine **9**, phosphatidylserine **10**, phosphatidylinositol **11** and phosphatidic acid **12**.[31,33]

Sphingolipids form another structural lipid group. The major sphingolipids in mammalian cells are sphingomyelin **13** (Figure 8) and glycosphingolipids containing mono-, di- or oligosaccharides. Sphingolipids have saturated tails so they can form longer and narrower cylindrical structures than phosphatidylcholine **8**. Sterols are the most important nonpolar cell membrane lipids of which cholesterol plays the main role in mammals and ergosterol in yeasts.[31,33]

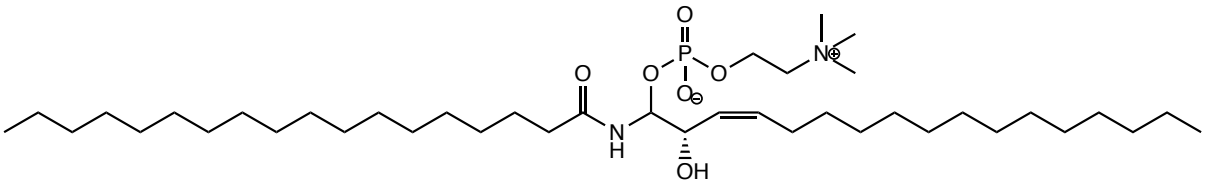

Figure 8: The structure of sphingomyelin **13**, which is one of the most common sphingolipids in mammalian cells.[31,33]

3.2 THE IMPORTANCE OF CHOLESTEROL IN BIOLOGICAL MEMBRANES

Cholesterol **14** (Figure 9) affects cell processes by interacting with other membrane lipids and specific proteins. The unique skeleton of cholesterol consisting of four fused rings. Because of the rigid steroidal backbone, cholesterol is located close to the saturated hydrocarbon chains of adjacent lipids in the cell membrane. The ability of cholesterol to organize the membrane lipids is mostly explained by its structure. The small headgroup of cholesterol is insufficient to shield the hydrophobic ring system from water molecules, so it is proposed that neighboring lipids fulfil this role, which is why cholesterol exists close to the other larger lipid molecules.[34]

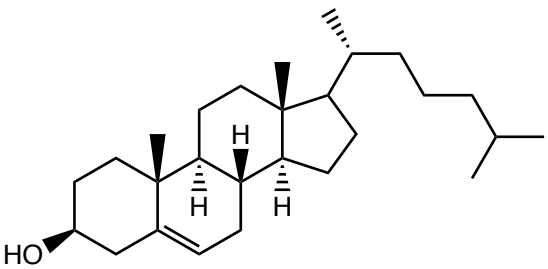

14

Figure 9: Schematic structure of cholesterol **14**.

The increased lateral association of lipids due to cholesterol affects the biophysical properties of the membrane. For example, the fluidity of the film decreases, and the permeability of the polar molecules is reduced. By controlling the permeability of the membrane, it is possible to form different ionic and solution conditions on different sides of the membrane.[34]

3.3 THE CHOLESTEROL BALANCE IN THE CELL

Cholesterol regulation is important because cholesterol is needed in several cellular processes. On the other hand, excessive free cholesterol is harmful to cells. Cholesterol regulation is a dynamic process, as cells constantly switch cholesterol with their environment. There are various mechanisms for controlling cholesterol levels in the cell, including cholesterol biosynthesis, cholesterol intake and outflow, and storage. To cope with these tasks, cells have developed feedback mechanisms that strictly regulate cholesterol balance.[32]

3.3.1 CHOLESTEROL BIOSYNTHESIS

All nucleolus cells can synthesize cholesterol from acetyl-CoA *via* a mevalonate pathway (Figure 10). Limiting enzyme of the pathway is hydroxymethylglutaryl-CoA reductase (HMG-CoAR), which catalyzes the synthesis of mevalonate and is under strict regulation at the beginning of the pathway. Six enzyme reactions convert mevalonate to squalene **16**. Then squalene is converted to lanosterol in the reaction catalyzed by squalene cyclase. The reaction requires one molecule of O_2 meaning that it depends on aerobic conditions. A complex 20-step-reaction that consumes 10 additional O_2 molecules produces cholesterol through sequential demethylations and reductions of double bonds. The post-lanosterol steps are divided into Bloch[35] and Kandutsch-Russel[36] pathways. These pathways share the same enzymatic steps but are distinguished by the stage at which the C-24 double bond is reduced. Cholesterol may be acylated to form cholesterol esters, such as cholesterol oleate **18**, or it can also be oxidized to form oxysterols, such as 25-hydroxycholesterol **19**. Cholesterol may further oxidize to bile acids, such as cholic acid **20**, or to steroid hormones, such as pregnenolone **21**. Key enzymes in these metabolic reactions are acetyl-CoA cholesterol acyltransferase and cholesterol-7α-hydroxylase which is a cholesterol side-chain cleaving enzyme involved in steroidogenesis.[34]

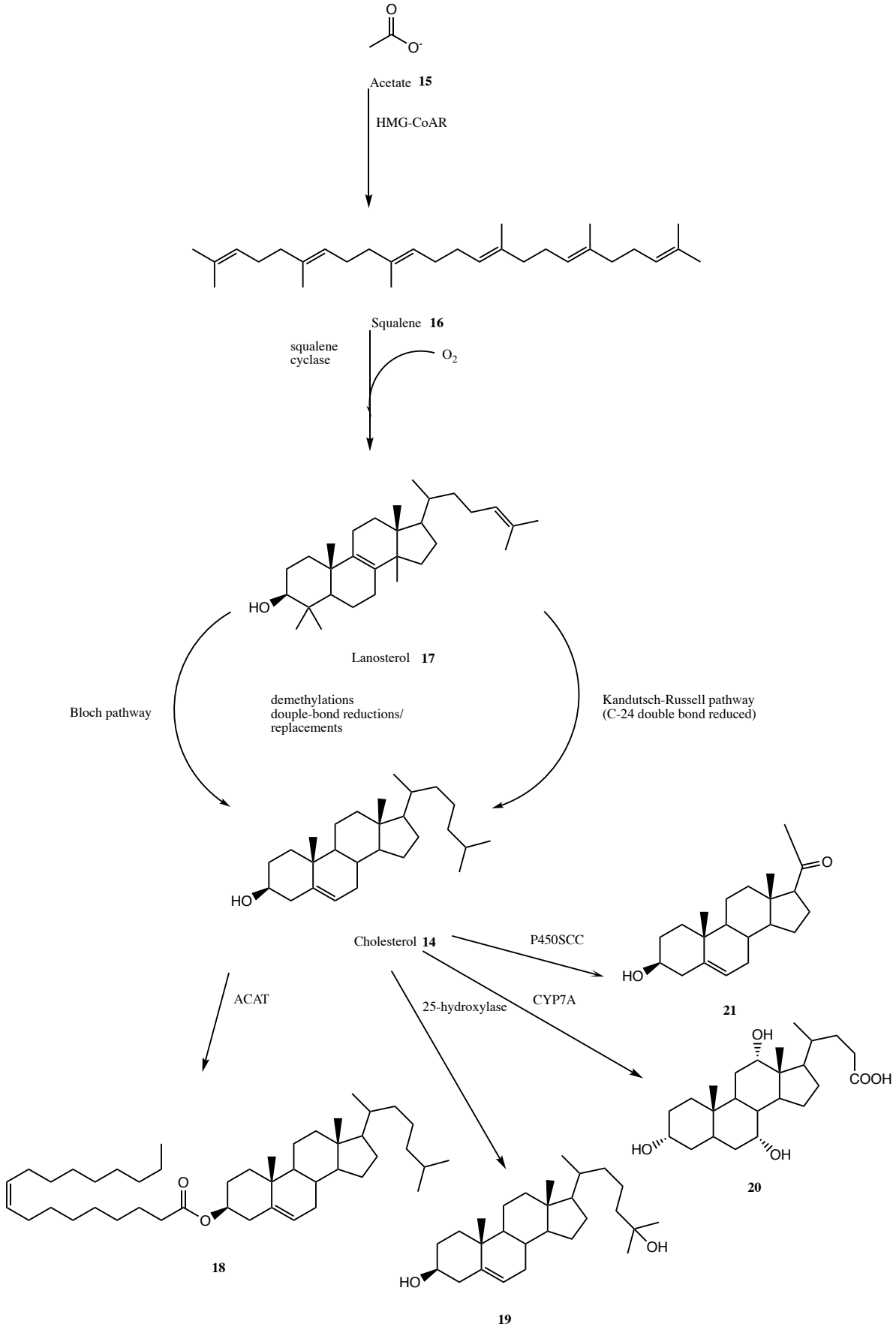

Figure 10: Representation of cholesterol biosynthesis simplified. After the lanosterol intermediate, the synthesis continues through Bloch or Kandutsch-Russell pathway.[34,35,36]

3.3.2 CONTROL OF CHOLESTEROL BIOSYNTHESIS

Cell cholesterol synthesis, intake, and processing are regulated by two different receptor systems; one involving sterol regulatory element binding proteins (SREBP), and the other liver X receptors (LRXs).[34] Regulation of cholesterol homeostasis by SREBP is one of the most well-known mechanisms in cholesterol metabolism (Figure 11). SREBP is located in the endoplasmic reticulum (ER) and activated when cholesterol levels are low. Activation of SREBP increases the transcription of genes encoding cholesterol synthesis.[35] SREBP is bound to a sterol regulatory element binding protein cleavage-activating protein (SCAP) in the ER. SCAP acts as a cholesterol-carrying protein for Golgi. When the cholesterol levels are low, the conformation of SREBP changes. The activated SCAP-SREBP complex is transported to the Golgi apparatus in COPII-coated vesicles. Then, SREBP is removed from SCAP. SREBP is proteolytically modified, wherein the complex reveals transcription factors.[35] The modified fragment is then transported to the nucleus, where it initiates the transcription of genes regulation sterol synthesis. Cholesterol transport is regulated in many different ways but the most well-known regulatory protein is an insulin-induced gene 1 protein (INSIG). SCAP is a Golgi-mediated protein of SREBP, whereas INSIG is an ER-anchoring protein. Binding of cholesterol to SCAP and 25-hydroxycholesterol **19** to INSIG causes binding of SCAP and INSIG to one another (Figure 11).[37,38,39] This leads to inactivation of SCAP`s sorting signal to COPII complex after which SCAP no longer enters in ER-Golgi transport vesicles.[40]

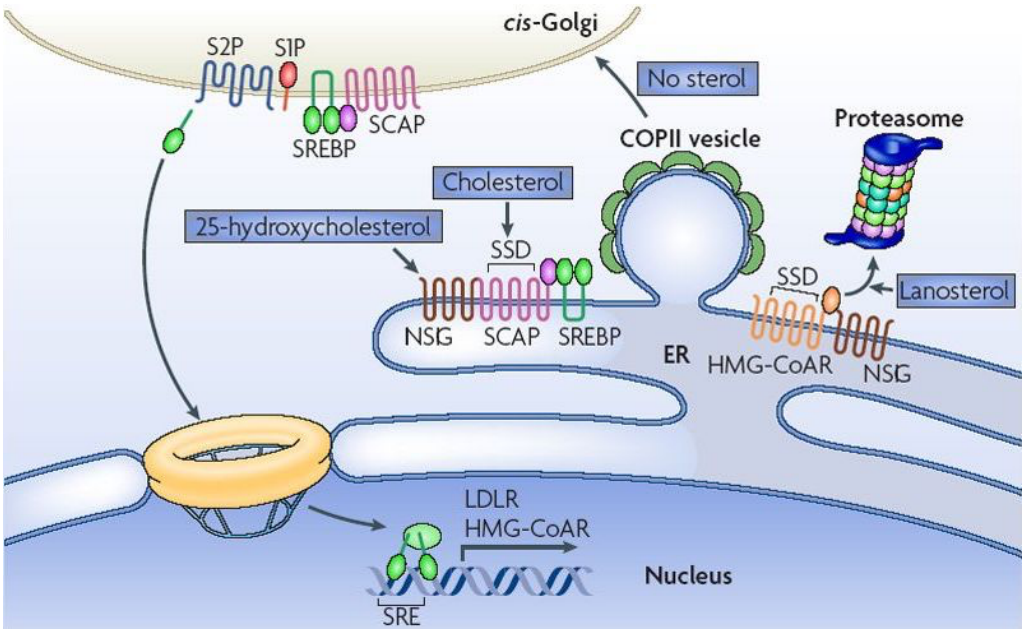

Figure 11: Regulation of cholesterol metabolism by SREBP.[34]
(Adapted from Ref.[34] with permission from Springer Nature.)

LRX activation facilitates reverse cholesterol transport i. e. processes that lead to cholesterol removal from the cell and increase in the secretion of bile acids.[41] LRX is activated by oxysterol, but the interaction between the membrane cholesterol levels, oxysterol production, and LRX activation are not completely understood. It has been shown that a particular oxysterol-related protein (OPR) could control this activation.[42]

3.3.3 CHOLESTEROL INTAKE, OUTFLOW, AND STORAGE

In addition to the biosynthesis of cholesterol, mammalian cells may obtain cholesterol in esterified form from the extracellular environment, *via* a process called forward cholesterol transport. It is mainly facilitated by receptor-mediated uptake of low-density lipoprotein (LDL) particles. When a cell needs cholesterol, for example, for synthesizing membrane structures, it prepares LDL receptors for the cell membrane. In the vasculature, circulating free LDL cholesterol is capable of attaching to an LDL receptor. This leads to a conformational change in the receptor, which induces a signal inside the cell. This leads to the attachment of the active membrane-binding adapter protein (AP2) to the intracellular portion of the LDL receptor. Attachment of AP2 to receptors leads to the formation of clathrin coating on the surface of the endocytic vesicle. Due to clathrin, the vesicle begins to separate from the cell membrane, the clathrin coating on the vesicle surface is rapidly degraded, and the vesicle content is transported to the early endosome. The LDL receptors are returned to the cell membrane by vesicles or transported for destruction if they are no longer needed. On the endosomal pathway, the change in pH causes cholesterol release from the receptor. Free LDL cholesterol is transported through the late endosome to the lysosome. In the lysosome, LDL cholesterol is hydrolyzed to free cholesterol, which is then available to the cell to be used as a building block.[32,34]

Because mammalian cells are unable to break down cholesterol, cells need a dedicated route to remove it. This is called inverse cholesterol transport. Since cells are not able to encode lipids genetically, direct changes in the genome or transcription factors do not affect cholesterol itself, but rather proteins maintaining the cholesterol homeostasis. In order to remove cholesterol, cells must excrete it homeostasis-maintaining proteins. Peripheral cholesterol is finally eliminated and transformed in the liver to bile acids through oxidation and cleavage of the side chain.[32,34]

Cells can regulate their intracellular cholesterol levels also by storing cholesterol in lipid droplets. Lipid droplets are cellular organelles that function as storage sites for cholesterol and fatty acids and thus regulate energy reservoirs in a cell.[43] The amount of cholesterol in the lipid droplets varies with cell types and depends on the metabolic state of the cell. Lipids are stored in a hydrophobic core which is surrounded by a lipid monolayer.[44] Although lipid droplets contain some free cholesterol, it is usually stored in esterified form.[32]

3.3.4 CHOLESTEROL DISTRIBUTION BETWEEN CELLULAR ORGANELLES

Cholesterol is distributed unevenly over the membranes of the various cellular compartments. Endoplasmic reticulum (ER), where cholesterol is synthesized, is actually relatively poor in cholesterol. Low cholesterol levels may facilitate the SCAP-SREBP complex to sense small changes in cholesterol levels, enabling the regulation of the cellular cholesterol levels. About 65-80 % of the cellular cholesterol resides in the plasma membrane. Around one of three of the plasma membrane lipids are cholesterol.[45] The amount of cholesterol in the Golgi apparatus lies between that of the ER and plasma membrane. In the Golgi apparatus, the concentration of cholesterol increases from cis-Golgi to trans-Golgi.[46] Other cellular organelles with high cholesterol levels include the endocytic recycling compartment. Mitochondria, which are involved in steroidogenesis, and lysosomes are generally cholesterol poor.[47]

3.3.5 INTRACELLULAR CHOLESTEROL TRANSPORT

To preserve the intracellular cholesterol distribution, cells must transport cholesterol from the biosynthesis sites (Figure 12). In general, the intracellular cholesterol transport pathways are vesicular or non-vesicular mediated. Vesicular transport takes place along the cytoskeleton by the means of transport proteins. Non-vesicular transport takes place either directly between the membrane contacts or by various lipid carrier proteins, or by the combination of both mechanisms. Precise mechanisms for cholesterol transport are yet not fully understood.[32,48]

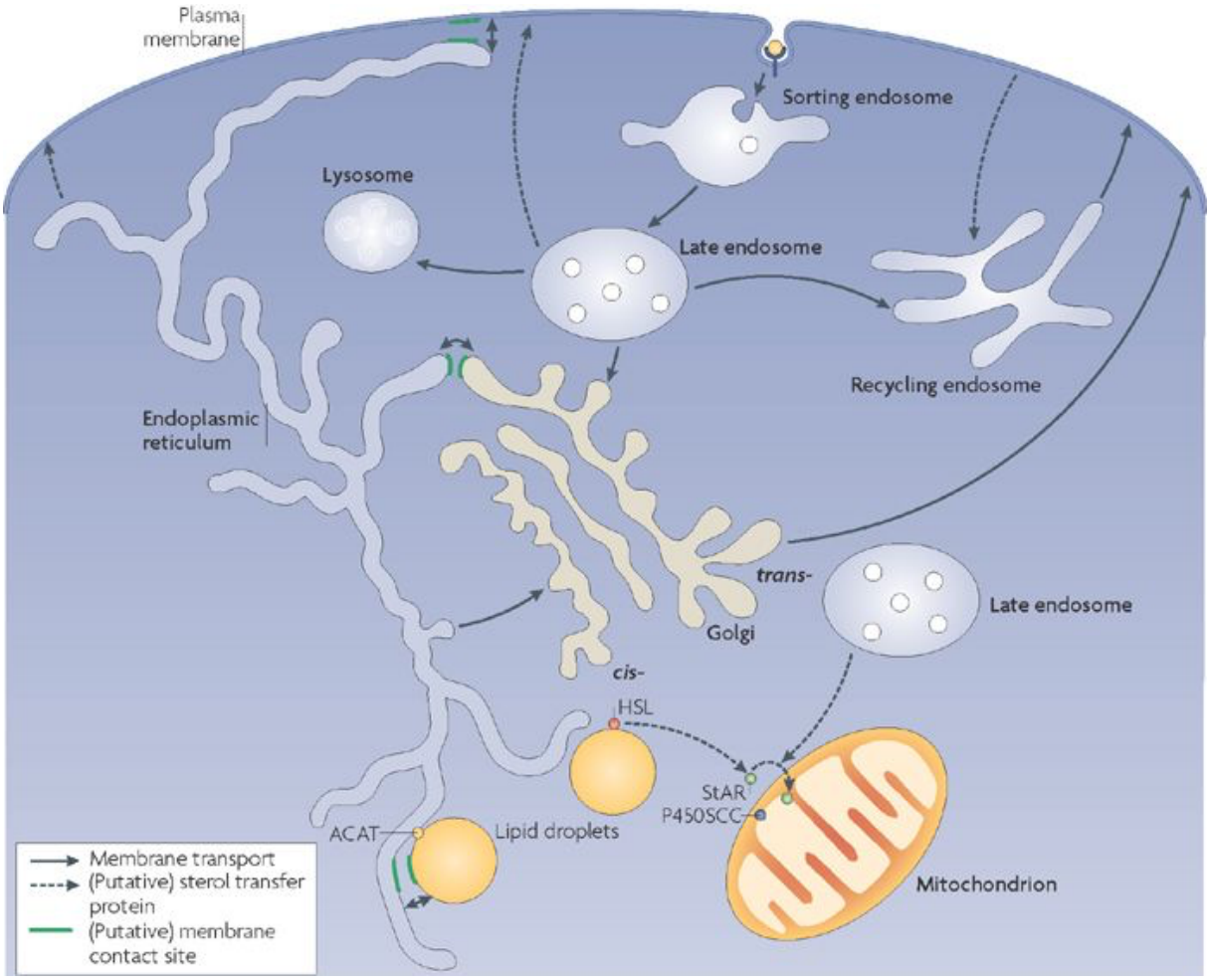

Figure 12: Cholesterol transport between membranes.[34]

(Adapted from Ref.[34] with permission from Springer Nature.)

3.3.5.1 FROM ENDOPLASMIC RETICULUM TO PLASMA MEMBRANE

Although the final stages of cholesterol synthesis are catalyzed by enzymes in the endoplasmic reticulum, most of the cholesterol is located on the cell membrane. An important transport route leads from the endoplasmic reticulum to the cell membrane. This takes place by the non-vesicular mechanism. The newly produced cholesterol is rapidly transported by an ATP-dependent mechanism to the cell membrane. The mechanism that carries the newly prepared cholesterol seems to be so effective that the cholesterol precursors are also carried to the surface of the cell. They are then returned back to the endoplasmic reticulum to be converted to cholesterol.[32,45]

3.3.5.2 TRANSPORT TO LIPID DROPLETS

The accumulation of cholesterol in lipid droplets is essential for maintaining cholesterol homeostasis. Most of the cholesterol migrating to lipid droplets originates from the cell membrane and passes through the endoplasmic reticulum. It is yet not fully understood how cholesterol and its esters migrate to lipid droplets. No carrier protein for the transport between the endoplasmic reticulum and the lipid droplets has yet been identified.[32]

For reducing the sterol levels in the endoplasmic reticulum, a buffering mechanism where cholesterol molecules are esterified to steryl esters has developed. Cholesterol is able to penetrate lipid vesicles more easily in ester form. Esterification is catalyzed by acetyl-CoA cholesterol acyltransferase, ACAT. Cholesterol esters are packed in lipid vesicles that are bulging. In some cells, unesterified cholesterol can be directly be packed into lipid vesicles. Caveolae protein has been shown to play an important role in maintaining cholesterol levels in lipid droplets.[32,34]

3.3.5.3 TRANSPORT TO MITOCHONDRIA

The main steroidogenic organs in the body include gonads, adrenal glands, and the brain. Rapid production of steroid hormones is necessary because the cells store only small amounts of steroid hormones. For the successful production of steroid hormones, cholesterol needs to be transmitted to mitochondria, where it must reach the inner membrane. The synthesis of steroid hormones from cholesterol is namely catalyzed by the cholesterol side-chain cleavage enzyme, P450SCC, which resides in the inner membrane of mitochondria. The migration of cholesterol from the outer membrane of mitochondria to the inner membrane facilitates a steroidogenic acute regulatory protein (StAR), which has a specific cholesterol-binding pocket. The activation of the StAR protein requires a conformational change. When the tertiary structure becomes a secondary one, the cholesterol-binding site in the carrier protein is revealed. The StAR-associated lipid carrier protein family includes StARD3, StARD4, and StARD5, which are all able to bind cholesterol and participate in its transport across the cytoplasm to the outer membrane receptors of mitochondria. Especially, the StARD3 carrier protein is able to transport cholesterol via non-vesicular mechanism directly to the mitochondria without passing through the endoplasmic reticulum or the cell membrane. StARD3 has also been found to bind cholesterol to late endosomes and thus reduce cholesterol levels in the cellular membrane.[34]

3.3.5.4 OTHER TRANSPORTERS

Oxysterol signals are mediated by several protein classes. These proteins are involved in non-vesicular sterol transport, lipid recognition, cellular signaling, and vesicle transport. The importance of oxysterol-binding proteins, OSBPs, for the intracellular transport of cholesterol has been studied mainly in yeasts. In mammalian cells, it is impossible to mute all genes and encoding OPRs, which is why their examination is more challenging. Mammals including humans have 12 different genes that are capable of encoding OPRs. In yeasts, OPRs are known to exist OSBP homologs, OSHs, seven of which have been identified.[49]

Inactivation of all Osh genes in yeasts significantly reduced the transport of sterols between the cell membrane and the endoplasmic reticulum. This was found to lead to apoptosis. On the other hand, inactivation of one of the Osh genes did not lead to apoptosis. This suggests that OSH proteins may have similar properties to each other.[49]

OSH proteins are involved in the identification and transport of phosphatidylinositol **11**, which participates in the identification and transport of sterols. Osh4 has a hydrophobic pocket that can bind sterols. Based on this, ORPs are believed to be involved in the transport of sterols. OPRs are able to bind the oxidized forms of cholesterol, such as oxysterol. Oxysterol is mainly present on lipid membranes, but due to the increased oxidation-induced hydrophilicity, it is much easier to move between the membrane structures than cholesterol. Oxysterol has been shown to be involved in the self-regulation of cholesterol homeostasis by participating in SREBP signaling.[49]

Several studies have shown that human OPRs are involved in the transport of sterols. For example, the increase in OPR2 level increased the delivery of the freshly synthesized cholesterol out from the cell. Similarly, its inactivation increased the amount of cholesterol esters. OPR2 is found, for example, in the lipid vesicles, on the cell membrane, and in the cytoplasm. Based on its distribution, OPR2 is suggested to be involved in the transport of cholesterol to the endoplasmic reticulum. The mechanism, however, is still unknown.[50]

OSBP and OPR9 have been shown to carry cholesterol *in vitro* but the transport depends on phosphatidylinositol-4-phosphatase (PI(4)P), that is located on the Golgi apparatus and endoplasmic reticulum. Overproduction of OSBP increases the biosynthesis of cholesterol and reduces cholesterol esterification. The attenuating of ORP9 led to the fragmentation of the Golgi apparatus. OPRs are likely to affect the transport of sterols, but transportation through them is

not the most important route since the distribution of ORPs leads to minor effects on the transport of sterols between the cell membrane and endoplasmic reticulum only.[51]

3.4 CHOLESTEROL METABOLISM DISORDERS

Cholesterol metabolism disorders have shown to affect the development of many neurobiological diseases such as Alzheimer`s, Parkinson`s, Huntington`s, and Niemann Pick disease, type C. Abnormal cholesterol metabolism also appears to have an effect on the development of tumors. In the tumor microenvironment, the activity of CD8+ T cells is suppressed, and the reactivation of their cytotoxicity is of great clinical interest in cancer immunotherapy. Recent studies have proved that the activity of the $CD8^+$ T cells can be influenced by cholesterol metabolism. The inhibition of the cholesterol esterification in the T cells by genetic modification or by pharmacological inhibition of ACAT-1 led to increased production of the $CD8^+$ T cells. This restrained the growth of melanoma tumor and metastasis effectively in mice.[52,53]

3.4.1 THE ROLE OF CHOLESTEROL IN ALZHEIMER`S DISEASE

Alzheimer`s disease (AD), a neurodegenerative disorder, is the most common cause of dementia in developed countries. It is a complex and genetically heterogeneous disease characterized by a progressive memory loss, cognitive impairment, and personality changes that involve specific structural abnormalities in the brain. The most important histological feature of AD is the build-up of amyloid-β in extracellular form, which contributes to damage to the nerves and brain cells. The damage begins in the inner part of the cerebral precursors and spreads over the years over the cortex.[52]

The brain is the organ exhibiting the highest cholesterol concentration. In the brain, cholesterol is mostly present as its free form and is derived from *de novo* synthesis. The blood-brain barrier prevents plasma lipoproteins entering from the peripheral bloodstream into the brain. Cholesterol has suggested affecting amyloid-β production, although the mechanisms are not fully understood. However, changes in the properties of the cell membrane have been suggested. Cholesterol is mainly located on the cell membrane in microdomains called lipid rafts through which the amyloidogenic pathway occurs. At the same site, amyloid precursor protein is processed into toxic amyloid-β peptides.[52,54]

It has been demonstrated that the elevation of cholesterol levels of lipid bilayer facilitates the binding of amyloid-β peptides to the membranes. This promotes the amyloid-β-conformation change from the helix to the β-sheet, resulting in permanent amyloid. The conversion of soluble and non-toxic monomeric amyloid-β to the insoluble and toxic oligomer and the aggregation of the amyloid-β are the critical steps in the development of Alzheimer`s disease. It appears that the distribution and transport of cholesterol in the brain cells are important factors in the accumulation of amyloid-β leading to the progression of Alzheimer`s disease.[52]

3.4.2 THE ROLE OF CHOLESTEROL IN NIEMANN-PICK DISEASE, TYPE C

In Niemann-Pick disease, type C (NPC), defect in cholesterol transport does not affect plasma lipoprotein levels or lead to vascular disease, but instead NPC patients suffer from progressive degeneration of the central nervous system and viscelar storage of cholesterol, sphingomyelin, and glycosphingolipids. The clinical phenotype of the disease is quite heterogeneous. Typically, the symptoms of NPC patients begin at school age, after which life expectancy is in the early teenage years. NPC has no therapeutic approach that would alleviate progressive neurodegeneration.[45]

The structure of the NPC1 protein contains a similar sterol-recognizing domain that is found in two ER proteins 3-hydroxy-3-methylglutaryl-CoA reductase and sterol regulated-binding protein cleavage acting protein (SCAP). They respond to the cholesterol content of the ER membrane. The homologous sterol-recognizing domain in NPC1 protein could function in targeting cholesterol-containing vesicles.[45]

A broad homology between the proteins NPC1 and Patched, the latter of which is a membrane receptor that mediates the Hedgehog signal transduction pathway. Because the Hedgehog signaling pathway transmits information to embryonic cells required for proper cell differentiation, the role of an NPC1 ligand triggering a signal shift cascade culminating in controlling cholesterol homeostasis may be speculated. The build-up display joins the developmental problems affecting the homologous sterol identifier Patched. So far, there is no evidence that NPC1 mutations influence development.[45]

Cholesterol is not the major storage product in the brain in NPC. Instead, the level of glycosphingolipids, such as GM2 gangliosides is elevated. Neuronal accumulation of GM2 is seen early in the disease and is closely related to the progression of the disease. This may mean that NPC1 protein carries a number of lipids found in plasma membranes. Sterol-specific

detection refers to the role of NPC1 protein in cholesterol homeostasis, but its presence does not rule out the role of ganglioside metabolism. The biological activity of NPC1 protein is not properly known, and it is not clear how lipid degradation leads to brain pathology.[45]

4 FLUORESCENT MARKERS FOR STUDYING THE INTRACELLULAR CHOLESTEROL

Quantitative fluorescent microscopy is a commonly used method to study intracellular cholesterol transport. Since cholesterol and its physiological esters are not fluorescent, their fluorescent analogs must be employed. The major challenge is to synthesize cholesterol analogs with suitable brightness. Furthermore, the structure and chemical properties of cholesterol analogs should be similar to those of cholesterol. Cholesterol analogs can be intrinsically or extrinsically fluorescent. Dehydroergosterol **22** (Figure 13) is an example of an intrinsically fluorescent cholesterol analog and BOBIDY-tagged cholesterol **31** (Figure 19) of an extrinsically fluorescent cholesterol analog. The fluorescent probe may also be a combination of these. An alternative approach is to use cholesterol-binding fluorescent molecules. The common problem related to the previous approach is that these probes cannot be used when studying inter-organelle transport of cholesterol.[4]

4.1 DEHYDROERGOSTEROL

As already mentioned, dehydroergosterol **22** (DHE) is an example of an intrinsically fluorescent cholesterol analog. DHE belongs to the group of P-sterols and is the most widely used molecule studying cholesterol trafficking. DHE is a derivative of ergosterol **23**, which differs from DHE by only one double bond in the ring system (Figure 13). The conjugated system of three double bonds makes DHE slightly fluorescent in the ultraviolet (UV) range. DHE is a sterol that occurs naturally in yeast cells and fungi.[4]

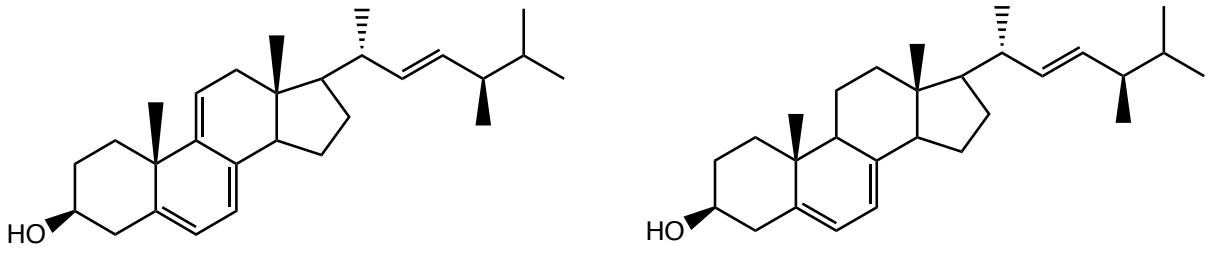

22 **23**

Figure 13: Structures of dehydroergosterol **22** and ergosterol **23**.[4]

The commercially available DHE usually contains a significant amount of impurities. This is detrimental in imaging because impurities can compete with DHE itself or may have other effects, including cytotoxicity.[55] Fortunately, DHE can be synthesized in the laboratory. In the first step, ergosterol is converted to its ethyl acetate form **24** (Figure 14).

Thereafter, oxidation with mercury acetate is performed forming the product **25**. Finally, sodium hydroxide is added to remove the ester protection of 3-position obtaining the product **22**.[4]

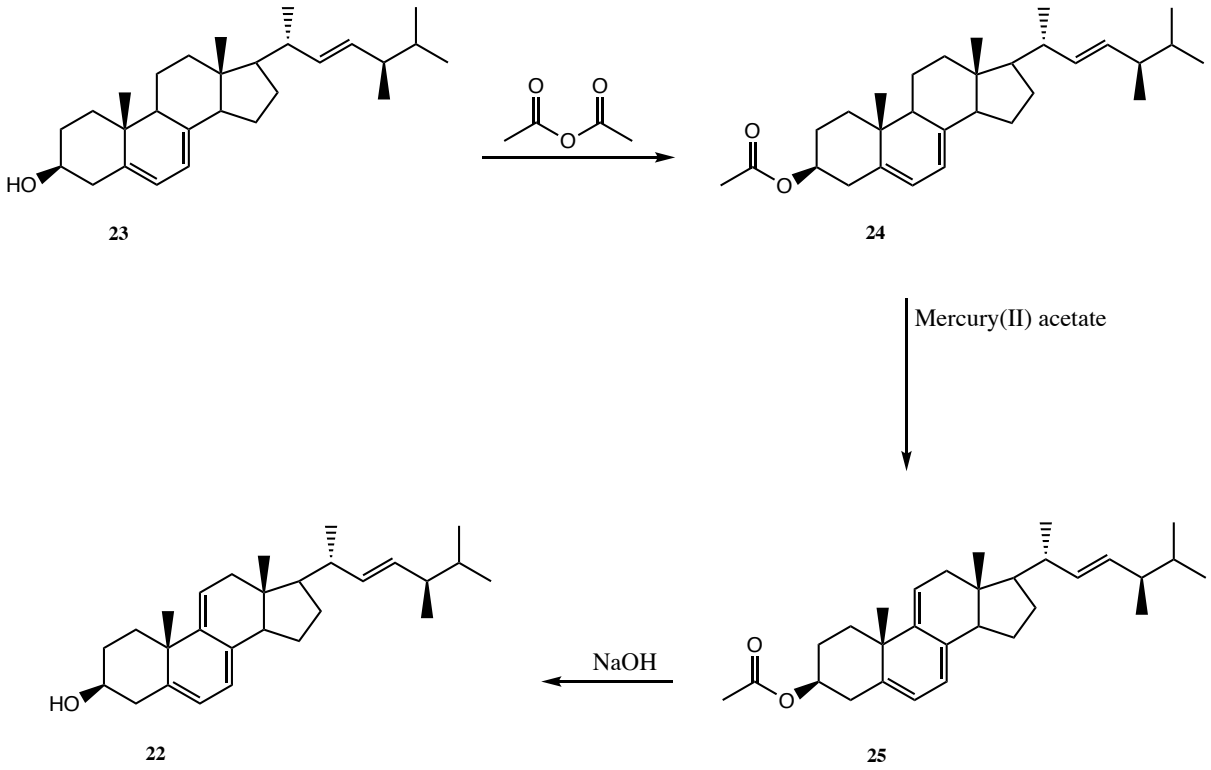

Figure 14: Schematic pathway for the synthesis of DHE **22**.[4]

DHE has been used for decades for spectroscopic studies of cholesterol distribution in the membranes. Based on the experimental and computational studies, it has been proved that **22** mimics cholesterol well in membranes. Concentrations up to 10-mole percent enable the organization of phospholipid acyl chains by **22**. Above this concentration, its organization ability ceases, which is different from cholesterol. DHE exhibits a fluorescence lifetime of approximately 0.3 nanoseconds. The maximum emission of DHE is about 373 nm in phosphatidylcholine membranes.[4,56]

The low excitation factor and quantum yield of DHE results in low molecular brightness. This requires UV-optimized optics combined with highly sensitive detectors to display DHE in cells. For example, a charge-coupled device is suitable for this task. The image quality can be significantly improved by averaging several frames to obtain a single image with a good signal-to-noise ratio.[4,57]

4.2 CHOLESTATRIENOL

Cholestatrienol (CTL) **26** (Figure 15) is the structurally closest intrinsically fluorescent derivative of cholesterol. Similar to dehydroergosterol **22**, cholestatrienol has a ring system with two additional double bonds compared with cholesterol. However, the aliphatic side chain of cholestatrienol is similar to cholesterol. Fluorescent properties and bleaching of CTL are comparable to those of DHE. The CTL is poorly fluorescent, but detection is possible, for example by using a UV-adapted wide field microscope.[4,58]

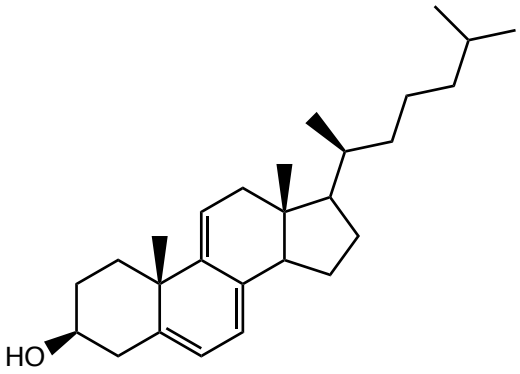

26

Figure 15: The chemical structure of cholestatrienol (CTL) **26**.[4]

The properties of cholestatrienol, in biological membranes, are close to cholesterol. Exactly like cholesterol, CTL shows a linear relationship between the ordering capacity of the fatty acid chains and its concentration in phosphatidylcholine bilayers.[59] One of the first studies using CTL was to gather information on micellar structures of sterols and sterol-protein interaction using sterol transporter protein, SCAP2. CTL was later used as the closest fluorescent cholesterol analog in many spectroscopic studies. CTL has been found to resemble natural and deuterated cholesterol, a property that can be utilized in NMR-spectroscopy and related techniques.[58] A CTL derivative, having a hydroxylated side chain, has been used to detect the transport and metabolism of 25-hydroxycholesterol **22** (Figure 14).[4,60]

4.3 CHOLESTATRIENOL ESTERS AND CHOLESTERYL PARINARIC ACID

Cholestatrienol **26** can be converted into esters by a reaction requiring an excess of fatty acid anhydride and a coupling reagent, such as dicyclohexylcarbodiimide and a catalytic amount of 4-dimethylaminopyridine. The most common fatty acids used in the esterification are linoleic acid and oleic acid leading to CTL-linoleate **27** and CTL-oleate **28** (Figure 16), respectively. CTL-esters can be added to LDL and other lipoproteins by two different methods. One alternative is to use sterol exchange proteins, such as proteins found in human plasma that catalyze the exchange of sterol esters. The other alternative is cholesterol ester extraction with heptane from lipoprotein and reconstitution of the core with **28**. The first method is useful for coupling sterol esters to HDL. The second method is most suitable for the coupling to LDL. For example, **26**, and its esters **27** and **28** have been used for spectroscopic analysis of sterol distribution in LDL and HDL.[4,61]

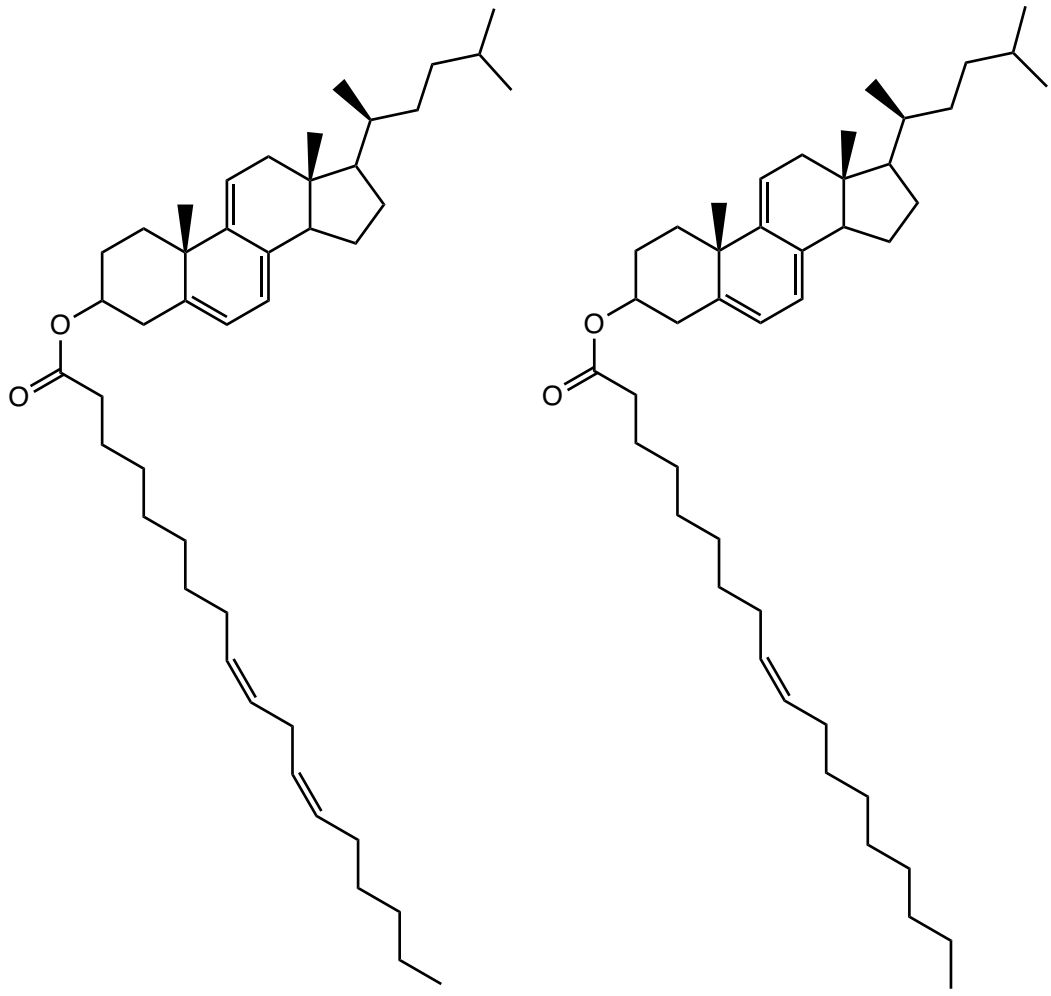

27 **28**

Figure 16: The structures of intrinsically fluorescent CTL-linoleate **27** and CTL-oleate **28**.[4]

Another approach in the development of intrinsically fluorescent cholesterol esters is to use a fluorescent fatty acid, such as parinaric acid **29** (Figure 17). It occurs naturally in a large quantity in Makita seeds, from which it can be extracted and purified by repeated recrystallization from petroleum ether. It can also be prepared synthetically using α-linoleic acid as a starting molecule or by iterative cross-couplings.[62] Parinaric acid has been used as a fluorescent probe for studying the membrane structure[63] as well as human plasma lipoproteins.[4]

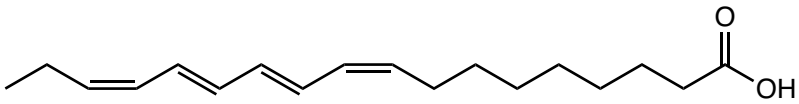

Figure 17: Parinaric acid **29** is an intrinsically fluorescent polyunsaturated fatty acid.[4]

4.4 NBD-CHOLESTEROL ANALOGS

NBD-cholesterol analogs are synthesized by adding a fluorescent 7-nitrobenz-2-oxa-1,3-diazole (NBD) group to cholesterol. There are several NBD-cholesterol analogs, that differ from each other according to the position of the NBD group. The most commonly used NBD-analogs are extrinsically fluorescent 22-NBD-cholesterol **30** and 25-NBD-cholesterol **31** (Figure 18). Typically, the NBD group has good fluorescent properties with the excitation wavelength of 470 nm and the emission wavelength of 530 nm. NBD-cholesterol analogs also have good quantum yield. **30** has been shown to interact with sterol binding sites of cholesterol-regulating enzymes, such as HMGR and ACAT. NBD-cholesterol derivatives have also been used to study the binding sites between STAR, SCAP-2, and sterols.[4,64,65]

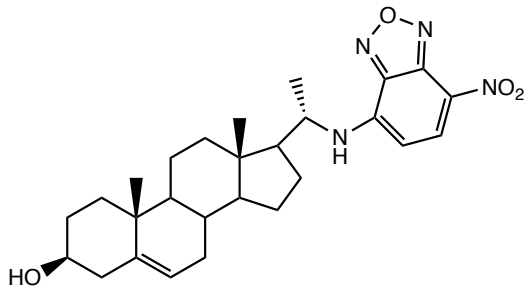

30

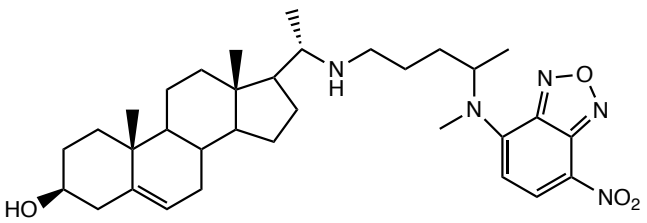

31

Figure 18: The structure of extrinsically fluorescent 22-NBD-cholesterol **30** and 25-NBD-cholesterol **31**.[4]

Many sterol binding enzymes recognize NBD-sterols similarly to cholesterol. However, the biophysical properties of NBD-sterols differ from those of cholesterol, for example on a lipid bilayer, where NBD-sterols are not distributed in cholesterol-rich domains. Moreover, the behavior of NBD-sterols in the cell differs from cholesterol; for example, **30** accumulate in mitochondria. Because the biophysical properties of NBD-sterols differ markedly from those of cholesterol, the intracellular targeting by them is of NBD-sterol inaccurate.[4,32]

4.5 BODIPY-TAGGED CHOLESTEROL

Boron-dipyrromethene (BODIPY)-tagging is a versatile and common approach for generating fluorescent lipid probes. They have preferable photophysical properties and acceptable impact on the native lipid structure.[66] BODIPY-cholesterol was first introduced by Li *et al*.[67] in 2006. In their study, they have synthesized several BODIPY-tagged cholesterol derivatives. The derivatives were obtained by coupling the carboxylic acid derivative of BODIPY to a sterol analog containing a hydroxyl group in the side chain. The coupling reagent in the reaction was *N,N′*-dicyclohexylcarbodiimide (DCC). Based on the study, only BODIPY-cholesterol (B-Chol) **32** and BODIPY-P-cholesterol **33**, are preferably distributed in the cholesterol-rich liquid ordered (lo) phase in ternary model membranes (Figure 19).[4]

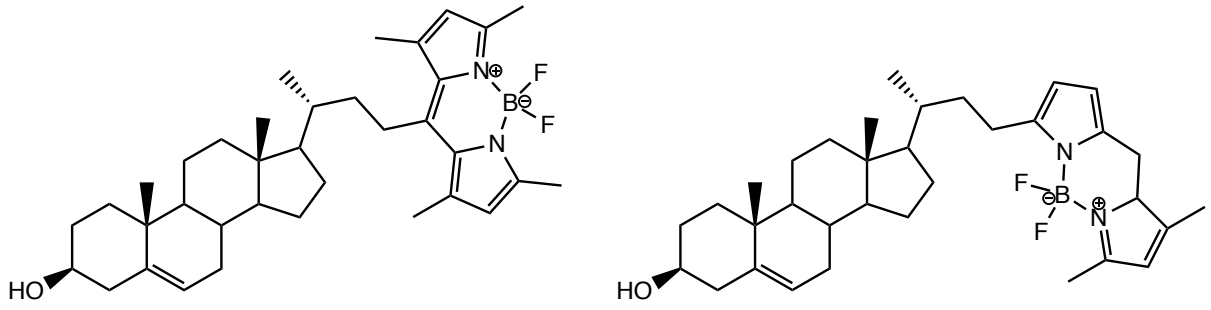

32 **33**

Figure 19: The structures of commercially available BODIPY-cholesterol **32** and BODIPY-P-cholesterol **33**.[4]

The distribution of **32** and **33** in the cholesterol-rich liquid ordered (Lo) phase, along with comparable trafficking kinetics, makes them useful for cholesterol research. BODIPY-based cholesterol derivatives have at least 600-fold higher brightness compared to **22** and **26**. BODIPY-cholesterols **32** and **33** behave more like cholesterol than NBD-sterols **30** and **31**. One of the main reasons for this difference is the higher hydrophobicity of the BODIPY-group, which makes it similar to the natural side chain of cholesterol.[4,67]

Cholesterol probes **32** and **33** can be used for long-term imaging and fluorescence correlation microscopy in living cells because of their high photostability.[68] They are also useful for evaluating the orientation of the probe with two photon-based fluorescence polarimeters on models and cell membranes.[69] These properties make BODIPY-tagged extrinsic cholesterol analogs very useful.[70]

4.6 DANSYL-CHOLESTEROL

Dansyl chloride **3** is commonly used as a fluorophore for labeling lipids, proteins, and other biomolecules. Its features include environmental sensitivity, solvent polarity, and a long lifetime.[71] Wiegand *et al.*[72] were the first to synthesize a cholesterol analog having a dansyl group. 6-ketocholestanol and dansyl hydrazine were condensed with HCl acting as a catalyst to yield 6-dansyl-cholesterol **34**, also known as dansyl-cholestanol (Figure 20). In the reaction, the double bond of between carbon five and six is reduced.[4]

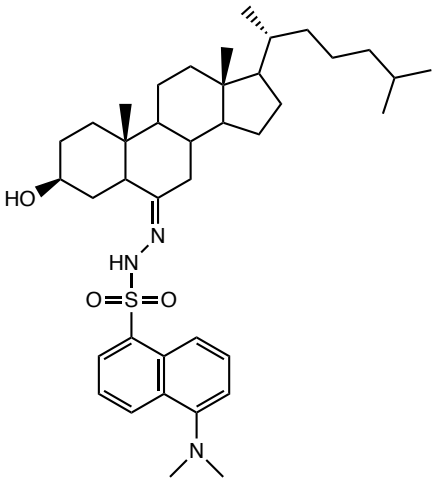

34

Figure 20: The structure of extrinsically fluorescent cholesterol analog dansyl-cholestanol (Dchol) **34**.[4]

Dansyl-cholestanol **34** has a broad excitation and emission spectrum with maximum values of 366 and 522 nm, respectively. It is a relatively small fluorophore having a high quantum yield and prone to photobleaching similar to NBD-tagged cholesterol derivatives **30** and **31**. The emission of **34** is environmentally sensitive and is affected by the polarity of the solvent and pH. The emission of **34** shifts to lower wavelengths at neutral pH and in a polar solvent. Correspondingly, as the pH drops, the emission intensity at 509 nm shifts to 490 nm. The mean fluorescence lifetime of **34** is 13.2-15.2 nanoseconds. When **34** has been used to study the transport of sterols, it was found that it is esterified similar to cholesterol. It can be introduced into the membranes of living cells in three different ways; directly from the culture media, by using specific vesicles, or as a complex with β-cyclodextrin. In the last case, the incubation time is reduced from 1-2 hours to 2-30 minutes.[4,72]

Dansyl-cholestanol has been found to be distributed in the cholesterol-poor liquid disordered (ld) phase in model membranes. When NPC1 disease cells were studied, 34 was found to be distributed to a small extent in cholesterol-rich cells.73 These results, together with the high bleaching ability of this probe, make the use of 34 in live-cell imaging studies questionable.4

4.7 PYRENE-TAGGED CHOLESTEROL AND ITS ESTERS

When pyrene-containing lipids gather in close proximity, the pyrene groups exhibit typical red-shifted excited state emission. This feature has been used in many applications. Guyader *et al.*[74] have studied 21-methylpyrenylcholesterol **35** (Figure 21), which was obtained by a condensation reaction between 1-pyrenecarboxaldehyde and pregnenolone. 21-Methylpyrenylcholesterol was shown to easily incorporated into membranes. By measuring the extent of excimer formation, it was found that it tends to self-associate in the membranes. 21-Methylpyrenylcholesterol is delivered to cells via introduction into lipoproteins which act as transporters to deliver this probe to cells.[4,74]

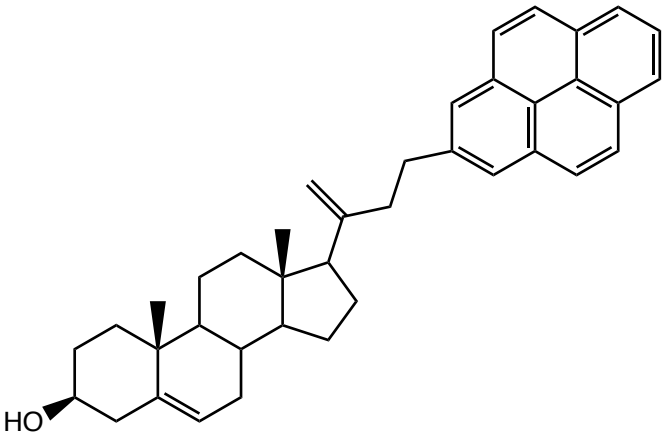

35

Figure 21: The structure of 21-methylpyrenylcholesterol **35**.[4]

Other examples of pyrene-labeled probes are acyl chain labeled pyrene cholesteryl esters, where the pyrenyl part is attached to the 3-position of cholesterol. Their exchange between HDL-particles catalyzed by a transfer protein has been studied. The same probe, when inserted into LDL, was used to follow trafficking and lysosomal degradation of cholesteryl esters in human fibroblasts. These studies suggest that cholesteryl esters tagged in the acyl chain with a pyrene group are suitable surrogates of native cholesterol esters.[4,75]

4.8 DERIVATIVES OF ALKYNE CHOLESTEROL

Click chemistry concept was introduced by K. B. Sharpless in 2001 to describe a modular approach that uses only the most practical, reliable and high yielding reactions for joining functional chemical groups together.[76] The method was developed in parallel with the interest within the pharmaceutical and other industries in capabilities for generating large libraries of compounds. The most well-known click chemistry reaction is the azide-alkyne Huisgen cycloaddition, where an azide group reacts with an alkynyl group. Copper ions (Cu^{+}) act as a catalyst in the reaction. Generally, the reaction can be carried out *in situ* the product being a 1,2,3-triazole ring. Hoffmann *et al.*[77] have investigated cell cholesterol metabolism and localization using alkyne-cholesterol **36**. They have also linked alkyne-cholesterol **36** to fluorescent BODIPY-dye using click chemistry to forming a product **37** (Figure 22).[76,77]

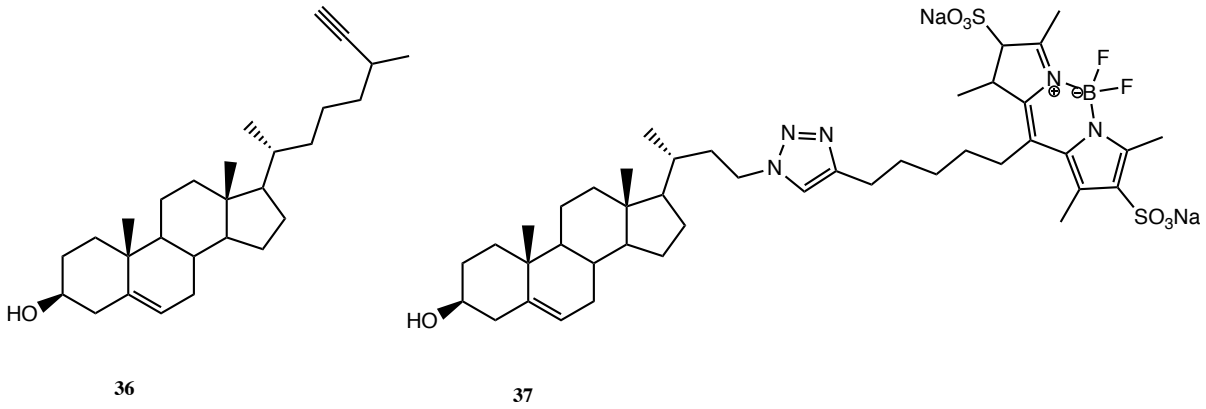

36 **37**

Figure 22: The structures of alkyne-cholesterol **36** and alkyne-cholesterol derivative **37** with BODIPY dye.[77,78]

Alkyne analogs **36** and **37** offers several advantages over cholesterol radioisotopes. The alkyl moiety replaces the terminal portion of the cholesterol side chain, so that compound **36** is structurally quite similar to natural cholesterol. It has been tested for various biological systems and its employing both *in vivo* and *in vitro*. Neither **36** nor **37** did show cytotoxicity in mammalian or in yeast cells. Alkyne-cholesterol **36** represents a versatile, sensitive, and useful tool for monitoring cellular cholesterol metabolism and localization. It can be detected by mass spectrometry or by fluorography. In addition, compound **37** can be detected by fluorescent microscopy.[77]

5 STEROIDS HORMONES AND BILE ACIDS

Steroid hormones regulate various physiological functions, such as reproduction, blood salt balance, maintenance of secondary sexual characteristics, response to stress, neuronal function, and various metabolic processes.[79] The steroids hormones, as of all the other steroids, consists of a perhydro-1,2-cyclopentanophenanthrene ring system **38** (Figure 23).[80] Steroid hormones are synthesized from cholesterol mainly in adrenal gland and gonads. After synthesis, they are released into the circulatory system. When they achieve their target cells, they interact with the hormone receptors and cause-specific physiology responses by regulating the expression of certain genes. The analysis of steroid hormones is of particular interest due to their abuse in sports as well as their potential roles as disease biomarkers. Steroid hormones are linked, for example, to Alzheimer`s disease[81], cancer[82], and diabetes[83].

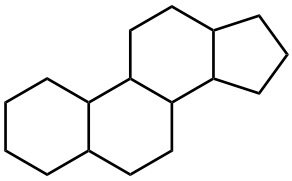

38

Figure 23: Schematic structure of steroidal skeleton **38**.[80]

Sex hormones are hormones that produce sex differences or support reproduction. This group includes androgens, estrogens, and progestogens. Examples of sex hormones include testosterone **39**, and its metabolite dihydrotestosterone **40**, progesterone **41**, and estradiol **42** (Figure 24). Corticosteroids include glucocorticoids, such as cortisol **43**, and mineral corticoids, such as aldosterone **44** (Figure 24). Glucocorticoids regulate metabolic processes and immune responses, while mineralocorticoids help to main blood pressure and to regulate electrolyte excretion in the kidneys.[79]

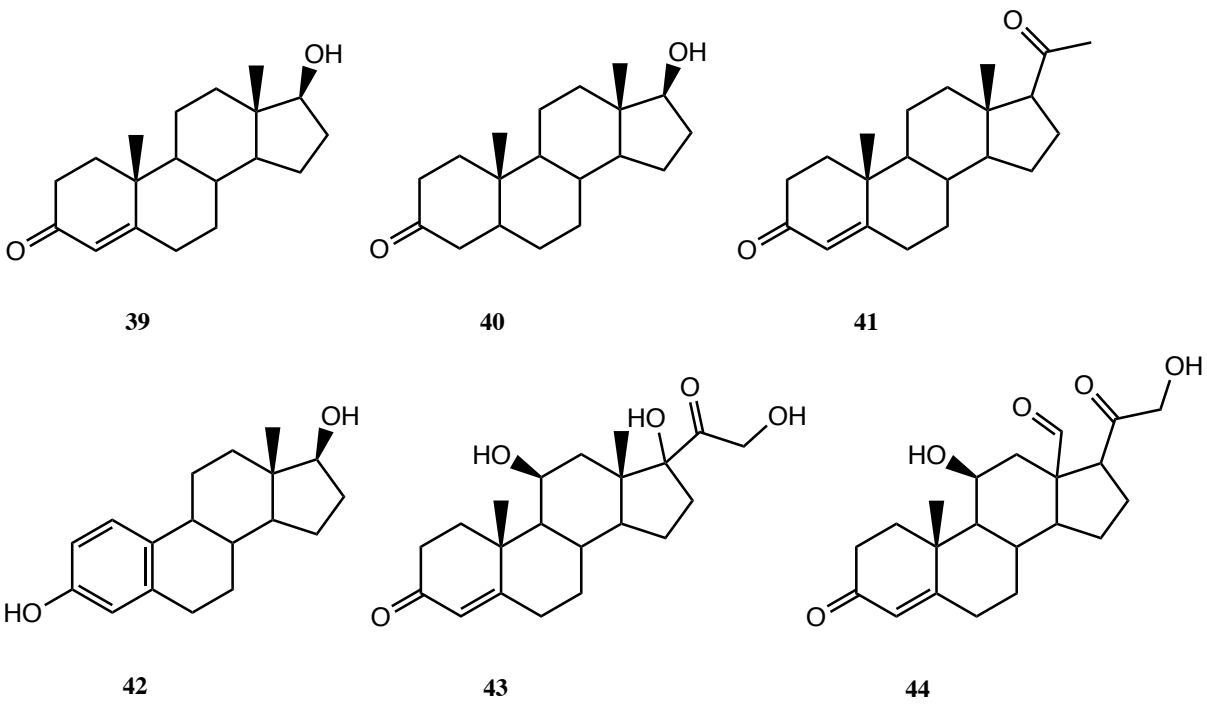

Figure 24: Structures of most common steroid hormones in the human body are testosterone **39**, dihydrotestosterone **40**, progesterone **41**, estradiol **42**, cortisol **43** and aldosterone **44**.[79,80]

Bile acids are part of cholesterol catabolism because they are involved in removing cholesterol from the body. Bile acids present in the human body can be divided into primary and secondary bile acids by structure and function. Primary bile acids are formed as part of the enterohepatic circulation in the liver, where their starting material is cholesterol. Primary bile acids are transported by the glycine and taurine conjugates to the gallbladder where they concentrated and stored. When primary bile acids are exposed to the bacteria in the gut, they form secondary bile acids. Primary bile acids include cholic acid **20** (Figure 30) and chenodeoxycholic acid **45**, whereas deoxycholic **46** and lithocholic acid **47** (Figure 25) represent secondary bile acids.[84,85,86]

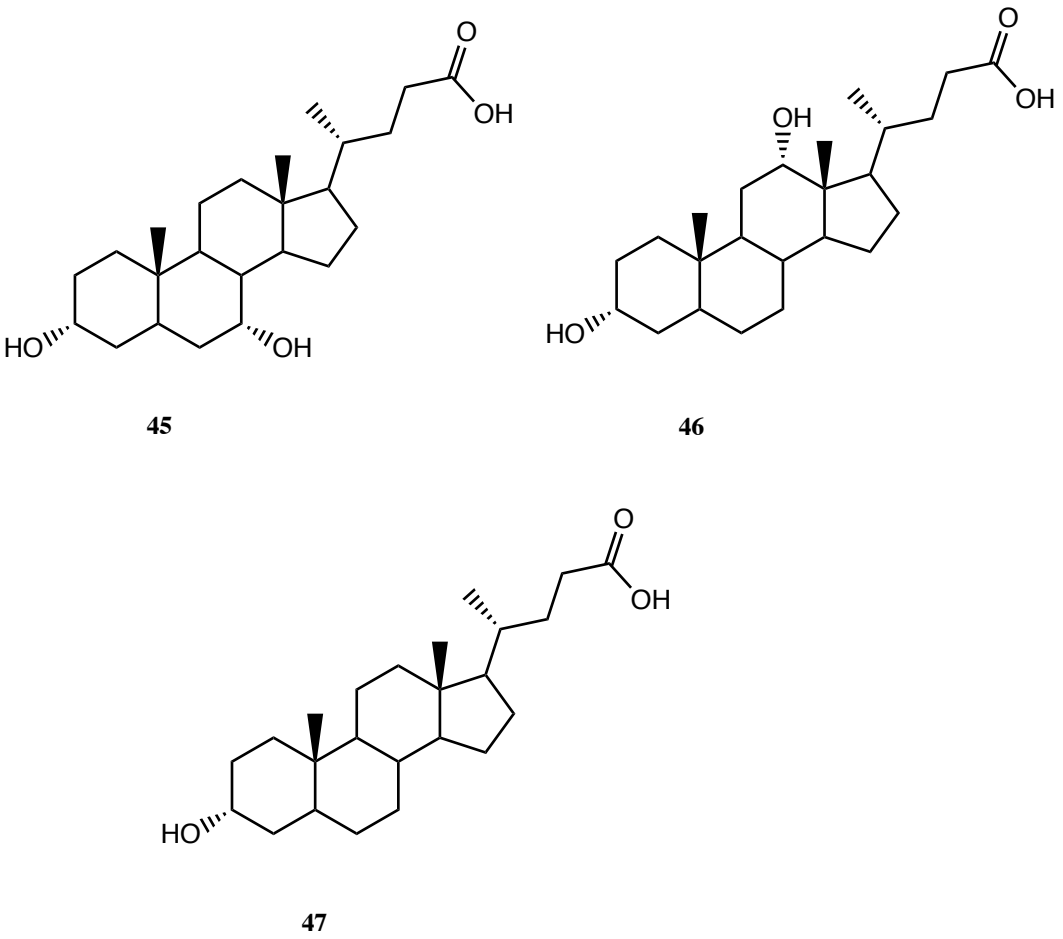

Figure 25: The structure of one of the primary bile acid, chenodeoxycholic acid **45**, and the secondary bile acids deoxycholic **46** and lithocholic acid **47**.[84,85,86]

As part of the enterohepatic circulation, bile acids circulate along the route intestine-liver-gallbladder-intestine. When fatty food is released from the stomach into the small intestine, the bile is secreted from the gallbladder. When the fats were absorbed in the intestine, most of the bile acids are reabsorbed from the intestines via transporter proteins and delivered back to the liver via the portal vein. This cycle is called the enterohepatic cycle, and it takes place 6-16 times per day. Less than 5 % of the bile acids are excreted with urine and feces, making bile acids the only natural way to remove excess cholesterol. Bile acids also have hormonal functions. They act, for example, as signaling molecules in the liver and are involved in the activation of the tumor hormone receptor FRX. In addition, they promote the absorption of fat-soluble vitamins in the small intestine.[84,85,86]

5.1 SELECTED APPLICATIONS OF USING FLUORESCENT PROBES IN STUDYING SYSTEMS INVOLVING STEROIDS

There exists a specific protein that binds gonadal steroids in the plasma. The human and non-human primate proteins have the highest affinity for testosterone **39** and dihydrotestosterone **40**. Estradiol **42** is also bound but with lesser affinity.[87] Ross *et al*.[88] developed a fluorescent probe to investigate the interaction between the steroid and the gonadal steroid-binding proteins. For that they used two approaches; in the first one, the fluorescent dye was linked to the dihydrotestosterone analogs, whereas the second one utilized fluorescent analogs of the gonadal steroids having a high affinity to the target protein. Since the ground and excited states of aromatic fluorescent dyes are very sensitive to the local environment, the fluorescence studies can provide significant information on the nature of the steroid binding site of the gonadal steroid-binding protein.[88]

In their study, Ross *et al.* determined the association constant of equilenin **48** (Figure 26) with the human gonadal steroid-binding protein. Equilenin is naturally fluorescent steroid with a high binding affinity to the human gonadal steroid-binding protein. In addition to the determination of the equilibrium constant the steady-state fluorescence excitation and emission spectra of **48** bound to the gonadal steroid-binding protein was investigated.[88]

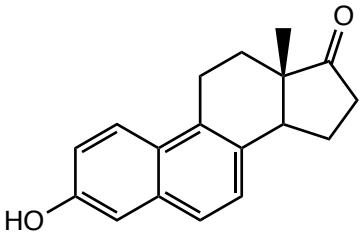

48

Figure 26: The structure of equilenin **48**, which is a potential probe for studying the interactions of steroids and proteins.[88]

Based on the study, the fluorescent excitation and emission spectra of the steroid-protein complex showed that both hydrophobic interactions and hydrogen bonding of the 3-hydroxyl group of the equilenin are important in its binding to the protein. The equilibrium association constant of the equilenin was $6 \times 10^7\ M^{-1}$. It is strong enough to displace the natural steroid, such as dihydrotestosterone, from the binding pocket. The results show that equilenin may be a useful probe for studying the interactions of steroids and proteins.[88]

Estrogens regulate a wide range of physiological functions through target cells that overexpress receptors, such as MCF7 breast cancer cells, and are one of the most widely studied classes of biological systems.[89] The estrogen receptors are mainly located in the nucleus or cytoplasm and to the lesser extent also on the plasma membrane of the cell. Like other steroids, estradiol **42** is a small molecule with lipophilic nature and neutral charge. Interest in developing fluorescent ligands that could act as specific probes in estrogen-binding sites within the tissues and cells has stimulated the development and characterization of fluorescent estrogen probes. Early attempts to develop fluorophore-conjugated estrogen probes have received criticism regarding the specificity. For example, high ligand concentrations were required for reasonable staining, or the staining was primarily located in the cytoplasm.[90,91,92]

Tsai *et al.*[89] prepared a novel gold nanocluster (AuNC)-conjugated estrogen probe for selective and rapid detection of estrogen receptors in living cells. The study showed that relatively large and hydrophilic bovine serum albumin (BSA)-protected AuNCs conjugated with 17β-estradiol **49** (Figure 27) are able to specifically bind to the steroid receptors. In contrast, a small organic dye Cy3 conjugated with 17β-estradiol **50** (Figure 27) showed non-specific binding to the cytoplasmic components.[89]

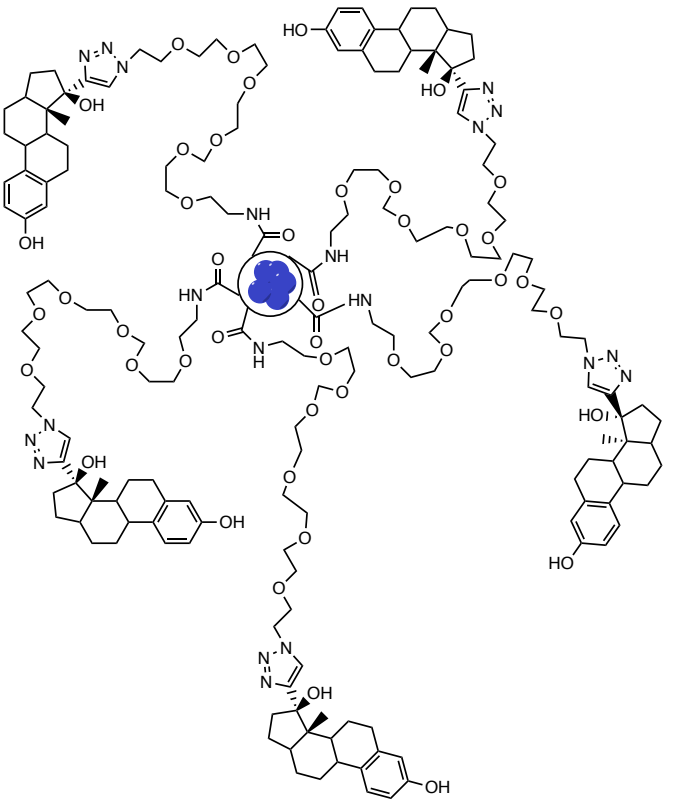

49

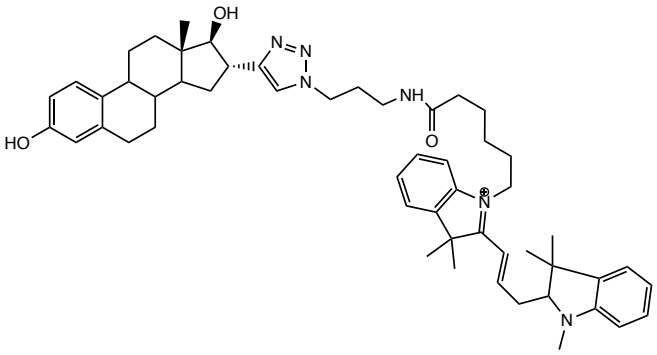

50

Figure 27: A schematic representation of the conjugate of a BSA-protected AuNC and 17β-estradiol **49** and Cy3-conjugated 17β -estradiol **50**.[89]

The BSA-AuNC-based probe can be utilized in the basic studies on a cell model and has the potential for the development of diagnostic applications of tissue samples. The efficiency of the probe can be increased, for example, by increasing the number of 17β-estradiol conjugates attached to each probe. A similar approach may be developed to fabricate other steroid probes requiring rapid and specific in-situ detection of target cells or tissues. For example, cell counting using flow cytometer and *in-situ* diagnosis of tumor versus normal tissues could be such application.[89]

Steroids are considered to act as endocrine disruptors, which may impact on the fertility of aquatic organisms and even have direct effects on humans.[93-96] Environmental research has so far focused on estrogen-induced environment impacts. Androgens, such as testosterone and its derivatives, have shown to act as hormone distributors as well, and consequently, bacteria capable of breaking down testosterone are becoming more frequent in wastewater treatment.[97]

Stahl *et al.*[97] have studied a fluorescent supramolecular assay, which can be used to screen for the depletion of steroids from the bacterial cultures containing steroid-degrading bacteria. The assay is based on the macrocyclic fluorescence dye encapsulation and the competitive binding of testosterone **39** as a model steroid (Figure 28).[97] The study is based on the indicator displacement assay (Figure 28), which is a well-established in biochemistry.[98] The method is based on the fact that the supramolecular receptor may bind either the dye or the analyte. In the study of Stahl *et al.* the supramolecular receptor was a macrocyclic cucurbit[8]uril (CD8).[97]

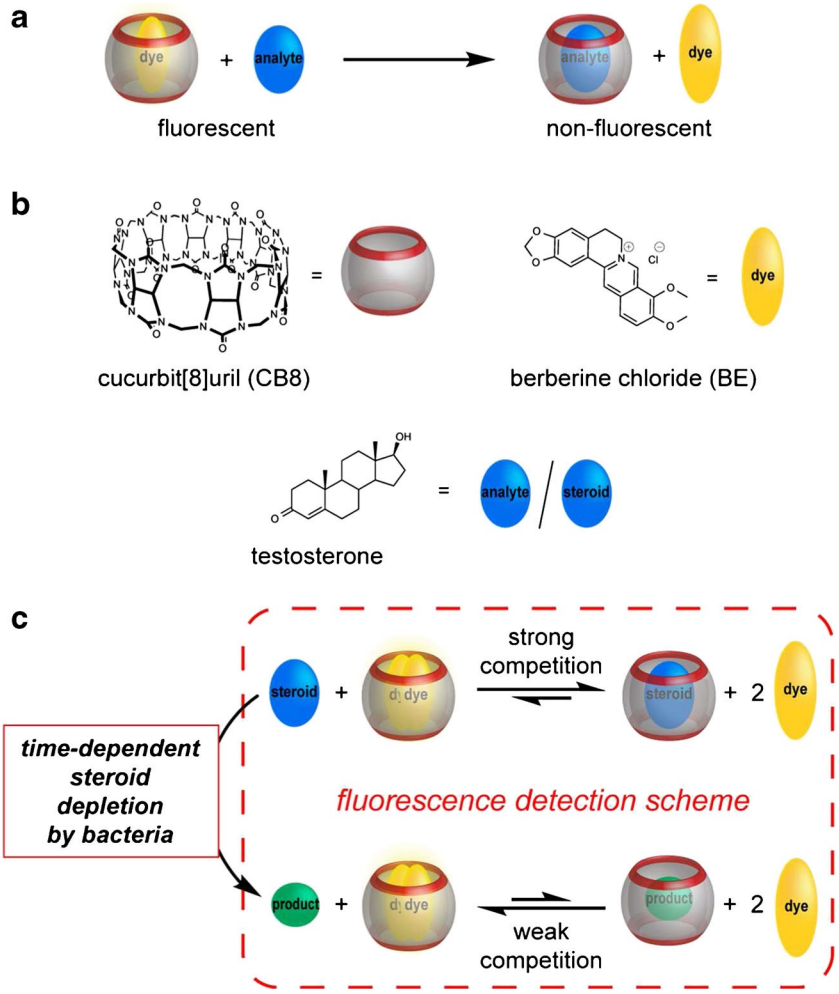

Figure 28: a) The principle of supramolecular indicator displacement assays. b) Structures of the receptor, the dye, and an analyte. c) Supramolecular tandem assays for monitoring the depletion of steroids in bacterial cultures.[97]

(Adapted from Ref.[97] with permission from Springer Nature.)

In the absence of the steroid, the cavity is free to bind the dye, leading to a strong increase of fluorescence. In the presence of the steroid, the remains in the solution. It was shown that cucurbit[8]uril is able to detect testosterone at concentrations above 0.7 µM with no heat or photodegradation. The excitation of the system was approximately 450 nm, and the maximum emission at about 525 nm.[97]

From the studies, it was obvious that CD8 combined with a fluorescent dye can be used to follow depletion of testosterone from the bacterial culture broth by degradation. The reliability of the chemosensor on screening applications was demonstrated to be excellent. The established screening system was proven to quickly identify steroid degradation under different conditions. The assay principle can be applied to the evolution of other environmentally harmful substances such as polyaromatic hydrocarbons or aid to produce enzymes and bacterial strains for sustainable biotransformation of hydrocarbons into high-quality raw chemicals.[97]

Deoxycholic acid (DCA) is supposed to be a promoter of carcinogenicity in the intestine. It can cause fragmentation of DNA, oxidative stress, Golgi fragmentation, and apoptosis. In contrast, the clinically used ursodeoxycholic acid (UDCA) is cytoprotective and anti-apoptotic and has immunomodulatory as well as anti-inflammatory properties. DCA and UDCA have opposite effects based on cell suspension and *in vivo* studies. For example, pre-treatment with UDCA can prevent apoptosis and Golgi fragmentation of colon cancer cells caused by DCA. The use of fluorescent analogs of DCA and UDCA may shed light on their interactions and distribution in cells. Màjer *et al.* have synthesized isomeric 3α- and 3β-(7-nitro-1,2,3-benzoxadiazole) analogs of DCA and UDCA **51-54** (Figure 29).[99-103]

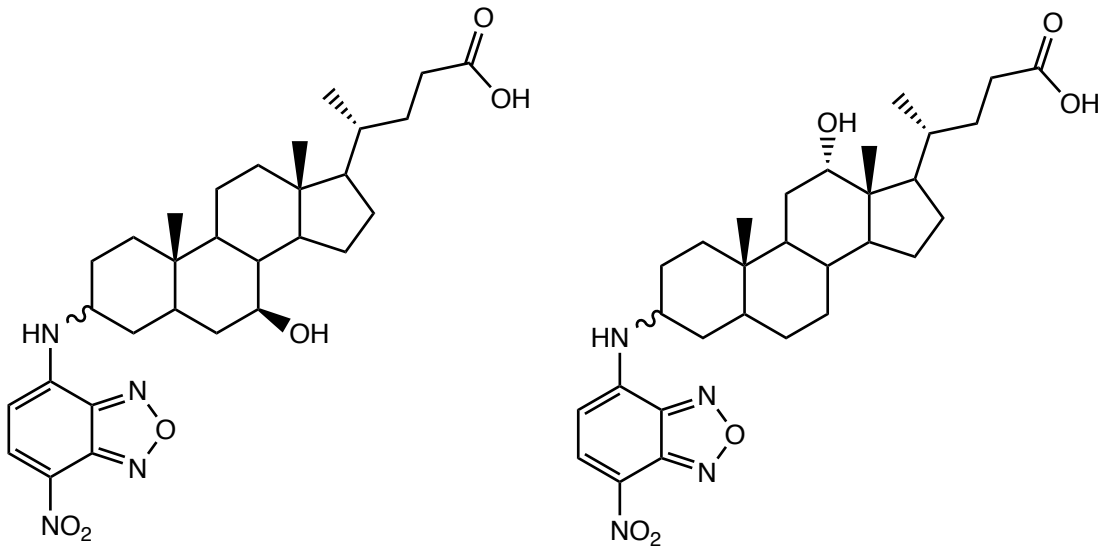

51 = 3α
52 = 3β

53 = 3α
54 = 3β

Figure 29: Fluorescent 7-nitro-1,2,3-benzoxadiazole (NB) analogs of UDCA and DCA **51-54**.[99]

Based on their studies, Màjer *et al.* found the fluorescent DCA and UDCA derivatives to be non-toxic on several cell lines. Their fluorescent properties were good. They absorbed at 465-470 nm and fluoresced at about 535 nm. The cell uptake of the compounds was diastereospecific. 3α-compounds **51** and **53** were taken in by active transport whereas 3β-compounds **52** and **54** were not. Compounds **51** and **53** may consequently find use in studying the functional aspect of DCA and UDCA in the intestinal biology.[99]

6 AIM OF THE EXPERIMENTAL WORK

Cholesterol **14** is lipid-soluble alcohol that serves as starting material for many physiologically important molecules.[104] It participates in constructing the cellular membranes of mammals and thus effects on signal transduction and cellular transport.[3] Intracellular cholesterol is in free form, whereby it is available to be used as a building block in the cell. Extracellular cholesterol is in esterified form which mammalian cells may obtain via a process called forward cholesterol transport. It has been shown that abnormalities in cholesterol metabolism have an impact on the development of certain neurodegenerative diseases and even cancer.[53] It is thus of utmost importance to work out the cholesterol composition as well as its transportation pathways in a cell. As mentioned before, fluorescence microscopy is the only method utilizable for studying living cells at the microscopic level. Since cholesterol itself is not fluorescent, new effective probes are needed. The cholesterol-binding fluorescent molecules currently in use are detrimental to living cells, and in addition, they generally do not recognize cholesteryl esters making identification between intracellular and extracellular cholesterol impossible.[4]

Cyclodextrin-based molecules have been found to bind cholesterol efficiently. Based on this observation, it can be assumed that steroid derivatives with amphiphilic properties behave in the same way. In addition, fluorescent labels can be attached to the functional groups of the bile acids enabling the detection and quantification of the formed cholesterol-probe complexes by fluorescence microscopy.[105] In this work, the aim was to attach fluorophoric derivatives with bile acids **20** (cholic acid), **46** (deoxycholic acid), and **47** (lithocholic acid) by esterification either on the 3-OH or on the 24-COOH functionality. The structures of the bile acids are presented in Figure 30.

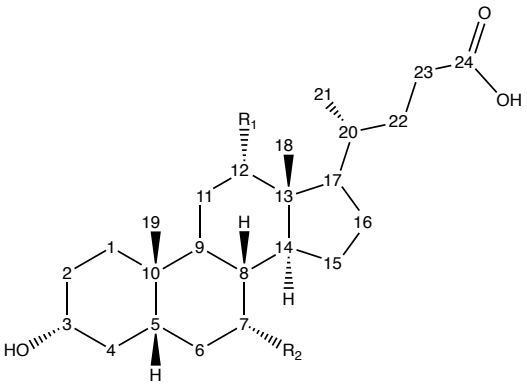

LCA (**47**) R_1 = H, R_2 = H
DCA (**46**) R_1 = OH, R_2 = H
CA (**20**) R_1 = OH, R_2 = OH

Figure 30: General structures of the bile acids **20**, **46**, and **47**.

7. SYNTHESIS OF THE FLUORESCENT BILE ACID-DERIVATIVES

7.1 HEAD-TO-HEAD DIMERS

The ultimate aim of the first sub-part of the project was to prepare cyclic bile acid derivatives with fluorophoric spacers on both the tail and the head. In order to accomplish the objective, two bile acid moieties were first combined via a fluorophoric spacer in order to get a tweezer-like system with two bile acid molecules lining the cavity suitable for accommodating cholesterol. The suitably functionalized fluorophore was conjugated to the 3-position of the bile acid, using a reaction between the activated fluorophore and the methyl ester of the bile acid. The methyl esters of the bile acids were prepared by sulphuric acid-catalyzed esterification reaction in excess of methanol (Scheme 1).[106] The structure of the methyl esters was assigned by measuring ^{1}H and ^{13}C NMR spectra and the yields were practically quantitative. ^{1}H NMR spectra suggested that esterification of lithocholic acid **47**, deoxycholic acid **46**, and cholic acid **20** had occurred because the spectra showed a peak at ~3.6 ppm with integral value 3 (Appendix 1-3). It corresponds to the signal of the esterified methyl group. ^{13}C NMR spectra showed that the carbonyl shift of **55** had moved upfield from δ = 179.27 ppm to δ = 174.74 ppm upon esterification (Appendix 1). Similarly, esterification of **56** could be deduced on the carbonyl shift which moved upfield to δ = 174.65 ppm (Appendix 2).

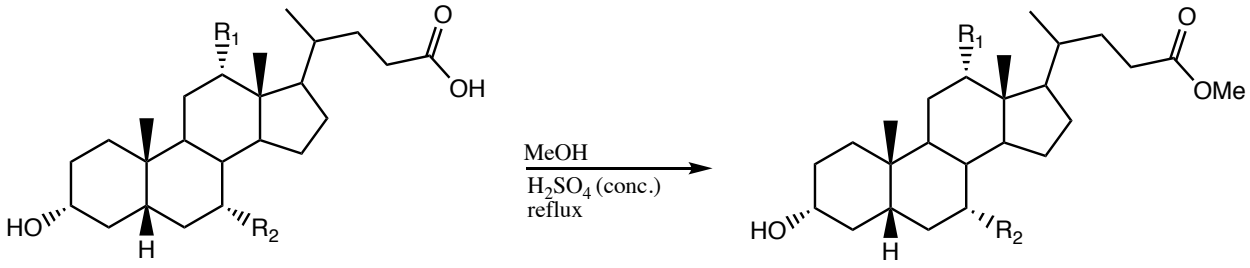

LCA (**47**) R_1 = H, R_2 = H
DCA (**46**) R_1 = OH, R_2 = H
CA (**20**) R_1 = OH, R_2 = OH

55 R_1 = H, R_2 = H
56 R_1 = OH, R_2 = H
57 R_1 = OH, R_2 = OH

Scheme 1: Synthesis of methyl ester of the bile acids.[106]

Dimers **59-61** were prepared by a modified Yamaguchi macrolactonization reaction, where 2,6-naphthalenedicarboxylic acid was first activated by 3,5-dichlorobenzoyl chloride (DCBC). The formed mixed anhydride should then react in the presence of 4-dimethylaminopyridine (DMAP) with the alcohol group of the bile acid in the molar ratio of 1:2 (naphthalenedicarboxylic acid : bile acid) to form the desired ester.[106-108] Since DCBC was not available in the laboratory, benzoyl chloride (BzCl) was used in the reaction (Scheme 2).

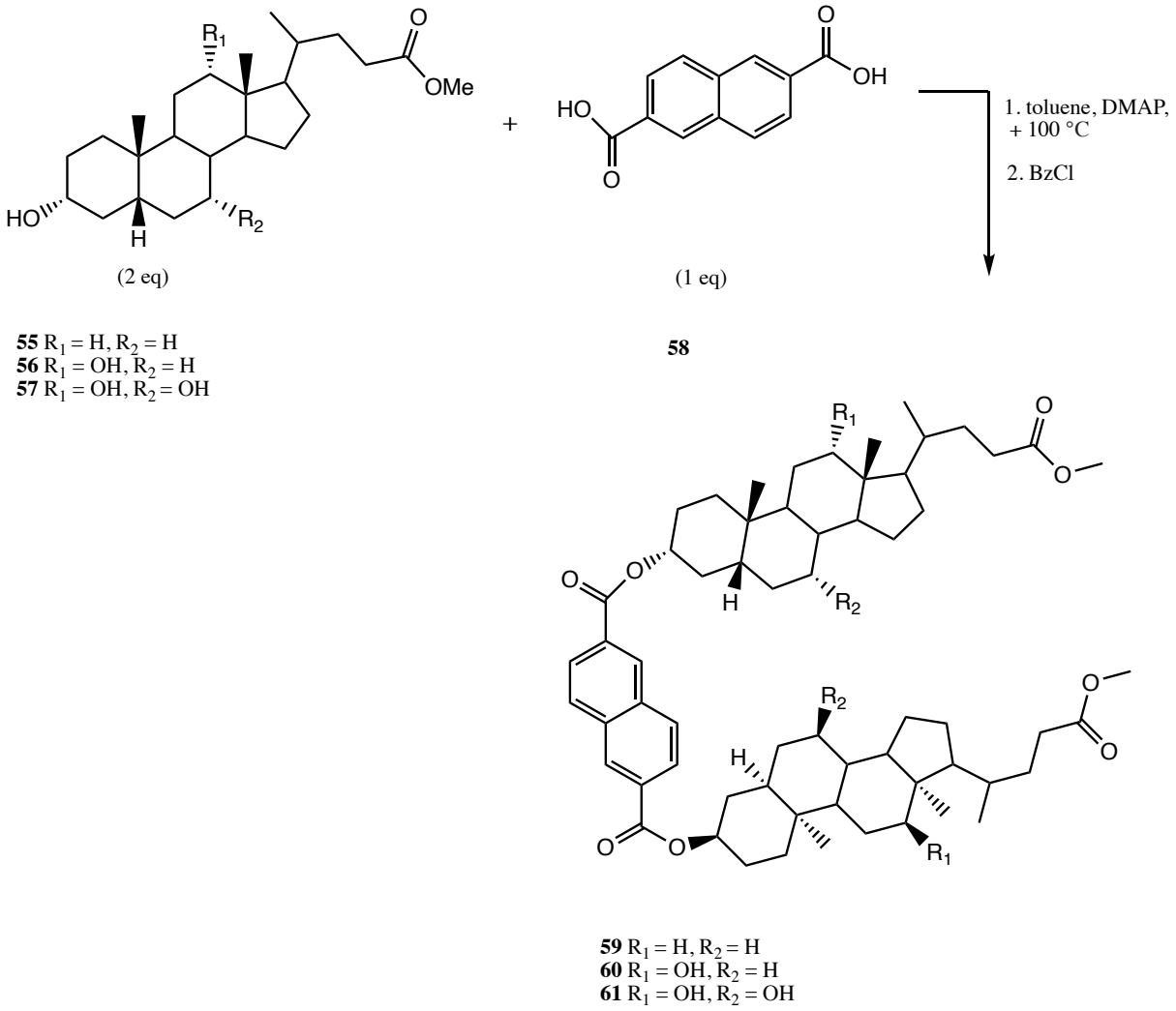

Scheme 2: General procedure for the synthesis of 2,6-naphthalenedicarboxylate of methyl lithocholate **59**, methyl deoxycholate **60** and methyl cholate **61**, using modified Yamaguchi esterification.[106-108]

The structures of the synthesized molecules were determined by ^{1}H and ^{13}C NMR combined with mass spectrometry. ^{1}H NMR spectra confirmed that esterification of the 3β-position of the bile acid methyl esters had occurred. This was obvious from the downfield shift of the 3β-protons; in the case of the methyl lithocholate derivative from 3.60 ppm to 4.97 ppm (Appendix 4), in the case of the deoxycholic acid derivative from 3.57 ppm to 4.96 ppm (Appendix 5), and in the case of the methyl cholate derivative from 3.60 ppm to 4.81 ppm (Appendix 6), respectively. In the ^{13}C NMR spectra of the synthesis products, esterification on position C-3 was obvious from the downfield shift of C-3 carbons; in the case of the methyl lithocholate derivative from 71.85 ppm to 75.02 ppm, in the case of the methyl deoxycholate derivative from 71.76 ppm to 74.84 ppm, and in the case of the methyl cholate derivative from ~71.00 ppm to 74.92 ppm. However, the four signals in the aromatic area (128.25 ppm, 129.54 ppm,

131.01 ppm, and 132.66 ppm) indicated the presence of only a single aromatic ring instead of the naphthyl ring. The measured mass spectra revealed ions at the *m/z* values of *m/z* = 518.06 for **59**, *m/z* = 543.03 for **60** and *m/z* 550.05 for **61** (Appendices 7-9). It was obvious that instead of the target products **59-61**, the reaction had yielded 3β-phenyl esters of methyl lithocholate **62**, methyl deoxycholate **63**, and methyl cholate **64** (Figure 31), respectively.

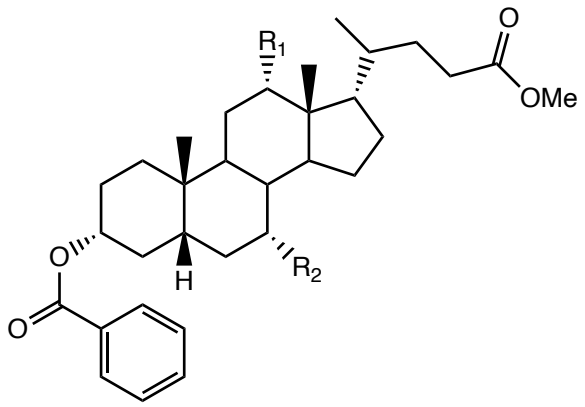

62 R_1 = H, R_2 = H
63 R_1 = OH, R_2 = H
64 R_1 = OH, R_2 = OH

Figure 31: The 3β-phenyl esters of the methyl lithocholate, methyl deoxycholate, and methyl cholate (**62-64**).

Since the first route did not yield the desired products, an alternative reaction route was tried. In this approach, 2,6-naphthalenedicarboxylic acid was first converted to its dianhydride by using ethyl chloroformate in the presence of Et_3N. The activated derivative of the dicarboxylic acid was then allowed to react with the bile acid methyl esters to form the desired products (Scheme 3).[109-111]

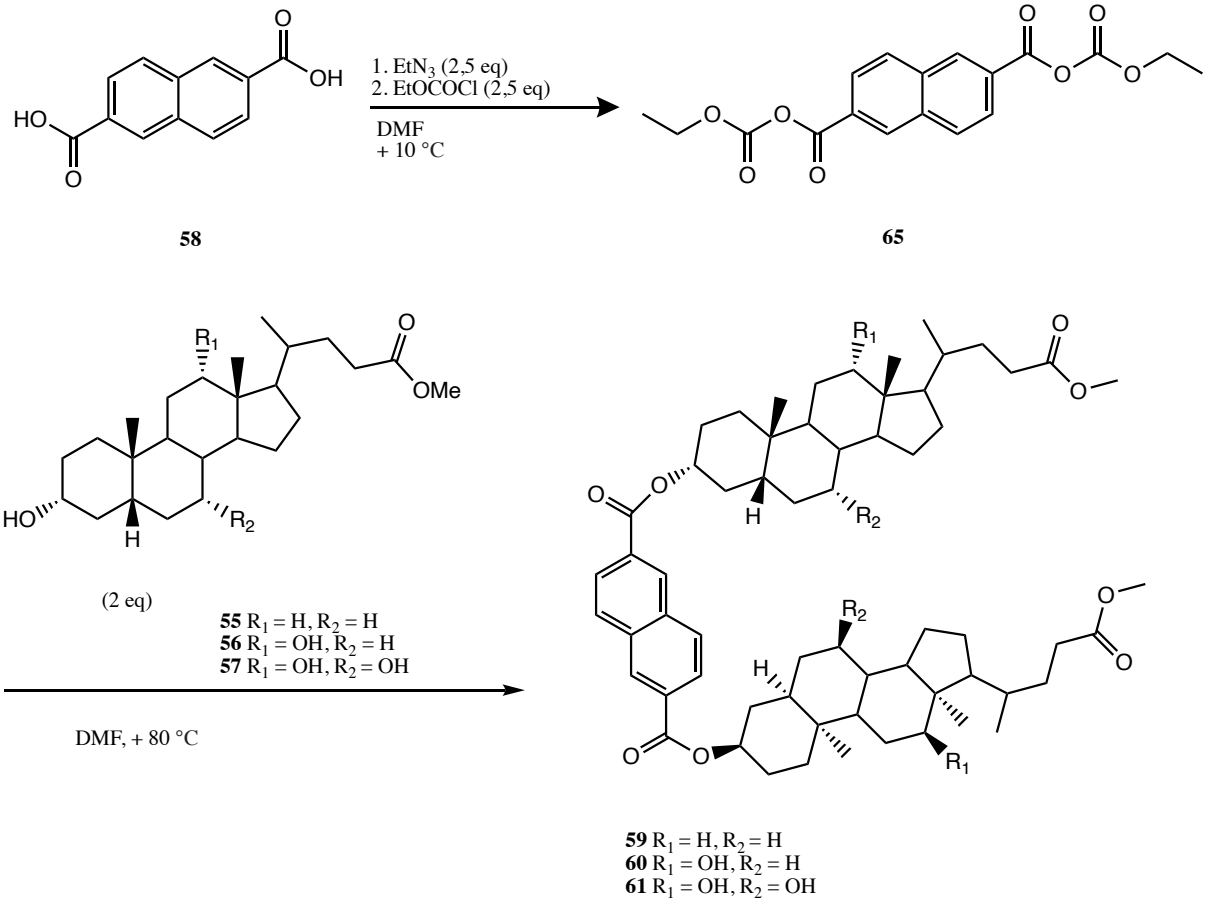

Scheme 3: General procedure for the synthesis of 2,6-naphthalenedicarboxylates of methyl lithocholate, methyl deoxycholate, and methyl cholate (**59**-**61**) using anhydride activation.[109-111]

^{1}H NMR spectra suggested that esterification of the methyl lithocholate **55** had occurred because the 3β-proton had shifted from 3.60 ppm to 4.85 ppm. Similarly, esterifications of methyl deoxycholate **56** and methyl cholate **57** could be deduced on the shift of the 3β-protons; in the case of the methyl deoxycholate derivative from 3.57 ppm to 4.43 ppm and in the case of methyl cholate derivative from 3.60 ppm to 4.65 ppm. The crude products were tried to be purified by column chromatography. In each case, the purification resulted in a mixture of the product and impurities. In the case of **60**, the crude product was recrystallized from acetonitrile, but no crystals were obtained. In the future, another chromatographic method, like high performance countercurrent chromatography (HPCCC), should be tried.

The low yield of the previous reactions led us to proceed to a Cs salt methodology reported by Pandey *et al*.[112] In this particular method, the bile acid methyl esters were first converted to their 3α-bromoacetyl derivatives **67** and **68** (Scheme 4). ^{1}H NMR spectra confirmed that esterification of the 3α-position of the bile acid methyl esters had occurred. This was obvious from the downfield shift of the 3β-protons; in the case of the methyl lithocholate derivative from 3.60 ppm to 4.78 ppm (Appendix 10) and the case of the deoxycholic acid derivative from 3.57 ppm to 4.78 ppm (Appendix 11).

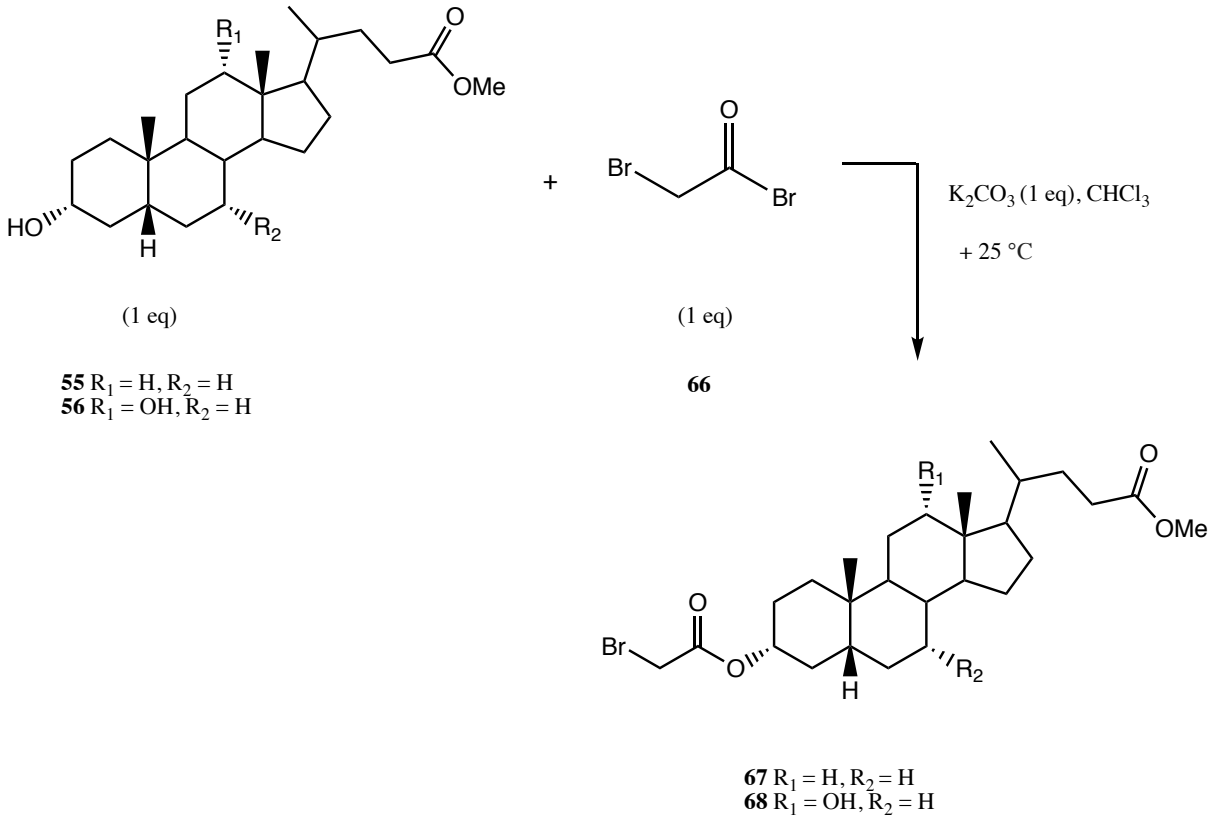

Scheme 4: The synthesis of the 3α-bromoacetyl derivatives of methyl lithocholate **67** and methyl deoxycholate **68**.[112]

At the same time, the fluorophore was converted to is dicaesium derivate (Scheme 5).[112] The structure of **70** was assigned by ^{13}C NMR spectrum (Appendix 12), which suggested that the reaction had occurred because the carbonyl shift of **58** had moved upfield from ~179.00 ppm to 175.50 ppm.

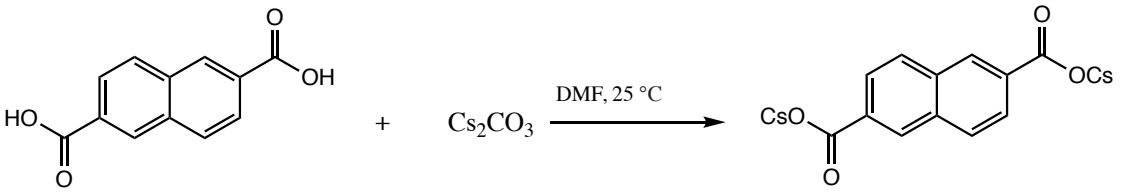

(1 eq) (1 eq)

58 **69** **70**

Scheme 5: The synthesis of dicaesium naphthalene-2,6-dicarboxylate **70**.[112]

Finally, 3α-bromoacetyl derivatives **67** and **68** were allowed to react with the Cs salt of the naphthalene dicarboxylic acid **70** in DMF at room temperature (Scheme 6).

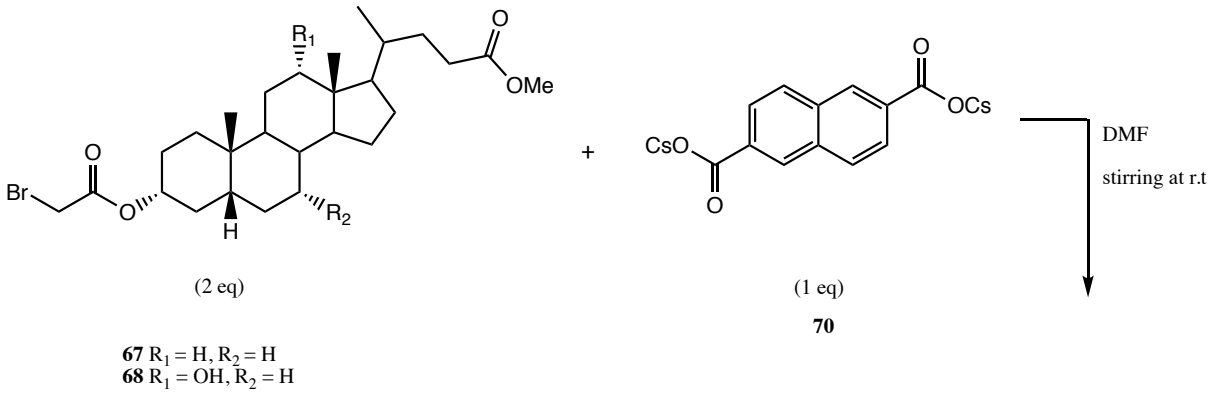

(2 eq) (1 eq)

70

67 R_1 = H, R_2 = H
68 R_1 = OH, R_2 = H

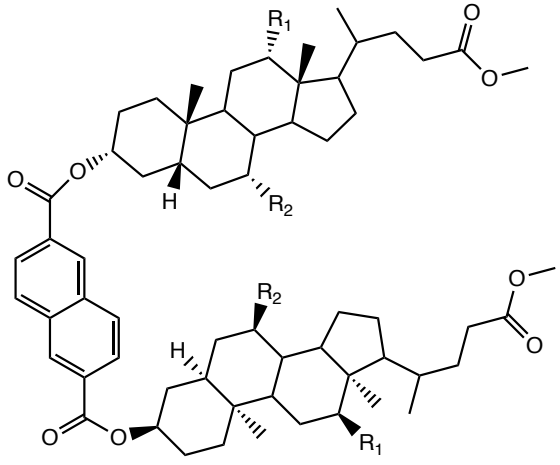

59 R_1 = H, R_2 = H
60 R_1 = OH, R_2 = H

Scheme 6: General procedure for the synthesis of 2,6-naphtalenedicarboxylate of methyl lithocholate **59** and 2,6-naphthalenedicarboxylate of methyl deoxycholate **60** by the Cs salt methodology.[112]

In the case of the lithocholic acid derivative **67**, ^{13}C NMR suggested that the reaction had occurred because the carbonyl shift of **70** had moved upfield from 175.50 ppm to 166.63 ppm. The crude product was tried to be purified by column chromatography, but it resulted in a mixture of the product and impurities. In the future, alternative chromatographic methods, like HPCCC, could be tried. For the deoxycholic acid derivative **68**, the reaction did not work, because in ^{13}C NMR spectrum the carbonyl shift of **70** from 175.49 ppm, was not observed.

The most promising method for synthesizing bile acid-fluorophore 2:1 head-to-head dimers seems to be using the conversion the fluorophore of diacid to the corresponding anhydride by ethyl chloroformate in the presence of triethylamine and then allowing the activated dicarboxylic acid derivative to react with the methyl esters of the bile acids in a ratio of 1:2. The method was the simplest to implement and the reaction worked for all of the bile acids, which were tested. The most challenging part of the syntheses was the purification, to which particular attention should be paid in the future. It was difficult to find a suitable eluent combination, which separates the components effectively. Alternative chromatographic method, like high performance countercurrent chromatography (HPCCC), could be tried.

7.2 TAIL-TO-TAIL DIMERS

In the second approach aiming at cholaphanes, the suitably functionalized fluorophore was intended to be conjugated to the carboxylic functionality of the bile acid. To yield this, the carboxylic functionality at position 24 of the bile acid was activated and then allowed to react with 2,7-naphthalenediol in a molar ratio of 2:1.

First, the 3α-hydroxyl group of the bile acid needed to be protected with trifluoroacetyl group, after which the carboxylic group was converted to the corresponding acid chloride with thionyl chloride. The reaction scheme for lithocholic acid is presented in Scheme 7. The structure of **72** was assigned by ^{1}H NMR spectrum (Appendix 13), which suggested that esterification of the litocholic acid had occurred, because the 3β-proton had shifted from 3.60 ppm to 4.93 ppm. The formation of the acid chloride **74** was checked by ^{13}C NMR (Appendix 14), where the carbonyl shift of the carbon C-24 had moved upfield from ~179.00 ppm to 174.18 ppm.

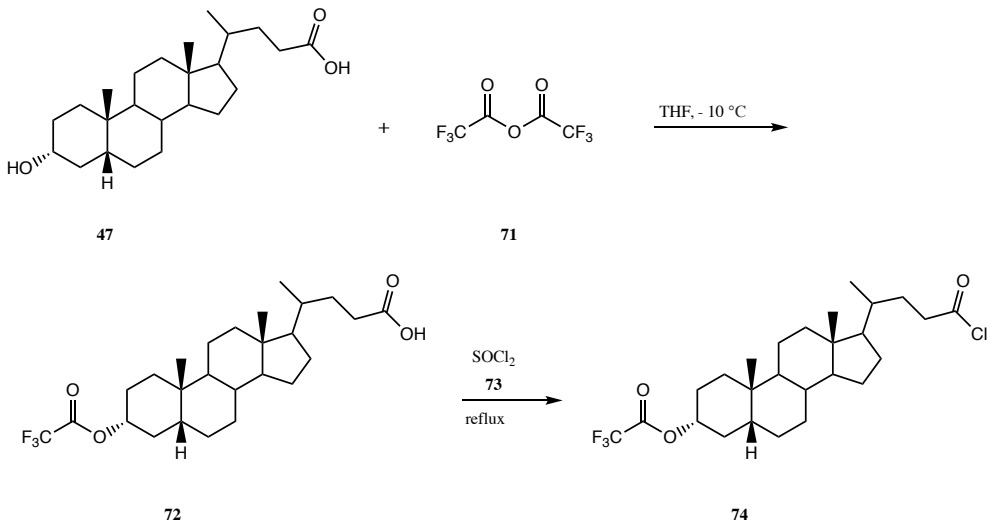

Scheme 7: Synthetic route to lithocholic acid derivatives **72** and **74**.[107]

The dimer, 2,7-dihydroxynaphthyl-bis(3α-trifluoroacetoxy-5β-cholan-24-oate) **76**, was first tried to be prepared by allowing 3α-trifluoroacetoxy-5β-cholan-24-oyl chloride and 2,7-dihydroxynaphthalene to react in a molar ratio of 2:1 with pyridine acting as a the HCl scavenger (Scheme 8).[107,113]

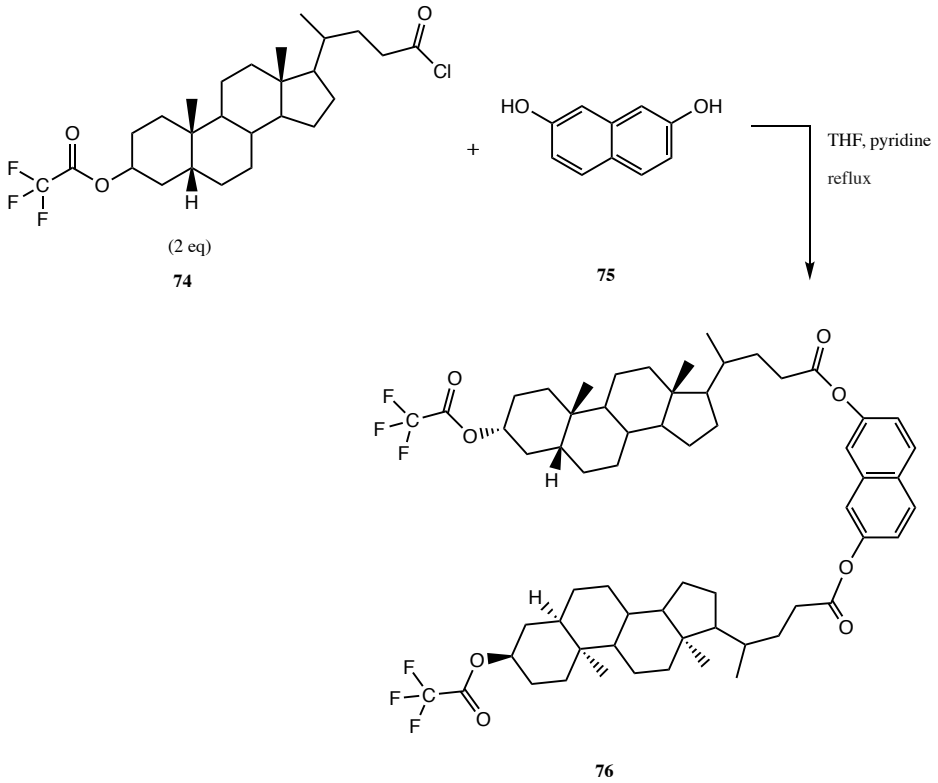

Scheme 8: The synthesis of 2,7-dihydroxynaphtyl-bis(3α-trifluoroacetoxy-5β-cholan-24-oate) **76**.[107,113]

Based on the ^{13}C NMR spectrum measured from the reaction mixture, the reaction had occurred. This was obvious since the carbonyl shift had moved from δ = 175.18 ppm to δ = 174.81 ppm upon esterification. Nor column chromatography neither size exclusion chromatography resulted in the pure product.

Next, compound **76** was attempted to be synthesized by allowing 3α-trifluoroacetoxy-5β-cholan-24-oyl chloride and 2,7-dihydroxynaphthalene to react without the presence of pyridine. HCl was absorbed by a water trap and the solvent changed from THF to DMF which is more polar solvent. Based on ^{13}C NMR spectrum the reaction had again occurred, because the carbonyl shift had moved upfield from δ = 175.18 ppm to δ = 174.81 ppm, upon esterification. Nor column chromatography neither size exclusion chromatography resulted in the pure product. The attempts to purify **76** remained resultless.

Because the acid chloride approach did not result in the desired product as pure form, Fischer esterification was tested for preparing 2,7-dihydroxynaphthyl-bis(3α-hydroxy-5β-cholan-24-oate) **77**.[107] This procedure lacks the need to remove the protecting groups of the hydroxyl groups. This was thought to be beneficial for the future reactions, such as closing of the ring. Unfortunately, the approach was unsuccessful. Based on ^{1}H and ^{13}C NMR spectra the product was not formed.

In the future, the easiest method to synthesize the tail-to-tail dimers, would be to use the anhydride method. Purification method of the possible products should discuss more because purification by column chromatography was mostly unsuccessful.

Next tail-to-tail dimers were aimed at by using a peptide coupling between the bile acid hydrazine and activated carboxylic acid groups of the fluorophore, which in this case was different from the previous attempts. At first, three different methods were tested to optimize the synthesis route.

To obtain *N,N′*-di(*p*-tolyl)-3,3′-dibenzoylpyrrolopyrrolyl bis(3α,7α,12α-trihydroxy-5β-cholan-24-yl-hydrazine) **83**, the dicarboxylic acid **78** was first activated by *N*-(3-dimethylaminopropyl)-*N*′-ethylcarbodiimide hydrochloride (EDC). EDC acted as base that removes the protons from the carboxylic acid groups. The formed dicarboxylate then esterifies with EDC while ethyl (hydroxyimino)cyanoacetate (OXYMA) binds to the carbonyl carbon of the formed ester by nucleophilic substitution. Finally, 3α,7α,12α-trihydroxy-5β-cholan-24-oic

hydrazine **82** attacks by nucleophilic substitution to the carbonyl group and OXYMA as a good leaving group is eliminated yielding the target compound **83** (Scheme 9).[114-116]

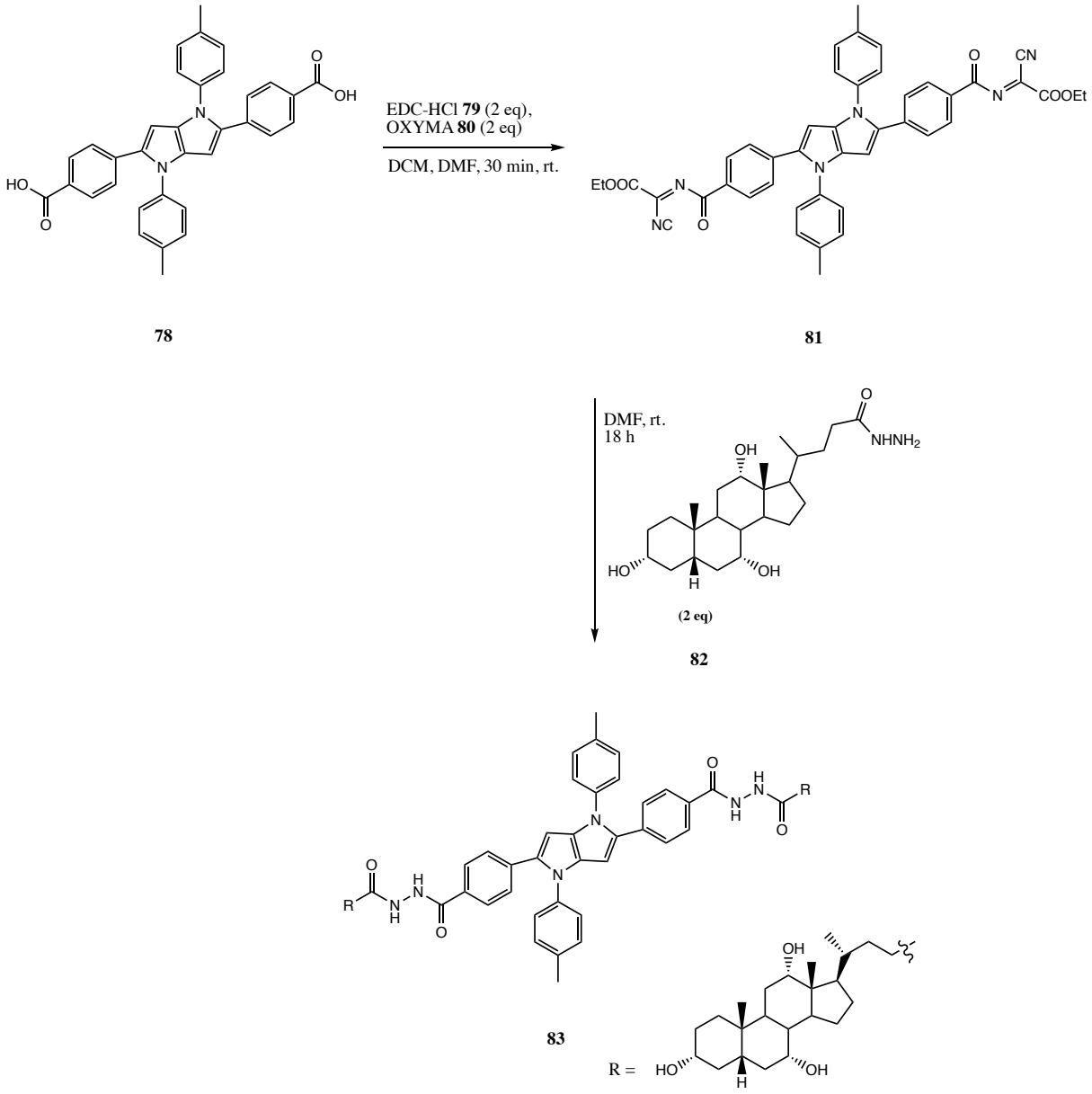

Scheme 9: The synthesis of *N,N′*-di(*p*-tolyl)-3,3′-dibenzoylpyrrolopyrrolyl bis(3α,7α,12α-trihydroxy-5β-cholan-24-yl-hydrazine) **83** with OXYMA as the coupling reagent.[114-116]

In addition to the EDC-OXYMA route an alternative strategy aiming at **83** was tested. In this approach *N,N*-diisopropylethylamine (DIPEA) acted as the base and *N,N,N′,N′*-tetramethyl-*O*-(1*H*-benzotriazol-1-yl)uronium hexafluorophosphate (HBTU) as the activating agent (Scheme 10).[114,117]

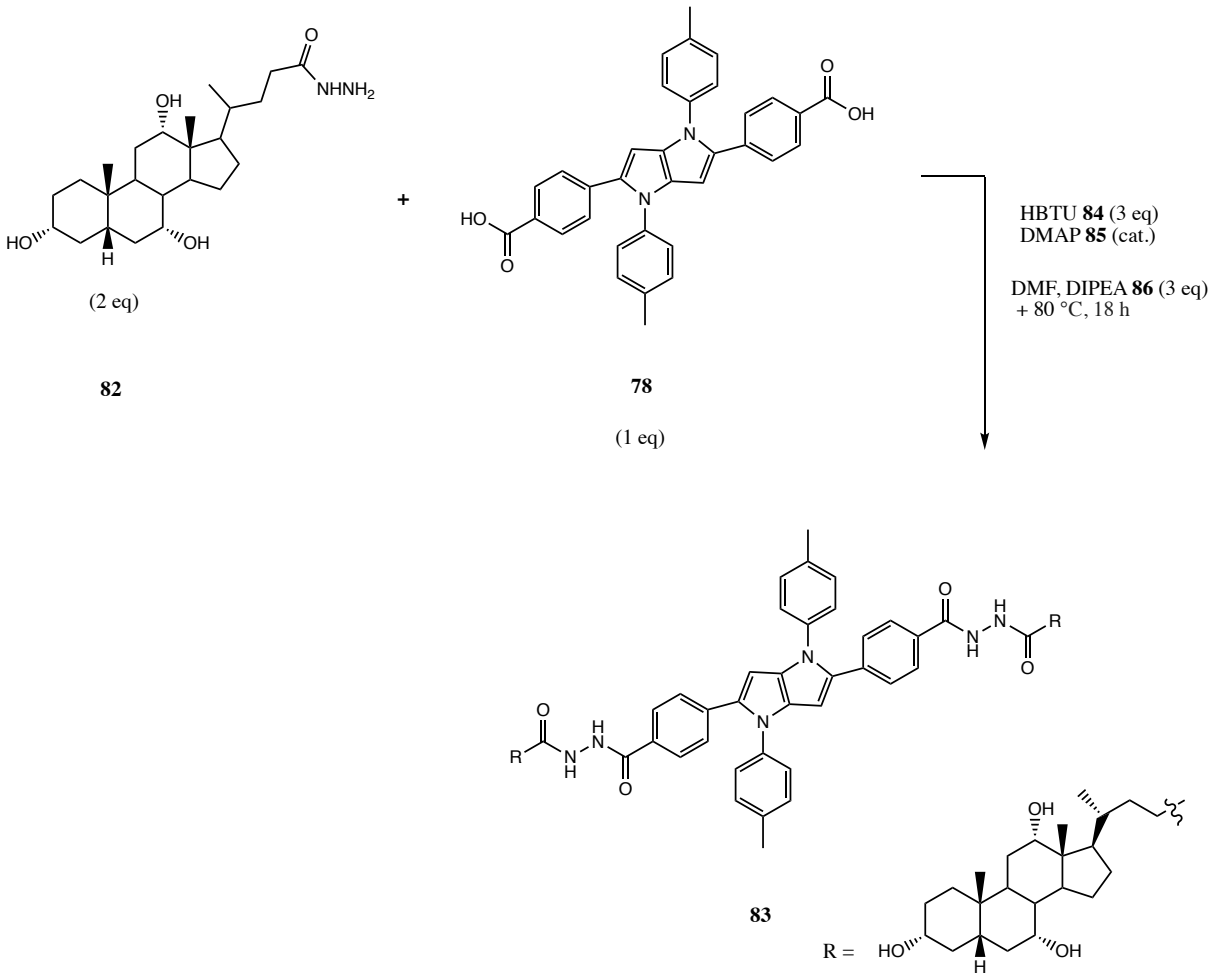

Scheme 10: The synthesis of *N,N′*-di(*p*-tolyl)-3,3′-dibenzoylpyrrolopyrrolyl bis(3α,7α,12α-trihydroxy-5β-cholan-24-yl-hydrazine) **83** with HBTU as the coupling reagent.[114,117]

In the third approach, 1-[bis(dimethylamino)methylene]-1*H*-1,2,3-triazolo[4,5-*b*] pyridinium 3-oxide hexafluorophosphate (HATU) was used to activate the diacid in the presence of DIPEA (Scheme 11).[114,117]

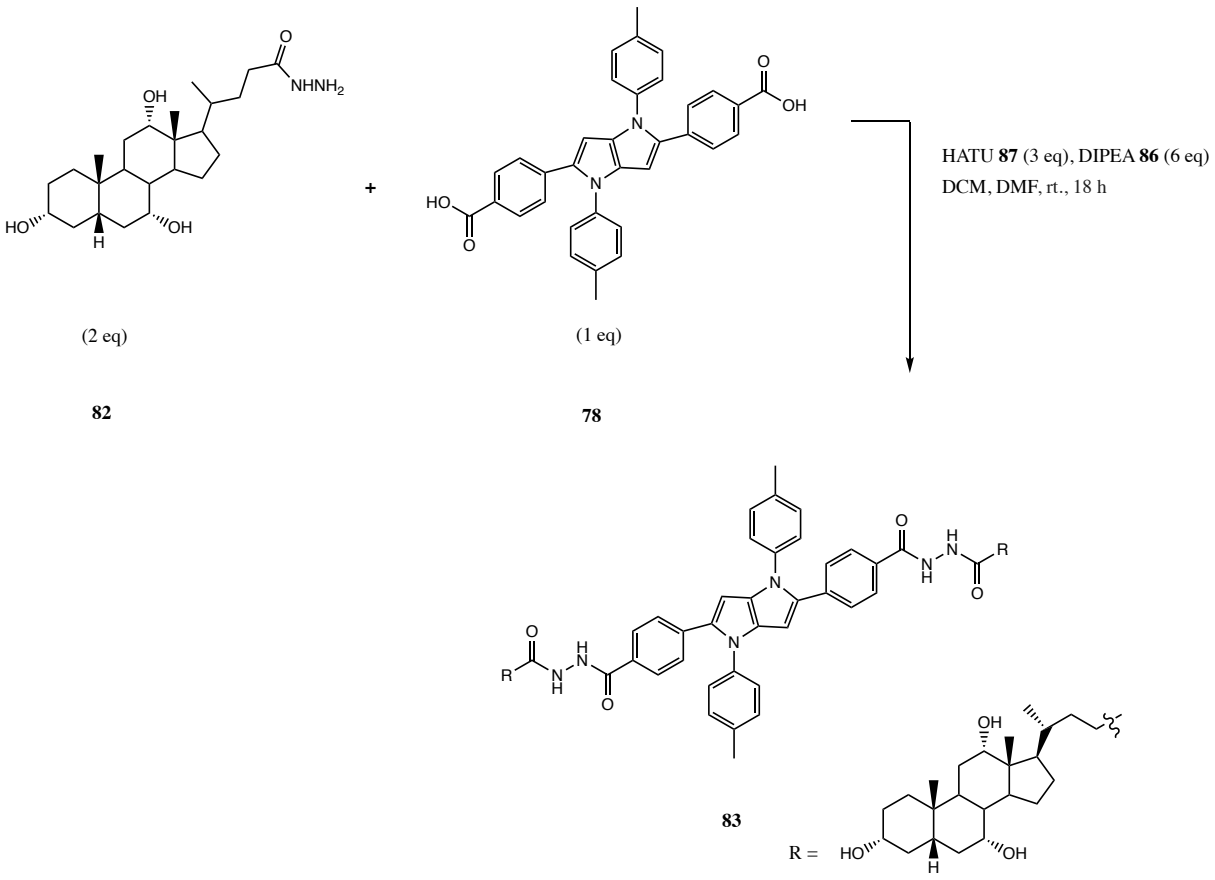

Scheme 11: The synthesis of *N,N′*-di(*p*-tolyl)-3,3′-dibenzoylpyrrolopyrrolyl bis(3α,7α,12α-trihydroxy-5β-cholan-24-yl-hydrazine) **83** HATU as the coupling reagent.[114,117]

The reactions were followed by TLC. The formation of the desired product **83** was evident from the appearance of an amide proton at the chemical shift value of 6.57 ppm in the ^{1}H NMR spectra. The crude product was tried to be purified by column chromatography but the purification resulted in a mixture of product and impurities in all cases.

For further reactions between bile acid hydrazines and fluorophores the route where OXYMA acts as a coupling reagent was chosen. It was the simplest of the three routes and could additionally be carried out at room temperature.

The synthetic route to derivatives of lithocholic and deoxycholic acid with *N,N´*-di(*p*-tolyl)pyrrolopyrrole-3,3´-dibenzoic acid (**90** and **91**) is represented in Scheme 12.[114-116]

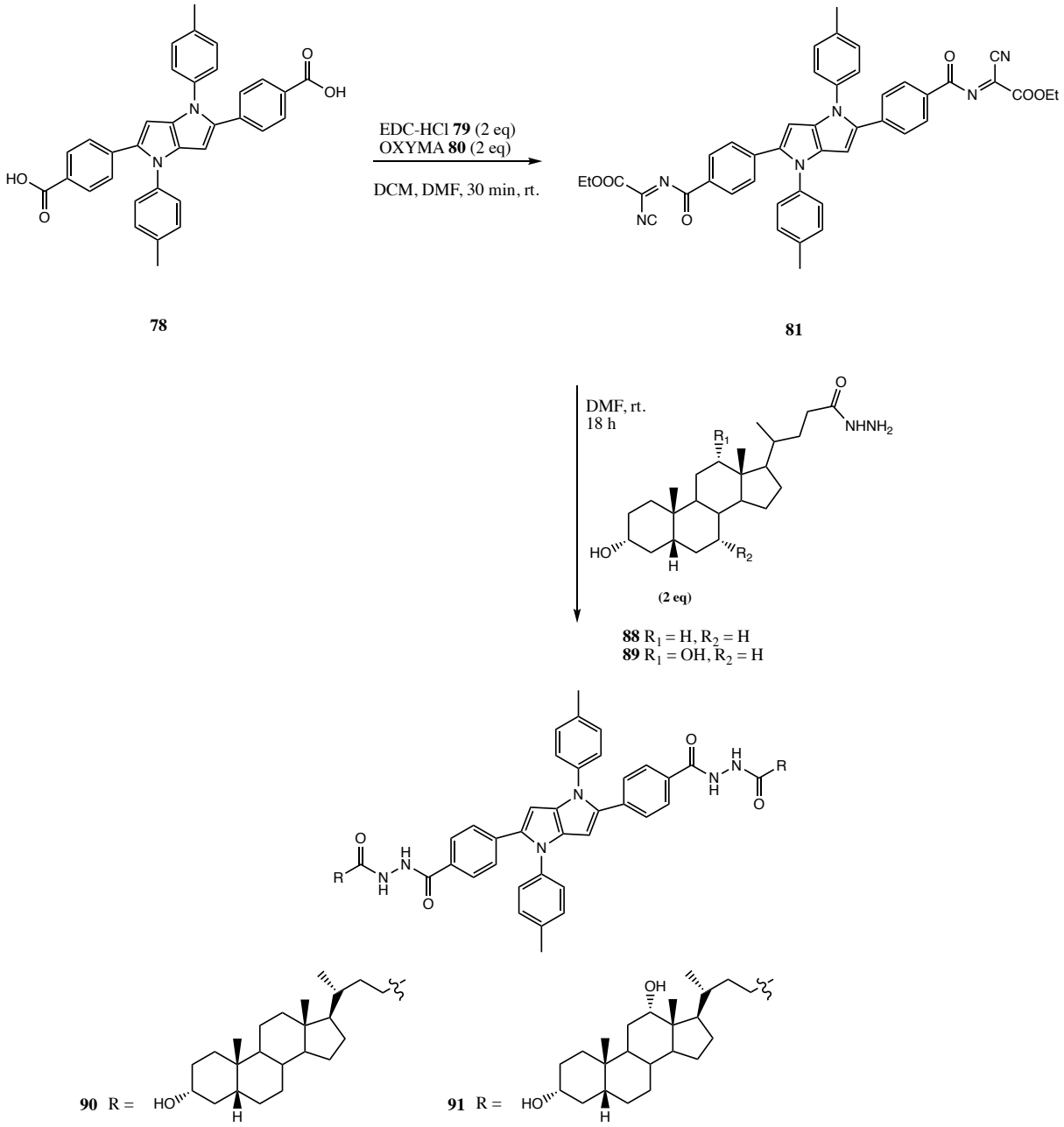

Scheme 12: General procedure to the lithocholyl and deoxycholyl derivatives of *N,N`*-di(*p*-tolyl)pyrrolopyrrole-3,3´-dibenzoates **90** and **91**.[114-116]

The reactions were followed by TLC and the formation of the desired products, **90** and **91**, was deduced from the appearance of amide protons at the chemical shift values of 6.57 ppm and 6.57 ppm, respectively, on the ^{1}H NMR spectra. Due to limited temporal resources, the crude products **90** and **91** were not purified.

The lithocholyl, deoxycholyl, and cholyl derivatives of 8-(1,2,3-trimethoxybenzene)-BODIPY-3,5-bis(*p*-ethenyl phenoxypentanoic acid) **94-96** were synthesized by using the EDC-OXYMA coupling (Scheme 13).[114-116]

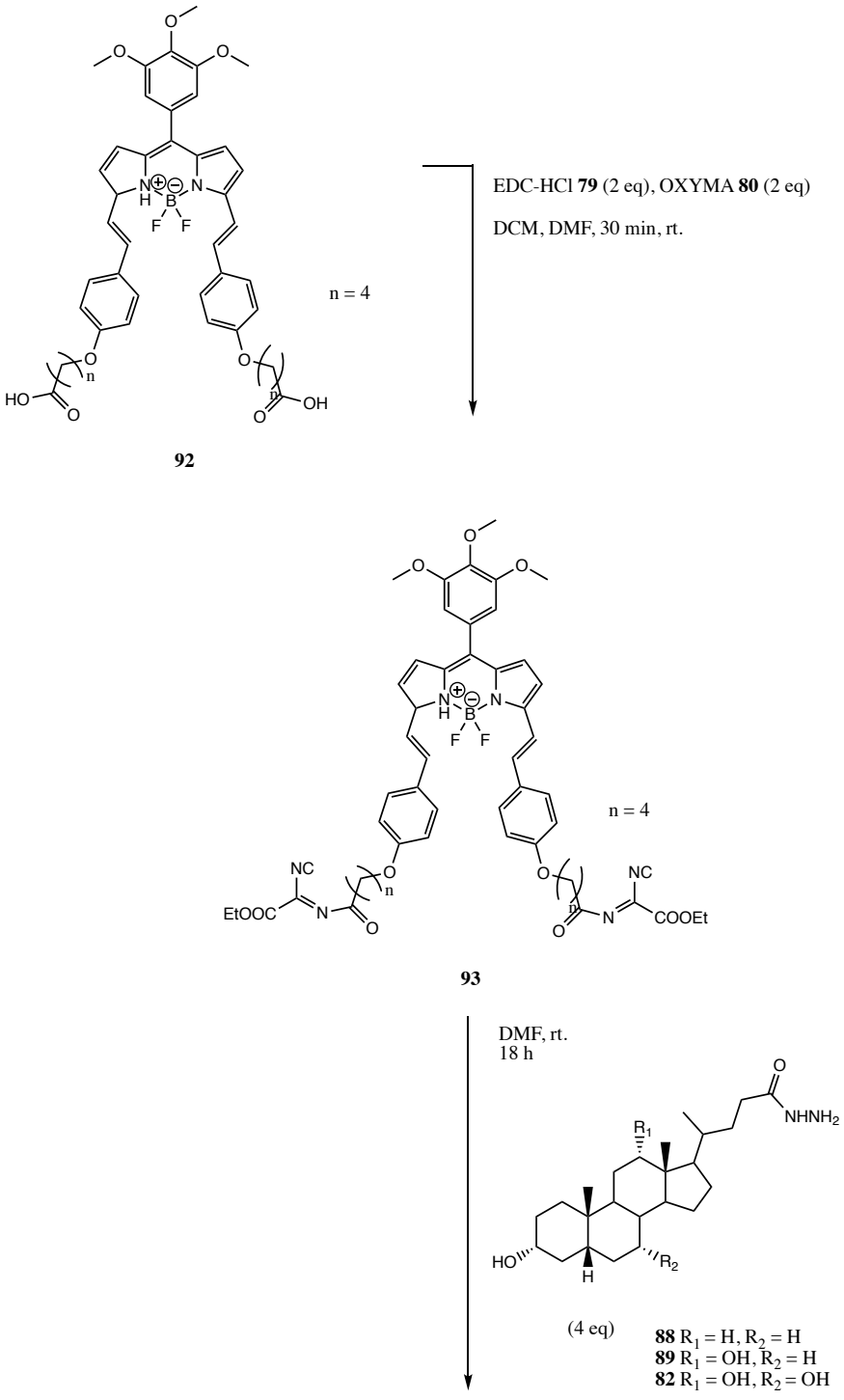

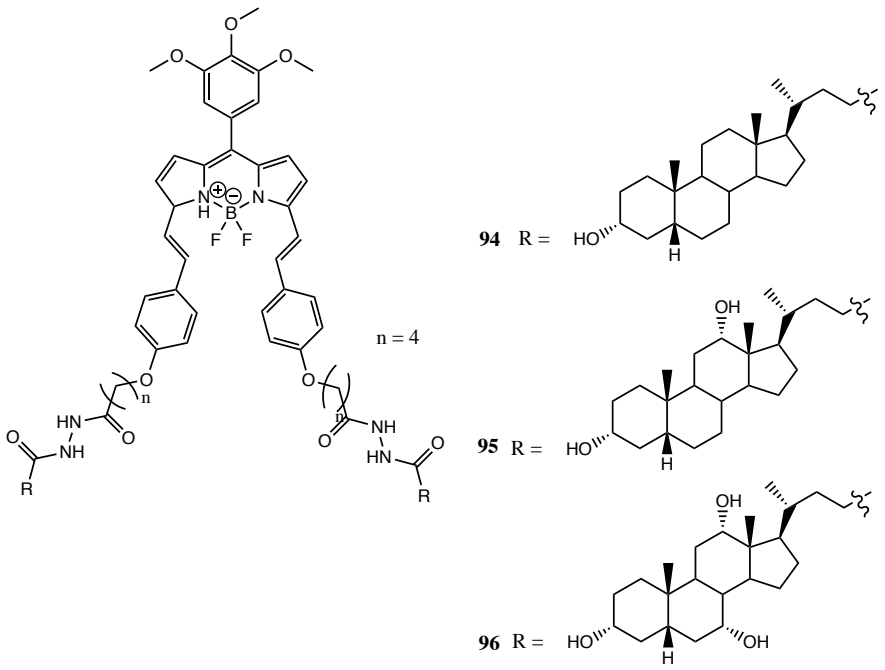

Scheme 13: General procedure to the lithocholyl, deoxycholyl, and cholyl derivatives of 8-(1,2,3-trimethoxybenzene)-BODIPY-3,5-bis(*p*-ethenyl phenoxypentanoic acid) **94**-**96**.[114-116]

The reactions were followed by TLC. The formation of **94** was evident from the appearance of the amide proton at the chemical shift value of 6.53 ppm in the ^{1}H NMR spectrum. The purification of compound **94** by using column chromatography was unsuccessful, resulting in a mixture of the desired product with impurities. In the case of **96**, the amide proton resonated at the chemical shift value of approximately 6 ppm. Additionally, in the ^{1}H NMR spectrum resonant signal of the unreacted hydrazine group appeared at ~5 ppm as well. Due to limited temporal resource, the crude product **96** was not purified. The synthesis of **95** resulted in traces of the crude product, which is why no characterizations could be made.

The lithocholyl, deoxycholyl, and cholyl derivatives of di(3,3′-dimethyl-3*H*-benzoindole-2,2′-(1,3,5-pentatrienyl)-*N,N′*-dipentanoic acid **99-101** were prepared by using the EDC-OXYMA coupling (Scheme 14).[114-116]

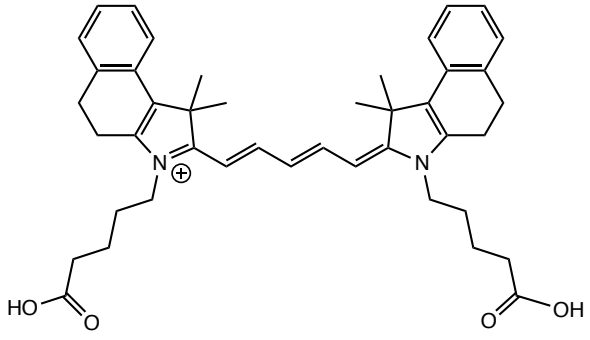

97

EDC-HCl **79** (2 eq), OXYMA **80** (2 eq)
DCM, DMF, 30 min, rt.

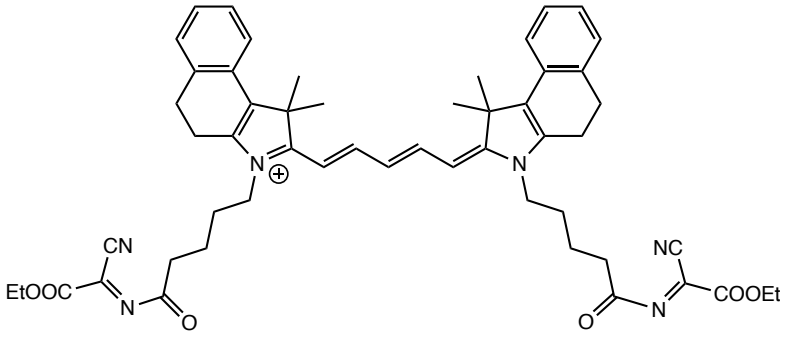

98

DMF, rt.
18 h

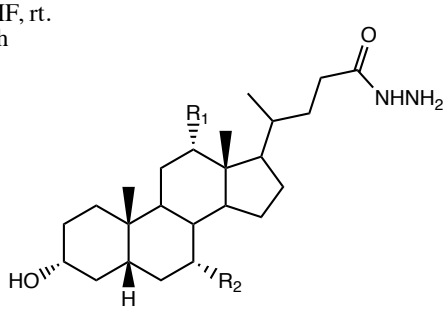

(4 eq)

88 R_1 = H, R_2 = H
89 R_1 = OH, R_2 = H
82 R_1 = OH, R_2 = OH

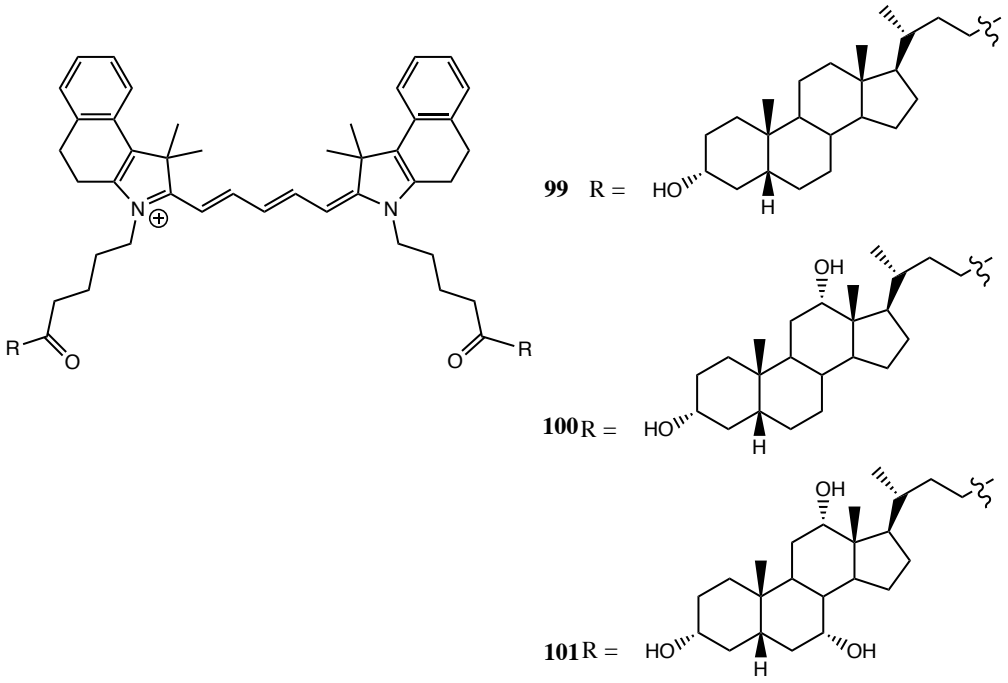

Scheme 14: General procedure to synthesis of the lithocholyl, deoxycholyl, and cholyl derivatives of di(3,3′-dimethyl-3*H*-benzoindole-2,2′-(1,3,5-pentatrienyl)-*N,N′*-dipentanoic acid **99-101**.[114-116]

The reactions were followed by TLC. The formation of **99** was obvious from the appearance of the amide proton at the chemical shift value of 6.53 ppm in the ^{1}H NMR spectrum. Some of the lithocholyl hydrazine had not reacted, which was evident from the resonant signal of the hydrazine protons at 5.75 ppm. Due to limited temporal resources, the crude products were not purified. The product could have been purified for example by using column chromatography. In the ^{1}H NMR spectra measured from the crude products from syntheses aiming at **100** and **101**, no amide signals were observed. It was thus deduced that these reactions had not proceeded.

7.3 MONOMERS

In the second sub-part of the project the objective was to prepare monomeric bile acid-fluorophore conjugates that could act as model compounds for the fluorescence microscopic studies. The derivatives were prepared by esterification reactions either on 3-OH or on 24-COOH functionalities. In both of the alternatives, the carboxylic acid functionality of the forming ester was activated as its anhydride.[110-112]

To yield 4-nitro-*N*-(2-hydroxyethyl)-1,8-naphthalimidyl 3α,7α,12α-trihydroxy-5β-cholan-24-oate **104**, cholic acid was first activated by converting the carboxylic acid functionality to the corresponding anhydride. Then, 4-nitro-*N*-(2-hydroxyethyl)-1,8-naphthalimide **103** was allowed to react with the anhydride (Scheme 15).[110-112]

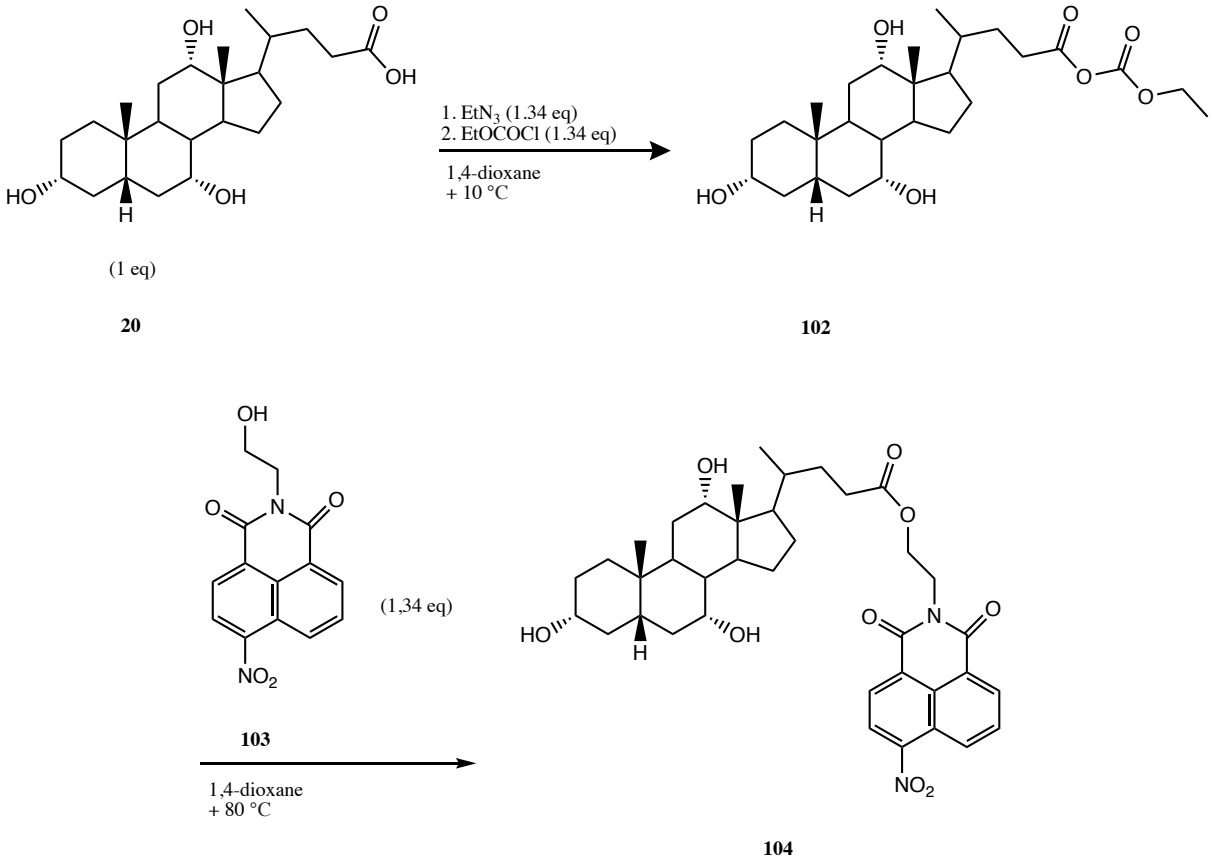

Scheme 15: The synthesis of 4-nitro-*N*-(2-hydroxyethyl)-1,8-naphthalimidyl 3α,7α,12α-trihydroxy-5β-cholan-24-oate **104**.[110-112]

Based on the ^{1}H NMR spectrum of the crude product the reaction had occurred. This was obvious from the disappearance of the hydroxyl group of **103** at the chemical shift value of 4.80 ppm upon esterification. The crude product was purified by column chromatography. Purification resulted in a mixture of product **104** and impurities.

Methyl 3α-(1-pyreneacetate)-5β-cholan-24-oate **107** was attempted to be prepared by converting the 1-pyreneacetic acid **105** to the corresponding anhydride and then allowing the anhydride **106** to react with methyl 3α-hydroxy-5β-cholan-24-oate **55** (Scheme 16).[110-112]

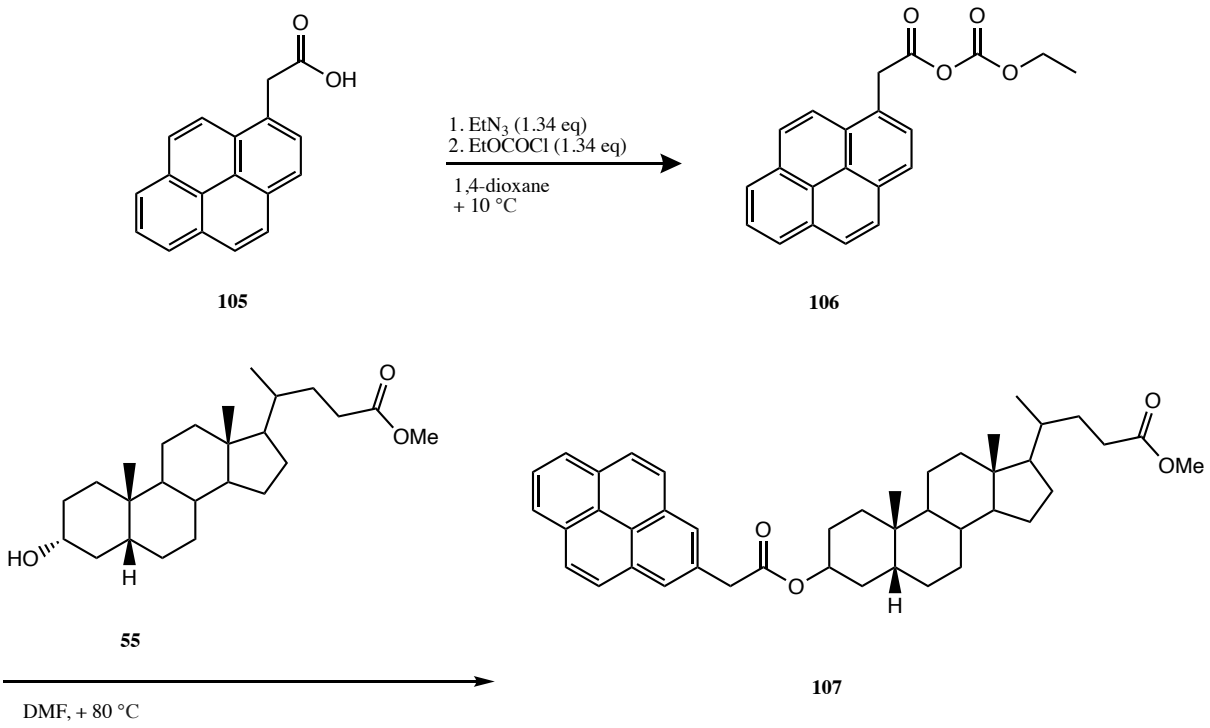

Scheme 16: The synthesis route to methyl 3α-(1-pyreneacetate)-5β-cholan-24-oate **107**.[110-112]

Based on ^{1}H NMR spectrum the reaction had not occurred, which could be deduced from the chemical shift of the 3β-proton at 3.57 ppm. Upon esterification the 3β-proton experiences a downfield shift to ~ 4.5 ppm. Because the anhydride is moisture sensitive, next time the reaction should be carried out under a nitrogen atmosphere in the future syntheses.

8. CONCLUSIONS

Based on the literature review, fluorescence microscopy provides a highly sensitive signaling mechanism to study events at the molecular level in chemistry, cell biology, and environmental sciences. Cholesterol is a crucial component of the cellular membranes, but the knowledge of its intracellular dynamics is scarce. It has been shown that abnormalities in cholesterol metabolism may have an impact on the development of certain neurodegenerative diseases and even cancer, which is why understanding the metabolic pathways of cholesterol is of utmost importance.

Intrinsically or extrinsically fluorescent cholesterol analogs can be used when detecting cholesterol by fluorescent microscopy. For example, alkyne cholesterol derivatives can be used in preparing extrinsically fluorescent cholesteryl derivatives by click chemistry. Intrinsically fluorescent sterols are structurally very similar to cholesterol, but their fluorescent properties are not as favorable as those of some extrinsically fluorescent cholesterol analogs. Intrinsically fluorescent probes usually require UV optics for good quality detection. The most widely used intrinsically fluorescent cholesterol analog is cholestatrienol. It is typically used for membrane biophysics and trafficking studies. Respectively, the most used and versatile extrinsically fluorescent analog is BODIBY-tagged cholesterol, which is used in many kinds of studies including screening assays for cholesterol efflux.

Steroid hormones are synthesized from cholesterol, and they regulate physiological functions. Various fluorescent probes have been developed for studying systems involving steroids or steroid hormones. The research is focused for example, in studying steroid-protein interactions, steroid depletion, and bile acid distribution in intestinal cells.

The objective of the experimental part was to synthesize fluorescent bile acid derivatives with the capability of binding cholesterol. First, cyclic bile acid derivatives with fluorophoric spacers on both the tail and the head were aimed at. In order to accomplish the objective, two bile acid moieties were first combined via a fluorophoric spacer either in a head-to-head or a tail-to-tail manner. 2,6-Naphthalenedicarboxylic acid was first allowed to react with the methyl esters of the bile acids in a molar ratio 1:2 in order to yield a diester in the 3α-position of the bile acid methyl esters. A modified Yamaguchi reaction proved not to result in the desired product, but instead a reaction between benzoyl chloride and the methyl ester of the bile acids took place. Naphthalenedicarboxylic acid was then activated as its anhydride or Cs salt and allowed to react with the corresponding bile acid methyl esters. Both of these reactions yielded the product, but

unfortunately the purification proved challenging. The anhydride method, however, seems to be the most promising synthetic route when preparing the head-to-head dimers of bile acids and a fluorophore.

In order to yield tail-to-tail dimers of the bile acid derivatives and the fluorophore, the carboxylic acid functionality at position 24 of the bile acid was activated and then allowed to react with 2,7-naphthalenediol in a molar ratio of 2:1. Tail-to-tail dimers were endeavored also by reactions between bile acid hydrazines and selected fluorophores **78**, **92**, and **97** in a molar ratio of 2:1. Most of the reactions were successful. Due to limited temporal resources, crude products were not purified. Moreover, attempts to synthesize monomeric derivatives between cholic acid or lithocholic acid and N-hydroxyethyl-4-nitro-1,8-naphthalimide or pyrene acetic acid were made. The products would have potential to act as model compounds for fluorescence microscopy studies.

This work provides perspectives for future research on the preparation of bile acid-based fluorophore derivatives. For purification of compounds, some other chromatographic method than column chromatography should be considered. For example, high performance countercurrent chromatography (HPCCC) could be tried. When synthetic procedures for the dimeric derivatives are established, the rings could be closed by the same or different difunctionalized fluorophores resulting in cholaphanes. Their cholesterol binding abilities may differ from the open and cleft-like compounds. It would then be interesting to study the cholesterol-binding of the different probes by using diffusion NMR measurements and mass spectrometry, and draw conclusions on the binding constants as a function of the construct.

9 EXPERIMENTAL

The starting materials used in the syntheses were purchased from commercial sources. Table 1 shows the used reagents, their purities and their manufactures. Triethylamine, ethyl chloroformate, and trifluoroacetic acid anhydride were distilled before use. Toluene, acetone, dimethylformamide, tetrahydrofuran, chloroform, and 1,4-dioxane were dried overnight with molecular sieves. All the other chemicals used without further purification.

Table 1: Used reagents, their purities and their manufacturers.

Reagent	Purity	Manufacturer
Acetone	AR	VWR
Benzoyl chloride	–	Merck
Bromoacetyl bromide	–	Sigma
CA	≥ 98 %	Sigma
$CHCl_3$	AR	VWR
Cholesterol	≥ 99 %	Sigma
Cs_2CO_3	≥ 98 %	Sigma
DCA	≥ 98 %	Sigma
DCM	AR	VWR
1,4-Dioxane	AR	VWR
2,7-Dihydroxynaphthalene	97 %	Sigma
DIPEA	99,5 %	–
DMAP	–	–
DMF	AR	VWR
4-(Dimethylamino)pyridine	–	Fluka
Di(3,3´-dimethyl-3*H*-benzoindole)-2,2´-(1,3,5-pentatrienyl)-*N*,*N*´-dipentanoic acid	–	Courtesy from M.Sc. M. Jurášek, UCT, Prague
3α,12α-Dihydroxy-5β-cholan-24-oic hydrazine	–	Courtesy from Ph.D. R. Kaplánek, UCT, Prague
EDC-HCl	–	Sigma
Ethyl chloroformate	–	–
EtOAc	AR	VWR
HATU	≥ 97 %	Sigma
HBTU	≥ 98 %	Sigma
3α-Hydroxy-5β-cholan-24-oic hydrazine	–	Courtesy from Ph.D. R. Kaplánek, UCT, Prague
K_2CO_3	–	–
LCA	≥ 95 %	Sigma/TCI Chemicals
MeOH	Analytical grade (AR)	VWR
2,6-Naphthalenedicarboxylic acid	95 %/98 %	Sigma/TCI Chemicals
N-hydroxyethyl-4-nitro-1,8-naphthalimide	–	Courtesy from M.Sc. M. Jurášek, UCT, Prague

N,N´-di(*p*-tolyl)-pyrrolopyrrole-3,3´-dibenzoic acid	–	Courtesy from M.Sc. M. Jurášek, UCT, Prague
OXYMA	97 %	Sigma
1-Pyreneacetic acid	97 %	Sigma
Pyridine	–	VWR
$SOCl_2$	–	Riedel-de Häen
Sulfuric acid (H_2SO_4)	95-98 %	–
TFAA	–	Merck
THF	AR	Sigma-Aldrich
Toluene	AR	VWR
Triethylamine	–	–
3α,7α,12α-Trihydroxy-5β-cholan-24-oic hydrazine	–	Courtesy from Ph.D. R. Kaplánek, UCT, Prague
8-(1,2,3-trimethoxybenzene)-BODIPY-3,5-bis(*p*-ethenyl phenoxypentanoic acid)	–	Courtesy from M.Sc. M. Jurášek, UCT, Prague

Thin layer chromatography was used to monitor the reactions. For this purpose, Merck Silica gel plates (20 cm x 20 cm) were used. The eluent used was a mixture of DCM and EtOAc or DCM and MeOH. Thin layer plates were visualized under ultraviolet light or by quickly dipping them into 5 % H_2SO_4 in MeOH solution and then heating the plates until spots appeared. The crude products were purified by column chromatography, size-exclusion chromatography, or recrystallization.

^{1}H and ^{13}C NMR spectra were measured from the synthesized products by using Bruker Avance III 300 MHz NMR spectrometer. The NMR samples were made in $CDCl_3$. Its residual proton signal, $\delta = 7.26$ ppm, was used as a reference for ^{1}H NMR spectrum. The corresponding signal for ^{13}C NMR spectrum was 77.00 ppm. NMR titrations and diffusion NMR experiments were performed by Bruker Avance III 500 MHz NMR spectrometer.

Mass spectrometric measurements were performed by using Micromass LCT time of flight (TOF) mass spectrometer with electrospray ionization (ESI) using positive ion mode. MassLynx NT software system was used to control the spectrometer, and to acquire and process the data.

The molecules and reaction schemes were plotted with ChemDraw program.

9.1 METHYL-3α-HYDROXY-5β-CHOLAN-24-OATE

In a round-bottomed two-necked 100 ml flask lithocholic acid **47** (8.00 mmol; 3.01 g) was dissolved in methanol (50 ml) after which 5 drops of concentrated sulfuric acid was added to the solution. The resulting mixture was refluxed at +100 °C for 18 h. Then, $CHCl_3$ (50 ml) was added to the mixture. The organic layer was washed with saturated $NaHCO_3$ solution (4 x 25 ml) and water (1 x 25 ml). Then, the organic layer was dried ($MgSO_4$), filtered, and the volatiles evaporated under reduced pressure. The structure of **55** was assigned by ^1H and ^{13}C NMR spectra (Appendix 1). The yield of compound **55** was 3.12 g (8.00 mmol; 100 %, white powder).

^1H NMR (300 MHz, $CDCl_3$, ppm): δ 0.64 (s, 3H, 18-CH_3), 0.90 (s, 3H, 19-CH_3), 0.91 (d, 3H, 21-CH_3), 2.21/2.35 (m, 2H, 23-CH_2), 3.60 (m, 1H, 3β-H), 3.66 (s, 3H, 25-CH_3)

^{13}C NMR (75 MHz, $CDCl_3$, ppm): 12.02, 18.25, 20.82, 23.35, 24.19, 26.41, 27.19, 28.16, 30.57, 31.01, 31.06, 34.57, 35.36, 35.36, 35.86, 36.49, 40.17, 40.45, 42.11, 42.74, 51.43, 55.97, 56.50, 71.85 (C-3), 174.73 (C-24)

9.2 METHYL-3α,12α-DIHYDROXY-5β-CHOLAN-24-OATE

In a round-bottomed two-necked 100 ml flask deoxycholic acid **46** (8.00 mmol; 3.14 g) was dissolved in methanol (50 ml) after which 5 drops of concentrated sulfuric acid was added to the solution. The resulting mixture was refluxed at +100 °C for 18 h. Then, $CHCl_3$ (50 ml) was added to the mixture. The organic layer was washed with saturated $NaHCO_3$ solution (4 x 25 ml) and water (1 x 25 ml). Then, the organic layer was dried ($MgSO_4$), filtered, and the volatiles evaporated under reduced pressure. The structure of **56** was assigned by ^1H and ^{13}C NMR spectra (Appendix 2). The yield of compound **56** was 3.25 g (8.00 mmol; 100 %, white powder).

^1H NMR (300 MHz, $CDCl_3$, ppm): 0.67 (s, 3H, 18-CH_3), 0.90 (s, 3H, 21-CH_3), 0.97 (d, 3H, 19-CH_3), 2.22/2.36 (m, 2H, 23-CH_2), 3.58 (m, 1H, 3β-H), 3.65 (s, 1H, 25-CH_3), 3.96 (s, 1H, 12β-H)

^{13}C NMR (75 MHz, $CDCl_3$, ppm): 12.71, 17.28, 23.12, 23.62, 26.10, 27.11, 27.42, 28.67, 30.48, 30.89, 31.07, 33.65, 34.10, 35.09, 35.21, 36.03, 36.44, 42.07, 46.48, 47.30, 48.25, 51.44, 71.76 (C-3), 73.10 (C-12), 174.65 (C-24)

9.3 METHYL-3α,7α,12α-TRIHYDROXY-5β-CHOLAN-24-OATE

In a round-bottomed two-necked 100 ml flask cholic acid **20** (8.00 mmol; 3.27 g) was dissolved in methanol (50 ml) after which 5 drops of concentrated sulfuric acid was added to the solution. The resulting mixture was refluxed at +100 °C for 18 h. Then, $CHCl_3$ (50 ml) was added to the mixture. The organic layer was washed with saturated $NaHCO_3$ solution (4 x 25 ml) and water (1 x 25 ml). Then, the organic layer was dried ($MgSO_4$), filtered, and the volatiles evaporated under reduced pressure. The structure of **57** was assigned by ^{1}H NMR spectrum (Appendix 3). The yield of compound **57** was 3.38 g (8.00 mmol; 100 %, white powder).

^{1}H NMR (300 MHz, $CDCl_3$, ppm): δ 0.66 (s, 3H, 18-CH_3), 0.87 (s, 3H, 19-CH_3), 0.97 (d, 21-CH_3), 2.22/2.35 (m, 2H, 23-CH_2), 3.43 (m, 1H, 3β-H), 3.65 (s, 3H, 25-CH_3), 3.82 (s, 1H, 7β-H), 3.94 (s, 1H, 12β-H)

9.4 METHYL-3α-BROMOACETYL-5β-CHOLAN-24-OATE

In a round-bottomed two-necked 250 ml flask methyl-3α-hydroxy-5β-cholan-24-oate **55** (7.00 mmol; 2.77 g) was stirred at +60 °C in dry $CHCl_3$ (50 ml) until it completely dissolved. Anhydrous K_2CO_3 (8.00 mmol; 1.11 g) was then added. Next, bromoacetyl bromide **66** (8.00 mmol; 0.697 ml) in dry $CHCl_3$ (25 ml) was added dropwise from a dropping funnel. After 3 h, the heating was stopped, ice-cold water (50 ml) added, and the organic layer separated. The organic layer was dried ($MgSO_4$), filtered, and the volatiles evaporated under reduced pressure. The crude product was purified by column chromatography (silica gel; 1. DCM/EtOAc 90:10 and 2. DCM/EtOAc 92:8). The structure of **67** was assigned by ^{1}H NMR spectrum (Appendix 10). The yield of compound **67** was 0.47 g (13 %).

^{1}H NMR (300 MHz, $CDCl_3$, ppm): δ 0.64 (s, 3H, 18-CH_3), 0.89 (s, 3H, 19-CH_3), 0.93 (d, 3H, 21-CH_3), 2.20/2.35 (m, 2H, 23-CH_2), 3.66 (s, 3H, 25-CH_3), 3.79 (s, 2H, Br-CH_2-), 4.78 (m, 1H, 3β-H)

9.5 METHYL-3α-BROMOACETYL-12α-HYDROXY-5β-CHOLAN-24-OATE

In a round-bottomed two-necked 250 ml flask methyl-3α,12α-dihydroxy-5β-cholan-24-oate **56** (8.00 mmol; 3.28 g) was stirred at +60 °C in dry $CHCl_3$ (50 ml) until it completely dissolved. Anhydrous K_2CO_3 (8.00 mmol; 1.11 g) was then added. Next, bromoacetyl bromide **66** (8.00 mmol; 0.697 ml) in dry $CHCl_3$ (25 ml) was added dropwise from a dropping funnel. After 15 minutes, the heating was stopped, ice-cold water (50 ml) added, and the organic layer separated. The organic layer was dried ($MgSO_4$), filtered, and the volatiles evaporated under reduced pressure. The crude product was purified by column chromatography (silica gel; 1. $CHCl_3$/MeOH 95:5 and 2. DCM/EtOAc 90:10). The structure of **68** was assigned by ^{1}H NMR spectrum (Appendix 11). The yield of compound **68** was 0.32 g (7.5 %).

^{1}H NMR (300 MHz, $CDCl_3$, ppm): δ 0.68 (s, 3H, 18-CH_3), 0.92 (s, 3H, 19-CH_3), 0.97 (d, 3H, 21-CH_3), 2.24/2.36 (m, 2H, 23-CH_2), 3.66 (s, 3H, 25-CH_3), 3.79 (s, 2H, Br-CH_2-), 3.99 (s, 1H, 12β-H), 4.78 (m, 1H, 3β-H). Traces of EtOAc and DCM are also visible in the NMR spectrum.

9.6 DICAESIUM NAPHTHALENE-2,6-DICARBOXYLATE

2,6-Naphthalenedicarbocylic acid **58** (4.00 mmol; 0.865 g) was dissolved in dry DMF (12 ml) and caesium carbonate **69** (4.00 mmol; 1.30 g) was added. After stirring for 3 h at room temperature, the solid obtained was filtered off and washed with acetone. The structure of **70** was assigned by ^{13}C NMR spectrum (Appendix 12). The yield of compound **70** was 1.23 g (64 %; white powder).

^{13}C NMR (75 MHz, $CDCl_3$, ppm): δ 126.22 (C-Ar), 128.79 (C-Ar), 129.01 (C-Ar), 133.25 (C-Ar), 133.78 (C-Ar), 175.50 (C=O)

9.7 2,6-NAPHTHALENEDICARBOXYLATE OF METHYL LITOCHOLATE

In a round-bottomed two-necked 250 ml flask methyl-3α-hydroxy-5β-cholan-24-oate **55** (6.90 mmol; 2.71 g), 2,6-naphthalenedicarbocylic acid **58** (3.50 mmol; 0.914 g), and 4-(dimethylamino)-pyridine (27.6 mmol; 3.37 g) were dissolved in dry toluene (150 ml) and the mixture heated to +100 °C in an oil bath. Then, benzoyl chloride (7.60 mmol; 0.88 ml) was added, and the mixture was kept at +100 °C for 72 h. After the reaction period, the solvent was evaporated under vacuum. The crude product was dissolved in $CHCl_3$ (75 ml) and washed with 2 M HCl solution (2 x 60 ml) and saturated $NaHCO_3$ solution (2 x 60 ml) to remove any unreacted benzoyl chloride and 4-(dimethylamino)pyridine. Finally, the mixture was washed with water (60 ml), dried ($MgSO_4$), and the volatiles were evaporated under reduced pressure.

The crude product was purified by column chromatography (silica gel, 1. DCM/EtOAc 85:15, 2. DCM/EtOAc 92:8 and 3. DCM 100). The final product was dried in a vacuum line. The structure of the synthesized compound was determined by ^{1}H and ^{13}C NMR (Appendix 4) combined with mass spectrometry (Appendix 7). Instead of compound **59** phenyl ester of methyl lithocholate **62** was formed. The yield of compound **62** was 1.05 g (2.12 mmol; 31 %, white powder).

^{1}H NMR (500 MHz, $CDCl_3$, ppm): δ 0.66 (s, 3H, 18-CH_3), 0.91 (d, 3H, 21-CH_3), 0.96 (s, 3H, 19-CH_3), 1.04-2.01 (26H, steroidal H), 2.35/2.22 (m, 2H, 23-CH_2), 3.66 (s, 3H, 25-CH_3), 4.97 (m, 1H, 3β-H), 7.43 (m, 2H, Ar-H), 7.54 (m, 1H, Ar-H), 8.04 (m, 2H, Ar-H)

^{13}C NMR (75 MHz, $CDCl_3$, ppm): δ 12.07, 18.30, 20.91, 23.38, 24.20, 27.37, 26.80, 27.08, 28.20, 31.05, 31.09, 32.41, 34.68, 35.13, 35.39, 35.86, 40.18, 40.54, 42.01, 42.79, 51.46, 56.06, 56.53, 75.02 (C-3), 128.25 (C-Ar), 128.25 (C-Ar), 129.54 (C-Ar), 129.54 (C-Ar), 131.01 (C-Ar), 132.66 (C-Ar), 166.14 (C=O of phenyl group), 174.74 (C-24)

MS (ESI-TOF) *m/z* 518.06 $[M+Na]^+$

Because the desired product did not achieved by previous method, another approach was tried.

In a round-bottomed two-necked 250 ml flask 2,6-naphthalenedicarbocylic acid **58** (8.00 mmol; 1.73 g) and DMF (60 ml) were cooled an ice-water bath to +10 °C under a nitrogen atmosphere. Then triethylamine (20.0 mmol; 2.79 ml) was added to the solution from a dropping funnel, followed by a dropwise addition of ethyl chloroformate (20.0 mmol; 1.91 ml) in DMF (10 ml). The mixture was stirred at room temperature for 30 minutes. Then, methyl-3α-hydroxy-5β-cholan-24-oate **55** (16.0 mmol; 6.50 g) in DMF (50 ml) was added dropwise to the solution. The mixture was heated at +80 °C in an oil bath for 42 h. After the reaction period, the solvent was evaporated under vacuum. The crude product was dissolved in $CHCl_3$ (75 ml) and washed with water (2 x 50 ml), 0.1 M HCl solution (2 x 50 ml), water (2 x 50 ml), and finally with brine (2 x 50 ml). The organic layer was dried ($MgSO_4$), filtered, and the volatiles evaporated under reduced pressure. The crude product was purified by column chromatography (silica gel; DCM/MeOH 96:4). Purification resulted a mixture of the product **59** and impurities.

Again, because the desired product did not achieved by previous method, another approach was experimented.

In a round-bottomed two-necked 100 ml flask dicaesium naphthalene-2,6-dicarboxylate **70** (0.30 mmol; 0.144 g) was dissolved in dry DMF (10 ml). At the same time in another flask methyl-3α-bromoacetyl-5β-cholan-24-oate **67** (0.60 mmol; 0.317 g) was dissolved in dry DMF (30 ml) and then it was added to the solution of **70** by dropwise from a dropping funnel. The resulting mixture was stirred at room temperature for 42 h. After the reaction period, the solvent was evaporated under vacuum. The crude product was purified by column chromatography (silica gel; DCM/MeOH 96:4). Purification resulted a mixture of the product **59** and impurities.

9.8 2,6-NAPHTHALENEDICARBOXYLATE OF METHYL DEOXYCHOLATE

In a round-bottomed two-necked 250 ml flask methyl-3α,12α-dihydroxy-5β-cholan-24-oate **56** (7.94 mmol; 3.23 g) was suspended in dried toluene (150 ml) after which 4-(dimethylamino)pyridine (31.8 mmol; 3.88 g), and benzoyl chloride (8.70 mmol; 1.01 ml) were added to the solution. The mixture was heated at +100 °C in an oil bath. Then, 2,6-naphthalenedicarbocylic acid **58** (3.98 mmol; 0.858 g) in dried toluene (50 ml) was added to the solution from a dropping funnel, and heating was continued for 48 h at +100 °C. After the reaction period, the solvent was evaporated under vacuum. The crude product was dissolved in $CHCl_3$ (75 ml) and washed with 2 M HCl solution (2 x 60 ml). Finally, the mixture was washed with saturated $NaHCO_3$ solution (2 x 60 ml) and water (1 x 60 ml). The organic layer was dried ($MgSO_4$), filtered, and the volatiles were evaporated under reduced pressure. The crude product was purified by column chromatography (silica gel, 1. DCM/EtOAc 60:40 and 2. DCM/EtOAc 92:8). The final product was dried in a vacuum line. The structure of the synthesized compound was determined by ^{1}H and ^{13}C NMR (Appendix 5) combined with mass spectrometry (Appendix 8). Instead of compound **60,** phenyl ester of methyl deoxycholate **63** was formed. The yield of compound **63** was 1.48 g (2.90 mmol; 37 %, white powder).

^{1}H NMR (500 MHz, $CDCl_3$, ppm): δ 0.69 (s, 3H, 18-CH_3), 0.95 (s, 3H, 19-CH_3), 0.98 (d, 3H, 21-CH_3), 1.06-2.01 (25H, steroidal H), 2.23/2.37 (m, 2H, 23-CH_2), 3.66 (s, 3H, 25-CH_3), 4.00 (s, 1H, 12β-H), 4.96 (m, 1H, 3β-H), 7.42 (m, 2H, Ar-H), 7.53 (m, 1H, Ar-H), 8.03 (m, 2H, Ar-H). Traces of EtOAc and DCM are also visible in the spectrum.

^{13}C NMR (75 MHz, $CDCl_3$, ppm): δ 12.77, 17.38, 23.17, 23.61, 26.06, 26.67, 27.01, 27.44, 28.81, 30.94, 31.07, 32.34, 33.78, 34.21, 34.97, 35.08, 36.05, 41.98, 46.55, 47.42, 48.37, 51.48, 73.30 (C-12), 74.87 (C-3), 128.25 (C-Ar), 128.25 (C-Ar), 129.56 (C-Ar), 129.56 (C-Ar), 130.93 (C-Ar), 132.67 (C-Ar), 166.17 (C=O of phenyl group), 174.66 (C-24)

MS (ESI-TOF) *m*/*z* 534.03 $[M+Na]^+$

Because the desired product did not achieved by previous method, another approach was tried.

In a round-bottomed two-necked 250 ml flask 2,6-naphthalenedicarbocylic acid **58** (4.00 mmol; 0.87 g) and DMF (40 ml) were cooled an ice-water bath to +10 °C under a nitrogen atmosphere. Then, triethylamine (10.0 mmol; 1.39 ml) was added to the solution from a dropping funnel, followed by a dropwise addition of ethyl chloroformate (10.0 mmol; 0.96 ml) in DMF (5 ml). The mixture was stirred at room temperature for 30 minutes. In another round-bottomed two-necked 250 ml flask methyl-3α,12α-dihydroxy-5β-cholan-24-oate **56** (8.00 mmol; 3.16 g) was dissolved in DMF (45 ml) under a nitrogen atmosphere. Then, 2,6-naphthalenedicarbocylic acid dianhydride **65** in DMF was added dropwise to the solution. The mixture was heated at +80 °C in an oil bath under a nitrogen atmosphere for 42 h. After the reaction period, the solvent was evaporated under vacuum. The crude product was dissolved in $CHCl_3$ (100 ml) and washed with water (2 x 70 ml), 0.1 M HCl solution (2 x 50 ml), water (2 x 50 ml), and finally with brine (2 x 40 ml). The organic layer was dried ($MgSO_4$), filtered, and the volatiles evaporated under reduced pressure. The crude product was purified by column chromatography (silica gel; DCM/MeOH 96:4) and recrystallized from acetonitrile, but no crystals were obtained.

Again, because the desired product did not achieved by previous methods, another approach was experimented.

In a round-bottomed two-necked 50 ml flask methyl-3α-bromoacetyl-12α-hydroxy-5β-cholan-24-oate **68** (0.60 mmol; 0.317 g) was dissolved in dry DMF (20 ml). Then, dicaesium naphthalene-2,6-dicarboxylate **70** (0.30 mmol; 0.144 g) was added to the solution. The resulting mixture was stirred at room temperature for 24 h. After the reaction period, the solvent was evaporated under vacuum. Based on ^{1}H NMR spectrum formation of product **60** was not observed.

9.9 2,6-NAPHTHALENEDICARBOXYLATE OF METHYL CHOLATE

In a round-bottomed two-necked 250 ml flask methyl-3α,7α,12α-trihydroxy-5β-cholan-24-oate **57** (7.34 mmol; 3.11 g) was suspended in dried toluene (150 ml) after which 4-(dimethylamino)-pyridine (29.4 mmol; 3.59 g) and benzoyl chloride (8.10 mmol; 0.94 ml) were added to the solution. The mixture was heated at +100 °C in an oil bath. Then, 2,6-naphthalenedicarbocylic acid **58** (3.7 mmol; 0,800 g) in dried toluene/acetone (5:1, 60 ml) was added to the solution from a dropping funnel, and heating was continued for 68 h at +100 °C. After the reaction period, the solvent was evaporated under vacuum. The crude product was dissolved in $CHCl_3$ (75 ml) and washed with 2 M HCl solution (2 x 60 ml). Finally, the mixture was washed with saturated $NaHCO_3$ solution (2 x 60 ml) and water (1 x 60 ml). The organic layer was dried ($MgSO_4$), filtered, and the volatiles evaporated under reduced pressure. The crude product was purified by column chromatography (silica gel, 1. DCM/EtOAc 60:40, 2. DCM/EtOAc 92:8 and 3. MeOH 100). The final product was dried in a vacuum line. The structure of the synthesized compound was determined by ^{1}H and ^{13}C NMR (Appendix 6) combined with mass spectrometry (Appendix 9). Instead of compound **61**, phenyl ester of methyl cholate **64** was formed. The yield of compound **64** was 1.69 g (3.21 mmol; 44 %, white powder).

^{1}H NMR (500 MHz, $CDCl_3$, ppm): δ 0.70 (s, 3H, 18-CH_3), 0.92 (s, 3H, 19-CH_3), 0.98 (d, 3H, 21-CH_3), 1.09-1.99 (24H, steroidal H), 2.34/2.38 (m, 2H, 23-CH_2), 3.66 (s, 3H, C-25), 3.87 (s, 1H, 7β-H), 4.00 (s, 1H, 12β-H), 4.82 (m, 1H, 3β-H), 7.41 (t, 2H, Ar-H), 7.52 (t, 1H, Ar-H), 8.01 (d, 2H, Ar-H)

^{13}C NMR (75 MHz, $CDCl_3$, ppm): δ 12.56, 17.39, 22.52, 23.20, 26.77, 27.47, 28.42, 30.30, 31.08, 34.54, 34.75, 34.94, 35.22, 35.29, 39.54, 41.30, 42.09, 46.60, 47.30, 51.50, 68.32 (C-7), 73.02 (C-12), 74.92 (C-3), 128.19 (C-Ar), 128.19 (C-Ar), 129.56 (C-Ar), 129.56 (C-Ar), 131.00 (C-Ar), 132.62 (C-Ar), 166.18 (C=O of phenyl group), 174.72 (C-24)

MS (ESI-TOF) *m*/*z* 550.05 $[M+Na]^+$

Because the desired product did not achieved by previous method, another approach was tried.

In a round-bottomed two-necked 250 ml flask 2,6-naphthalenedicarbocylic acid **58** (4.00 mmol; 0.87 g) and DMF (40 ml) was cooled an ice-water bath to +10 °C under a nitrogen atmosphere. Then, triethylamine (10.0 mmol; 1.39 ml) was added to the solution from a dropping funnel, followed by a dropwise addition of ethyl chloroformate (10.0 mmol; 0.96 ml) in DMF (5 ml). The mixture was stirred at room temperature for 30 minutes. In another round-bottomed two-necked 250 ml flask methyl-3α,7α,12α-trihydroxy-5β-cholan-24-oate **57** (8.00 mmol; 3.38 g) was dissolved in DMF (40 ml) under a nitrogen atmosphere. Then, 2,6-naphthalenedicarbocylic acid dianhydride **65** in DMF was added dropwise to the solution. The mixture was heated at +80 °C in an oil bath under a nitrogen atmosphere for 68 h. After the reaction period, the solvent was evaporated under vacuum. The crude product was dissolved in $CHCl_3$ (75 ml) and washed with water (2 x 50 ml), 0.1 M HCl solution (2 x 50 ml), water (2 x 50 ml), and finally with brine (2 x 40 ml). The organic layer was dried ($MgSO_4$), filtered, and the volatiles evaporated under reduced pressure. The crude product was purified by column chromatography (silica gel; DCM/MeOH 94:6). Purification resulted in a mixture of product **61** and impurities.

9.10 3α-TRIFLUOROACETOXY-5β-CHOLAN-24-OIC ACID

To the solution of lithocholic acid **47** (8.00 mmol; 3.01 g) in dry THF (75 ml) cooled to -10 °C in an ice-salt bath, trifluoroacetic acid anhydride **71** (130 mmol; 18.0 ml) was added dropwise. The mixture was kept at -10 °C for 1 h and stirred for 2 h at room temperature. Then, the mixture was poured into Et_2O/ice (120 ml:30 g). The organic layer was washed with water (1 x 60 ml), with saturated $NaHCO_3$ solution, (until the water solution was basic; monitored by pH-paper 4 x 60 ml), and with brine (1 x 60 ml). The organic layer was dried ($MgSO_4$), filtered, and the volatiles evaporated under reduced pressure. The structure of **72** was assigned by ^1H spectrum (Appendix 13). The yield was 3.78 g (8.00 mmol; 100 %, white powder).

^1H NMR (300 MHz, $CDCl_3$, ppm): δ 0.64 (s, 3H, 18-CH_3), 0.92 (s, 3H, 19-CH_3), 0.95 (d, 3H, 21-CH_3), 2.26/2.40 (m, 23-CH_2), 4.93 (m, 1H, 3β-H)

9.11 3α-TRIFLUOROACETOXY-5β-CHOLAN-24-OYL CHLORIDE

In a round-bottomed one-necked 100 ml flask 3α-trifluoroacetoxy-5β-cholan-24-oic acid **72** (8.00 mmol; 3.78 g) and distilled $SOCl_2$ **73** was refluxed for 15 minutes. After the reaction period, the excess of $SOCl_2$ was evaporated to dryness under vacuum. The crude product was dissolved in $CHCl_3$ (50 ml) and evaporated to the dryness under vacuum. The structure of **74** was assigned by ^{13}C NMR spectrum (Appendix 14). The yield of **74** was 3.93 g (8.00 mmol; 100 %, dark brown sticky solid).

^{13}C NMR (75 MHz, $CDCl_3$, ppm): 12.04 (C-18), 18.23 (C-21), 20.85 (C-11), 23.19 (C-19), 24.13 (C-15), 26.15 (C-7), 26.22 (C-2), 26.90 (C-6), 28.14 (C-16), 31.08 (C-22), 31.66 (C-4), 34.55 (C-10), 34.77 (C-1), 34.97 (C-20), 35.77 (C-8), 40.04 (C-12), 40.45 (C-9), 41.90 (C-5), 42.80 (C-13), 44.40 (C-23), 55.85 (C-17), 56.39 (C-14), 79.39 (C-3), 174.18 (C-24)

9.12 2,7-DIHYDROXYNAPHTHYL-BIS(3α-TRIFLUOROACETOXY-5β-CHOLAN-24-OATE)

To a solution of 3α-trifluoroacetoxy-5β-cholan-24-oyl chloride **74** (8.00 mmol; 3.93 g) in THF (20 ml) 2,7-dihydroxynaphthalene **75** (5.20 mmol; 0.833 g) in THF (10 ml) and pyridine (12.4 mmol; 1,00 ml) were added. The resulting mixture was refluxed for 69 h. Then $CHCl_3$ (30 ml) was added to the mixture. The organic layer was washed with saturated $NaHCO_3$ solution (3 x 30 ml), and water (1 x 30 ml). Then the organic layer was dried ($MgSO_4$), filtered, and the volatiles evaporated under reduced pressure. The crude product was attempted to be purified by column chromatography (silica gel; $CHCl_3$/MeOH 93:7) and size exclusion chromatography (Sephadex LH20). Purification resulted in a mixture of product **76** and impurities.

In order to improve the yield, pyridine was replaced by a water gas trap. The solution of 3α-trifluoroacetoxy-5β-cholan-24-oyl chloride **74** (8.00 mmol; 3.93 g) in DMF (40 ml) was heated at +90 °C in an oil bath, after which 2,7-dihydroxynaphthalene **75** (4.00 mmol; 0.641 g) in DMF (20 ml) was added dropwise. The resulting mixture was heated at +90 °C for 72 h. Then $CHCl_3$ (30 ml) was added to the mixture. The organic layer was washed with H_2O/MeOH (1:1, 4x 25 ml) solution, brine (4 x 25 ml), and water (1 x 25 ml). Next, the volatiles evaporated under reduced pressure and the crude product was dissolved in $CHCl_3$ (30 ml). The organic layer was washed with saturated $NaHCO_3$ solution (3 x 30 ml) and water (1 x 30 ml), the organic layer was dried ($MgSO_4$), filtered, and the volatiles evaporated under reduced pressure.

The crude product was purified by column chromatography (silica gel; $CHCl_3$/MeOH 93:7). Purification resulted in a mixture of product **76** and impurities.

9.13 2,7-DIHYDROXYNAPHTHYL-BIS(3α-HYDROXY-5β-CHOLAN-24-OATE)

In a round-bottomed two-necked 100 ml flask lithocholic acid **47** (1.30 mmol; 0.50 g) was dissolved in THF (30 ml). Then, 2,7-dihydroxynaphthalene **75** (0.66 mmol; 0.11 g) and 5 drops of concentrated sulfuric acid were added to the solution. The resulting mixture was refluxed for 6 h. After the reaction period $CHCl_3$ (30 ml) was added to the mixture. The organic layer was washed with saturated $NaHCO_3$ solution (2 x 20 ml) and water (1 x 20 ml). Then, the organic layer was dried ($MgSO_4$), filtered, and the volatiles evaporated under reduced pressure. Based on ^1H and ^{13}C NMR spectra, the formation of product **77** was not observed.

9.14 *N,N´*-DI(*p*-TOLYL)-3,3´-DIBENZOYLPYRROLOPYRROLYL BIS(3α,7α,12α-TRIHYDROXY-5β-CHOLAN-24-YL-HYDRAZINE)

In a round-bottomed 25 ml flask *N,N´*-di(*p*-tolyl)pyrrolopyrrole-3,3´-dibenzoic acid **78** (0.06 mmol; 0.03 g), *N*-(3-dimethylaminopropyl)-*N*′-ethylcarbodiimide hydrochloride (EDC-HCl) **79** (0.13 mmol; 0.02 g), and ethyl (hydroxyimino)cyanoacetate (OXYMA) **80** (0.13 mmol; 0.02 g) were dissolved in 5:1 mixture of DCM and DMF (6 ml). The mixture was stirred at room temperature for 30 minutes. Then, 3α,7α,12α-trihydroxy-5β-cholan-24-oic hydrazine **82** (0.25 mmol; 0.10 g) in DCM (5 ml) was added to the solution. The mixture was stirred at room temperature for 18 hours. After the reaction period, the volatiles were evaporated under vacuum. The crude product was purified by column chromatography (silica gel; 1. $CHCl_3$/MeOH 90:10 and 2. $CHCl_3$/MeOH 95:5). Product **83** was not obtained as a pure compound.

To improve the yield, an alternative synthesis route was attempted.

In a round-bottomed 5 ml flask 3α,7α,12α-trihydroxy-5β-cholan-24-oic hydrazine **82** (0.038 mmol; 0.016 g), *N,N´*-di(*p*-tolyl)pyrrolopyrrole-3,3´-dibenzoic acid **78** (0.019 mmol; 0.010 g), *N,N,N′,N′*-tetramethyl-*O*-(1*H*-benzotriazol-1-yl)uronium hexafluoro- phosphate (HBTU) **84** (0.057 mmol; 0.022 g), and few crystals of DMAP **85** were dissolved in DMF (0.5 ml). Then, *N,N*-diisopropylethylamine (DIPEA) **86** (0.057 mmol; 10.0 µl) was added to the solution. The mixture was heated at +85 °C in an oil bath for 18 h. After the reaction period the volatiles were evaporated under vacuum. The crude product was purified by column

chromatography (silica gel; $CHCl_2$/MeOH 96:4). Purification resulted a mixture of product **83** and impurities.

Again, because the desired product did not achieved by previous methods, another approach was experimented.

In a round-bottomed 5 ml flask 3α,7α,12α-trihydroxy-5β-cholan-24-oic hydrazine **82** (0.038 mmol; 0.016 g), *N,N´*-di(*p*-tolyl)pyrrolopyrrole-3,3´-dibenzoic acid **78** (0.019 mmol; 0.010 g), and 1-[bis(dimethylamino)methylene]-1*H*-1,2,3-triazolo[4,5-*b*]- pyridinium 3-oxide hexafluorophosphate (HATU) **87** (0.057 mmol; 0.022 g) were dissolved in 10:1 mixture of DCM and DMF (1.1 ml). Then, DIPEA **86** (0.014 mmol; 20.0 µl) was added to the solution. The mixture was stirred at room temperature for 18 h. After the reaction period, the volatiles were evaporated under vacuum. The crude product was purified by column chromatography (silica gel; 1. $CHCl_3$/MeOH 90:10 and 2. $CHCl_3$/MeOH 95:5). Product **83** could not be purified despite efforts.

9.15 *N,N´*-DI(*p*-TOLYL)-3,3´-DIBENZOYLPYRROLOPYRROLYL BIS(3α-HYDROXY-5β-CHOLAN-24-YL-HYDRAZINE)

In a round-bottomed 25 ml flask *N,N´*-di(*p*-tolyl)pyrrolopyrrole-3,3´-dibenzoic acid **78** (0.06 mmol; 0.03 g), EDC-HCl **79** (0.13 mmol; 0.02 g), and OXYMA **80** (0.13 mmol; 0.02 g) were dissolved in 5:1 mixture of DCM and DMF (6 ml). The mixture was stirred at room temperature for 30 minutes. Then, 3α-hydroxy-5β-cholan-24-oic hydrazine **88** (0.26 mmol; 0.10 g) in DCM (5 ml) was added to the solution. The mixture was stirred at room temperature for 18 hours. After the reaction period, the volatiles evaporated under vacuum. Due to limited temporal resources, the crude product was not purified.

9.16 *N,N´*-DI(*p*-TOLYL)-3,3´-DIBENZOYLPYRROLOPYRROLYL BIS(3α,12α-DIHYDROXY-5β-CHOLAN-24-YL-HYDRAZINE)

In a round-bottomed 25 ml flask *N,N´*-di(*p*-tolyl)pyrrolopyrrole-3,3´-dibenzoic acid **78** (0.06 mmol; 0.03 g), EDC-HCl **79** (0.13 mmol; 0.02 g), and OXYMA **80** (0.13 mmol; 0.02 g) were dissolved in 5:1 mixture of DCM and DMF (6 ml). The mixture was stirred at room temperature for 30 minutes. Then, 3α,12α-dihydroxy-5β-cholan-24-oic hydrazine **89** (0.24 mmol; 0.10 g) in DCM (5 ml) was added to the solution. The mixture was stirred at room temperature for 18 hours. After the reaction period, the volatiles were evaporated under vacuum. Due to limited temporal resources, the crude product was not purified.

9.17 8-(1,2,3-TRIMETHOXYBENZENE)-BODIPY-3,5-BIS(p-ETHENYL PHENOXYPENTANOYL)BIS(3α-HYDROXYL-5β-CHOLAN-24-YL HYDRAZINE)

In a round-bottomed 5 ml flask 8-(1,2,3-trimethoxybenzene)-BODIPY-3,5-bis(p-ethenyl phenoxypentanoic acid) **92** (0.02 mmol; 0.015 g), EDC-HCl **79** (0.08 mmol; 0.015 g), and OXYMA **80** (0.08 mmol; 0.012 g) were dissolved in 5:1 mixture of DCM and DMF (0.6 ml). The mixture was stirred at room temperature for 30 minutes. Then, 3α-hydroxy-5β-cholan-24-oic hydrazine **88** (0.2 mmol; 0.078 g) in DCM (0.5 ml) was added to the solution. The mixture was stirred at room temperature for 18 hours. After the reaction period, the volatiles were evaporated under vacuum. The crude product was purified by column chromatography (silica gel; $CHCl_3$/MeOH 95:5). Purification resulted in a mixture of the product **94** and impurities.

9.18 8-(1,2,3-TRIMETHOXYBENZENE)-BODIPY-3,5-BIS(p-ETHENYL PHENOXYPENTANOYL)BIS(3α,12α-DIHYDROXYL-5β-CHOLAN-24-YL HYDRAZINE)

In a round-bottomed 5 ml flask 8-(1,2,3-trimethoxybenzene)-BODIPY-3,5-bis(p-ethenyl phenoxypentanoic acid) **92** (0.006 mmol; 0.005 g), EDC-HCl **79** (0.012 mmol; 0.002 g), and OXYMA **80** (0.012 mmol; 0.002 g) were dissolved in 5:1 mixture of DCM and DMF (0.6 ml). The mixture was stirred at room temperature for 30 minutes. Then, 3α,12α-dihydroxy-5β-cholan-24-oic hydrazine **89** (0.024 mmol; 0.010 g) in DCM (1.0 ml) was added to the solution. The mixture was stirred at room temperature for 18 hours. After the reaction period, the volatiles were evaporated under vacuum. Due to limited temporal resources, the crude product was not purified.

9.19 8-(1,2,3-TRIMETHOXYBENZENE)-BODIPY-3,5-BIS(p-ETHENYL PHENOXYPENTANOYL)BIS(3α,7α,12α-TRIHYDROXY-5β-CHOLAN-24-YL HYDRAZINE)

In a round-bottomed 5 ml flask 8-(1,2,3-trimethoxybenzene)-BODIPY-3,5-bis(p-ethenyl phenoxypentanoic acid) **92** (0.006 mmol; 0.005 g), EDC-HCl **79** (0.012 mmol; 0.002 g), and OXYMA **80** (0.012 mmol; 0.002 g) were dissolved in 5:1 mixture of DCM and DMF (0.6 ml). The mixture was stirred at room temperature for 30 minutes. Then, 3α,7α,12α-trihydroxy-5β-cholan-24-oic hydrazine **82** (0.024 mmol; 0.01 g) in DCM (1.0 ml) was added to the solution. The mixture was stirred at room temperature for 18 hours. After the reaction period, the volatiles were evaporated under vacuum. Due to limited temporal resources, the crude product was not purified.

9.20 DI(3,3′-DIMETHYL-3*H*-BENZOINDOLE)-2-(1,3,5-PENTATRIENYL)-*N*,*N*′-DIPENTANOYL BIS(3α-HYDROXY-5β-CHOLAN-24-YL HYDRAZINE)

In a round-bottomed 5 ml flask di(3,3′-dimethyl-3*H*-benzoindole)-2,2′-(1,3,5-pentatrienyl)-*N*,*N*′-dipentanoic acid **97** (0.006 mmol; 0.005 g), EDC-HCl **79** (0.012 mmol; 0.002 g), and OXYMA **80** (0.012 mmol; 0.002 g) were dissolved in 5:1 mixture of DCM and DMF (0.6 ml). The mixture was stirred at room temperature for 30 minutes. Then, 3α-hydroxy-5β-cholan-24-oic hydrazine **88** (0.024 mmol; 0.010 g) in DCM (1.0 ml) was added to the solution. The mixture was stirred at room temperature for 18 hours. After the reaction period, the volatiles were evaporated under vacuum. Due to limited temporal resources, the crude product was not purified.

9.21 DI(3,3′-DIMETHYL-3*H*-BENZOINDOLE)-2-(1,3,5-PENTATRIENYL)-*N*,*N*′-DIPENTANOYL BIS(3α,12α-DIHYDROXY- 5β-CHOLAN-24-YL HYDRAZINE)

In a round-bottomed 5 ml flask di(3,3′-dimethyl-3*H*-benzoindole)-2,2′-(1,3,5-pentatrienyl)-*N*,*N*′-dipentanoic acid **97** (0.006 mmol; 0.005 g), EDC-HCl **79** (0.012 mmol; 0.002 g), and OXYMA **80** (0.012 mmol; 0.002 g) were dissolved in 5:1 mixture of DCM and DMF (0.6 ml). The mixture was stirred at room temperature for 30 minutes. Then, 3α,12α-dihydroxy-5β-cholan-24-oic hydrazine **89** (0.024 mmol; 0.010 g) in DCM (1.0 ml) was added to the solution. The mixture was stirred at room temperature for 18 hours. After the reaction period, the volatiles were evaporated under vacuum. Due to limited temporal resources, the crude product was not purified.

9.22 DI(3,3′-DIMETHYL-3*H*-BENZOINDOLE)-2-(1,3,5-PENTATRIENYL)-*N*,*N*′-DIPENTANOYL BIS(3α,7α,12α-TRIHYDROXY-5β-CHOLAN-24-YL HYDRAZINE)

In a round-bottomed 5 ml flask di(3,3′-dimethyl-3*H*-benzoindole)-2,2′-(1,3,5-pentatrienyl)-*N*,*N*′-dipentanoic acid **97** (0.006 mmol; 0.005 g), EDC-HCl **79** (0.012 mmol; 0.002 g), and OXYMA **80** (0.012 mmol; 0.002 g) were dissolved in 5:1 mixture of DCM and DMF (0.6 ml). The mixture was stirred at room temperature for 30 minutes. Then, 3α,7α,12α-trihydroxy-5β-cholan-24-oic hydrazine **82** (0.024 mmol; 0.010 g) in DCM (1.0 ml) was added to the solution. The mixture was stirred at room temperature for 18 hours. After the reaction period, the volatiles were evaporated under vacuum. Due to limited temporal resources, the crude product was not purified.

9.23 4-NITRO-*N*-(2-HYDROXYETHYL)-1,8-NAPHTHALIMIDYL-3α,7α,12α-TRIHYDROXY-5β-CHOLAN-24-OATE

In a round-bottomed two-necked 100 ml flask cholic acid **20** (0.021 mmol; 0.087 g) was dissolved in dry 1,4-dioxane (20 ml). The solution was cooled on an ice-water bath to +10 °C, after which triethylamine (0.028 mmol; 30.0 µl) and ethyl chloroformate (0.028 mmol; 21.0 µl) were added to the solution. The mixture was stirred at room temperature for 30 minutes. Then, 4-nitro-*N*-(2-hydroxyethyl)-1,8-naphthalimide **103** (0.028 mmol; 0.087 g) in 1,4-dioxane (15 ml) was added to the solution. The mixture was heated at +80 °C in an oil bath for 20 h. After the reaction period, the solvent evaporated under vacuum. The crude product was dissolved in $CHCl_3$ (50 ml) and washed with water (2 x 35 ml), 0.1 M HCl solution (2 x 35 ml), water (2 x 35 ml), and finally with saturated $NaHCO_3$ solution (2 x 35 ml). The organic layer was dried (Na_2SO_4), filtered, and the volatiles evaporated under reduced pressure. The crude product was purified by column chromatography (silica gel; DCM/MeOH 90:10). Purification resulted in a mixture of product **104** and impurities.

9.24 METHYL 3α-(1-PYRENEACETATE)-5β-CHOLAN-24-OATE

In a round-bottomed two-necked 100 ml flask 1-pyreneacetic acid **105** (2.00 mmol; 0.500 g) was dissolved in DMF (25 ml). The solution was cooled on an ice-water bath to +10 °C, after which triethylamine (3.00 mmol; 0.418 ml) and ethyl chloroformate (3.00 mmol; 0.287 ml) were added to the solution. The mixture was stirred at room temperature for 30 minutes. Then, methyl-3α-hydroxy-5β-cholan-24-oate **55** in DMF (25 ml) was added from a dropping funnel by dropwise to the solution. The mixture was heated at +80 °C in an oil bath for 42 h. After the reaction period, the solvent was evaporated under vacuum. The crude product was dissolved in $CHCl_3$ (50 ml) and washed with water (2 x 40 ml), 0.1 M HCl solution (2 x 40 ml), water (2 x 40 ml), and finally with brine (2 x 40 ml). The organic layer was dried ($MgSO_4$), filtered, and the volatiles evaporated under reduced pressure. Based on ^{1}H NMR spectra formation of product **107** was not observed.

10. BIBLIOGRAPHY

1. Sanderson M. J., Smith I., Parker I. and Bootman M.D., Fluorescence Microscopy, *Cold Spring Harb. Protoc.*, **2014**, 1042-1065.

2. Vegesna G. K., *Design, synthesis and applications of fluorescent and electrochemical probes*, Dissertation, Michigan Technological University, 2014, 14-17.

3. Maxfield F. R. and Wüstner D., Intracellular cholesterol transport, *J. Clin. Invest.,* **2002**, *110*, 891-898.

4. Solanko K. A., Modzel M., Solanko L. M. and Wüstner D., Fluorescent sterols and cholesteryl esters as probes for intracellular cholesterol transport, *Lipid Insights*, **2015**, *8*, 95-114.

5. Dobrucki J. W., *Fluorescence Microscopy: From Principles to Biological applications*, Wiley-VCH Verlag GmbH & Co. KGaA, Weinheim, Germany, 2013, 97-142.

6. Atkins P. and De Paula J., *Atkins' Physical Chemistry*, 10th edition, Oxford University Press, Oxford, 2014, 543-546.

7. Lavis L. D. and Raines R. T., Bright Building Blocks for Chemical Biology, *ACS Chem. Biol.*, **2014**, *9*, 855–866.

8. Lakowicz J. R., *Principles of Fluorescence Spectroscopy*, 3rd edition, Springer, New York, 2006, 529-569.

9. Lavis L. D. and Raines R. T., Bright Ideas for Chemical Biology, *ACS Chem. Biol.*, **2008**, *3*, 142-155.

10. Bright F. V. and Munson C. A., Time-resolved fluorescence spectroscopy for illuminating complex systems, *Anal. Chim. Acta,* **2003**, *500*, 71-104.

11. Owicki J. C., Fluorescence polarization and anisotropy in high throughput screening: perspective and primer, *J. Biomol.* Screening, **2000**, *5*, 297-306.

12. Kiyose K.; Kojima H. and Nagamo T., Functional near-infrared fluorescent probes, *Chem. Asian J.*, **2008**, *3*, 506-515.

13. Heilemann, M., Fluorescence microscopy beyond the diffraction limit, *J. Biotechnol*, **2010**, *149*, 242–251.

14. Microscopy Resource Center, https://www.olympus-lifescience.com/en/microscope-resource, Olympus Microscopy (8.3.2018).

15. Betzig E., Patterson G. H., Sougrat R., Lindwasser O. W., Olenych S., Bonifacino J. S., Davidson M. W., Lippincott-Schwartz J. and Hess H. F., Imaging Intracellular Fluorescent Proteins at Nanometer Resolution, *Science*, **2006**, *313*, 1642–1645.

16. Zaikova T. O., Rukavishnikov A. V., Birell G. B., Griff O. H. and Keana J. F. W., Synthesis of fluorogenic substrates for continuous assay of phosphatidylinositol-specific phospholipase C, *Bioconjugate Chem.*, **2001**, *12*, 307-313.

17. Jyaram S. and Verkmann A. S., Quenching mechanism of quinolinium-type chloride-sensitive fluorescent indicators, *Bio-phys. Chem.*, **2000**, *85*, 49-57.

18. Tsien R. Y., New calcium indicators and buffers with high selectivity against magnesium and protons: design, synthesis, and properties of prototype structures, *Biochemistry*, **1980**, *19*, 2396-2404.

19. Burdette S. C. and Lippard S. J., The rhodafluor family. An initial study of potential ratiometric fluorescent sensors for Zn^{2+}, *Inorg. Chem.*, **2002**, *41*, 6816-1823.

20. Martin V. V., Rothe A. and Gee K. R., Fluorescent metal ion indicators based on benzoannelated crown systems: a green fluorescent indicator for intracellular sodium ions, *Bioorg. Med. Chem. Lett.*, **2005**, *15*, 1851-1855.

21. Gonçalves M. S. T., Fluorescent labelling of biomolecules with organic probes, *Chem. Rev.*, **2009**, *109*, 190-212.

22. Basabe-Desmonts L., Reinhoudt D. N. and Crego-Calama M., Design of fluorescent materials for chemical sensing, *Chem. Soc. Rev.*, **2007**, *36*, 993-1017.

23. Kobayashi H., Ogawa M., Alford R., Choyke P. L. and Urano Y., New strategies of fluorescent probe design in medical diagnostic imaging, *Chem. Rev.*, **2010**, *110*, 2620-2640.

24. Komatsu H., Miki T., Citterio D., Kubota T., Shindo Y., Kitamura Y., Oka K. and Suzuki K., Single molecular multianalyte (Ca^{2+}, Mg^{2+}) fluorescent probe and applications to bioimaging, *J. Am. Chem. Soc.*, **2005**, *127*, 10798-10799.

25. Frade V. H. J., Coutinho P. J. G., Moura J. C. V. P. and Gonçalves M. S. T, Functionalised benzo[a]phenoxazine dyes as long-wavelength fluorescent probes for amino acids, *Tetrahedron*, **2007**, *63*, 1654-1663.

26. Chen X., Wang X., Wang S., Shi W., Wang K. and Ma H., A highly selective and sensitive fluorescence probe for the hypochlorite anion, *Chem. Eur. J.*, **2008**, *14*, 4719-4724.

27. Kwon J. Y., Jagn Y. J., Lee Y. J., Kim K. M., Seo M. S., Nam W. and Yoon J., A highly selective fluorescent chemosensor for Pb^{2+}, *J. Am. Chem. Soc.*, **2005**, *127*, 10107-10111.

28. Han J., Loudet A., Barhoumi R., Burghardt R. C. and Burgess K., A ratiometric pH receptor for imaging protein-dye conjugates in living cells, *J. Am. Chem. Soc.*, **2009**, *131*, 1642-1643.

29. Campbell N. A., Urry L. A., Chain M. L., Wasserman S. A., Minorsky P. V. and Reece J. B., *Biology: A Global Approach*, 11th edition, Pearson, Boston, 2018, 120-123.

30. Sud M., Fahy E., Cotter D., Brown A., Dennis E. A., Glass C. K., Merill A. H. Jr., Murphy R. C., Raetz C. R. H., Russell D. W. and Subramanian S., LMSD: Lipid maps structure database, *Nucleic Acids Res.*, **2007**, *35*, D527-D532.

31. van Meer G., Voelker D. R. and Feigenson G. W., Membrane lipids: where they are and how they behave, *Nat. Rev. Mol. Cell. Biol.*, **2008**, *9*, 112-124.

32. Jansen M. A. J., *Using Fluorescent and Non-Fluorescent Sterols to Study Rafts and Intracellular Cholesterol Transport in Mammalian Cells*, Dissertation, University of Helsinki, Faculty of Medicine, Institute of Biomedicine/Anatomy, Helsinki, 2011.

33. Dowhan W. and Bogdanov M., *Biochemistry of lipids, lipoproteins and membranes*, 4th edition, Elsevier Science B. V., 2002, 1-35.

34. Ikonen E., Cellular cholesterol trafficking and compartmentalization, *Nat. Rev. Mol. Cell. Biol.*, **2008**, *9*, 125-138.

35. Bloch K., The biological synthesis of cholesterol, *Vitam. Horm.*, **1957**, *15*, 119–150.

36. Kandutsch A. A. and Russell A. E., Preputial Gland Tumor Sterols III. A Metabolic Pathway from Lanosterol to Cholesterol, *J. Biol. Chem.*, **1960**, *235*, 2256–2261.

37. Goldstein J. L., DeBose-Boyd R. A. and Brown M. S., Protein sensors for membrane sterols, *Cell*, **2006**, *124*, 35-46.

38. Radhakrishnan A., Ikeda Y., Kwon H. J., Brown M. S. and Goldstein J. L., Sterol-regulated transport of SREBs from endoplasmic reticulum to Golgi: Oxysterols block transport by binding to Insig, *Proc. Natl Acad. Sci.*, **2007**, *104*, 6511-6518.

39. Sun L.-P., Seemann J., Goldstein J. L. and Brown M. S., Sterol regulated transport of SREBPs from endoplasmic reticulum to Golgi: Insig renders sorting signal in Scap inaccessible to COPII proteins, *Proc. Natl Acad. Sci*, **2007**, *104*, 6519-6526

40. Sun L.-P., Li L., Goldstein J. L. and Brown M. S., Insig required for sterol-mediated inhibition of Scap/SREBP binding to COPII proteins in vitro, *J. Biol. Chem.*, **2005**, *280*, 26483-26490.

41. Tontonoz P. and Mangelsdorf D. J., Liver X receptor signaling pathways in cardiovascular disease, *Mol. Endocrinol*, **2003**, *17*, 985-993.

42. Yan D., Mäyränpää M. J., Wong J., Perttilä J., Lehto M., Jauhiainen M., Kovanen P. T., Ehnholm C., Brown A. J. and Olkkonen V. M., OSBP-related protein 8 (ORP8) suppresses ABCA1 expression and cholesterol efflux from macrophages, *J. Biol. Chem.*, **2008**, *283*, 332-340.

43. Martin S. and Parton R. G., Caveolin, cholesterol and lipid bodies, *Semin. Cell Dev. Biol.*, **2005**, *16*, 163-174.

44. Tauchi-Sato K., Ozeki S., Houjou T., Taguchi R and Fujimato T., The surface of lipid droplets is a phospholipid monolayer with a unique fatty acid composition, *J. Biol. Chem.*, **2002**, *277*, 44507-44512.

45. Liscum L. and Munn N. J., Intracellular cholesterol transport, *Biochim. Biophys. Acta*, **1999**, *1438*, 19-47.

46. van Meer G, Lipids of the Golgi membrane, *Trends Cell Biol.*, **1998**, *8*, 29-33.

47. Möbius W., Donselaar E. van, Ohno-Iwashita Y., Shimada Y., Heijnen H. F., Slot J. W. and Gerize H. J., Recycling compartments and the internal vesicles of multivesicular bodies harbor most of the cholesterol found in the endocytic pathway, *Traffic*, **2003**, *4*, 222-231.

48. Hao M., Lin S. X., Karylowski O. J., Wurstner D., McGraw T. E. and Maxfield F. R., Vesicular and non-vesicular sterol transport in living cells, *J. Biol. Chem.*, **2002**, *277*, 609-617.

49. Vihervaara T., Jansen M., Uronen R.-L., Oksaki Y., Ikonen E. and Olkkonen V. M., Cytoplasmic oxysterol-binding proteins: sterol sensor or transporters?, *Chem. Phys. Lipids*, **2011**, *164*, 443-450.

50. Luo J., Jiang L, Yang H. and Song B.-L., Routes and mechanisms of post-endosomal cholesterol trafficking: a story that never ends, *Traffic*, **2017**, *18*, 209-217.

51. Pfisterer S. G., Peränen J. and Ikonen E., LDL-cholesterol transport to the endoplasmic reticulum: current concepts, *Curr. Opin. Lipids*, **2016**, *27*, 282-287.

52. Arenas F., Garcia-Ruiz C. and Fernandez-Chera J. C., Intracellular cholesterol trafficking and impact in neurodegeneration, *Front. Mol. Neurosci*., **2017**, *10*, 1-25.

53. Yang W., Bai Y., Xiong Y., Zhang J., Chen S., Zheng X., Meng X., Li L., Wang J., Xu C., Yan C., Wang L., Chang C. C. Y., Chang T.-Y., Zhang T., Zhou P., Song B.-L., Liu W., Sun S.-C., Liu X., Li B.-l. and Xu C., Potentiating the antitumour response of CD8+ T cells by modulating cholesterol metabolism, *Nature,* **2016**, *531,* 651–655.

54. Gamba P., Testa G., Sottero B., Gargiulo S., Poli G. and Leonarduzzi G, The link between altered cholesterol metabolism and Alzheimer disease, *Ann. N. Y. Acad. Sci.*, **2012**, *1529*, 54-64.

55. McIntosh A. L., Gallegos A. M., Asthaves B. P., Storey S. M., Kannoju D. and Schroeder F., Fluorescence and multiphoton imaging resolve unique structural forms of sterol in membranes of living cells, *J. Biol. Chem.*, **2003**, *278*, 6384-6403.

56. Pourmousa M., Ròg T., Mikkeli R., Vattulainen I., Solanko L. M., Würsteiner D., Holmgaar List N., Kongsted J. and Karttunen M., Dehydroergosterol as an analogue for cholesterol: Why it mimics cholesterol so well – or does it?, *J. Phys. Chem.*, **2014**, *118*, 7345-7357.

57. Wüstner D., Brewer J. R., Bagatolli L. and Sage D., Potential of ultraviolet wide-field imaging and multiphoton microscopy for analysis of dehydroergosterol in cellular membranes, *Microsc. Res. Tech.*, **2011**, *74*, 92-108.

58. Wüstner D. and Faergemann N. J., Spatiotemporal analysis of endocytosis and membrane distribution of fluorescent sterols in living cells, *Histochem. Cell. Biol.*, **2008**, *130*, 891-908.

59. Scheidt H. A., Müllers P., Herrmann A. and Huster D., The potential of fluorescent and spin-labeled steroid analogs to mimic natural cholesterol, *J. Biol. Chem.*, **2003**, *278*, 45553-45569.

60. Ngo M. and Ridgway N. D., Oxysterol binding protein-related protein 9 (OPR9) is a cholesterol transfer protein that regulates Golgi structure and function, *Mol. Biol. Cell.*, **2009**, *20*, 1388-1399.

61. Krieger M., Brown M. S., Faust J. R. and Goldstein J. L., Replacement of endogenous cholesteryl esters of low-density lipoprotein with exogenous cholesteryl linoleate – reconstitution of a biologically-active lipoprotein particle, *J. Biol. Chem.*, **1978**, *253*, 4093-4101.

62. Lee S. J., Gray K. C., Paek J. S. and Burke M. D., Simple, efficient, and modular syntheses of polyene natural products via iterative cross-coupling, *J. Am. Chem. Soc.*, **2008**, *130*, 466-468.

63. Sklar L. A., Hudson B. S. and Simoni R. D., Conjugated polyene fatty acids as fluorescent probes: Synthetic phospholipid membrane studies, *Biochemistry*, **1977**, *16*, 819-828.

64. Benson D. M., Bryan J., Plant A. L., Gotto Jr. A. M. and Smith L. C., Digital imaging fluorescence microscopy: spatial heterogeneity of photobleaching rate constant in individual cells, *J. Cell. Biol.*, **1985**, *100*, 1309-1323.

65. Craig J. F., Via D. P., Mantulin W. W., Pownall H. J., Gotto Jr. A. M. and Smith L. C., Low density lipoproteins reconstituted with steroids containing the nitrobenzoxadiazole fluorophore, *J. Lipid. Res.*, **1981**, *22*, 687-696.

66. Mark D. L., Bittman R. and Pagano R. E., Use of bodipy-labeled sphingolipid and cholesterol analogs to examine membrane microdomains in cell, *Histochem Cell Biol.,* **2008**, *130*, 819-832.

67. Li Z., Mintzer E. and Bittman R., First synthesis of free cholesterol-BODIPY conjugates, *J. Org. Chem.*, **2006**, *71*, 1718-1721.

68. Lund F. W., Lomholt M. A., Solanko L. M., Bittman R. and Wüstner D., Two-photon time-lapse microscopy of BODIPY-cholesterol reveals anomalous sterol diffusion in Chinese hamster ovary cells, *BCM. Biophys.*, **2012**, *5*, 1-15.

69. Solanko L. M., Honigmann A., Midtiby H. S., Lund F. W., Brewer J. R., Dekaris V., Bittman R., Eggeling C. and Wüstner D., Membrane orientation and lateral diffusion of BODIPY-cholesterol as a function of probe structure, *Biophys J.*, **2013**, *105*, 2082-2092.

70. Wüstner D., Lund F. W., Röhrl C. and Stangl H., Potential of BODIPY-cholesterol for analysis of cholesterol transport and diffusion in living cells, *Chem. Phys. Lipids.,* **2016**, *194*, 12-28.

71. Bernik D. L. and Negri R. M., Local polarity at the polar head level of lipid vesicles using dansyl fluorescent probes, *J. Colloid Interface Sci*., **1998**, *203*, 97-105.

72. Wiegand V., Chang T.-Y., Strauss, III, J. F., Fahrenholtz F and Gimpl G., Transport of plasma membrane-derivated cholesterol and the function of Niemann-Pick C1 protein, *FASEB J.,* **2003**, *17*, 782-784.

73. Sezgin E., Can F. B., Scheiner F., Clausen M. P., Galiani S., Stanly T. A., Waithe D., Colaro A., Honigmann A., Wüstner D., Platt F. and Eggeling C., A comparative study on fluorescent cholesterol analogs as versatile cellular reporters, *J. Lipid. Res.,* **2016**, *57*, 299-309.

74. Guyader L. L., Roux C. L., Mazéser S., Gaspard-Iloughmane H., Gornitzka H., Millot C., Mingotaud C. and Lopez A., Changes of the membrane lipids organization characterized by means of a new cholesterol-pyrene probe, *Biophys J.,* **2007**, *93*, 4462-4473.

75. Lusa S., Tanhuanpää K., Ezra T. and Somerharju P., Direct observation of lipoprotein cholesterol ester degradation in lysosomes, *Biochem J.,* **1998**, *332*, 451-457.

76. Kolb H. C. and Sharpless K. B., The growing impact of click chemistry on drug discovery, *Drug Discov. Today*, **2003**, *8*, 1128-1137.

77. Hoffmann K., Thiele C., Schött H.-F., Gaebler A., Shoene M., Kiver Y., Friedrichs S., Lütjohann D. and Kuerschner L., A novel alkyne cholesterol to trace cellular cholesterol metabolism and localization, *J. Lipid Res.*, **2014**, *55*, 583-591.

78. Supplemental Text, Reference 76.

79. Hu J., Zhang Z., Shen W.-J. and Azhar S., Cellular cholesterol delivery, intracellular processing and utilization for biosynthesis of steroid hormones, *Nutr. Metab.*, **2010**, *7*, 1-25.

80. Moss G. P., Nomenclature of steroids (Recommendations 1989), *Pure&Appl. Chem.*, **1989**, *61*, 1783-1822.

81. Olazarán J., Gil-de-Gómez L., Rodríguez-Martín A., Valentí-Soler M., Frades-Payo B., Marín-Munóz J., Antúnez C., Frank-García A., Acedo-Jiménez C., Morlán-Gracia L., Petidier-Torregrossa R., Concepción Guisasola M., Berjemo-Pareja F., Sánchez-Ferro A., Pérez-Marťinez D. A., Manzano-Palomo S., Farquhar R., Rábano A. and Calero M., A Blood-Based, 7-Metabolite Signature for the Early Diagnosis of Alzheimer's Disease, *J. Alzheimer`s Dis.*, **2015**, *45*, 1157-1173.

82. Qian X., Zhan Q., Lv L., Zhang H., Hong Z., Li Y., Xu H., Chai Y., Zhao L. and Zhang G., Steroid hormone profiles plus α-fetoprotein for diagnosing primary liver cancer by liquid chromatography tandem mass spectrometry, *Clin. Chim. Acta,* **2016**, *457*, 92-98.

83. Liu L., Wang M., Yang X., Bi M., Na L., Niu Y. and Sun C., Fasting serum lipid and dehydroepiandrosterone sulfate as important metabolites for detecting isolated postchallenge diabetes: serum metabolomics via ultra-high- performance LC-MS, *Clin. Chem.*, **2013**, *5*, 1338-1348.

84. Hofmann A. F. and Hagey L. R., Bile acids: Chemistry, Pathochemistry, Biology, Pathobiology, and Therapeutics, *Cell. Mol. Life Sci,* **2008**, *65*, 2461-2483.

85. Sjövall J., Fifty years with bile acids and steroids in health and disease, *Lipids,* **2004**, *39*, 703-722.

86. Hylemon P. B., Zhou H., Pandak W. M., Ren S., Gill G. and Dent P., Bile acids as regulatory molecules, *J. Lipid. Res.*, **2009**, *50*, 1509-1520.

87. Gosetti F., Mazzucco E., Gennamo M. C. and Mareny E., Ultra high performance liquid chromatography tandem mass spectrometry determination and profiling of prohibited steroids in human biological matrices, *J. Chromatogr. B*, **2013**, *927*, 22-36.

88. Tai C.-H., Lu C.-P., Wu S.-H. and Lo L.C., Synthesis and evaluation of turn-on fluorescent probes for imaging steroid sulfatase activities in cells, *Chem. Commun.*, **2014**, *50*, 6116-6119.

89. Tsai C.-Y., Li C.-W., Li J.-R., Jany B.-H. and Chen S.-H., Steroid probes conjugated with protein-protected gold nanocluster: specific and rapid fluorescence imaging of steroid receptors in target cells, *J. Fluoresc.*, **2016**, *26*, 1239-1248.

90. McCarthy K. S. Jr., Woodman B. H., Nichols D. E., Wilkinson W. and McCarthy K. S. Sr., Comparison of biochemical and histological techniques for estrogen receptor analyses in mammary carcinoma, *Cancer*, **1980**, *46*, 2842-2845.

91. Underwood J. C. E., Shen E., Reed M., Eisman J. A. and Martin T. J., Biochemical assessment of histochemical methods for oestrogen receptor localisation, J. Clin. Pathod., **1982**, *35*, 401-406.

92. Chamness G. C., Mercer W. D. and McGuire W. L., Are histochemical methods for estrogen receptor valid?, *J. Histochem. Cytochem.*, **1980**, *28*, 792-798.

93. Sumpter J. P., Endocrine disrupters in the aquatic environment: an overview, *Acta Hydrochim. Hydrobilol.,* **2005**, *33*, 9-16.

94. Gross-Sorokin M. Y., Roast S. D. and Brightly G. C., Assessment of feminization of male fish in english rivers by the environment agency of England and Wales, *Environ. Health Perspect.*, **2016**, *114*, 147-151.

95. Kidd K. A., Blanchfield P. J., Mills K. H., Palace V. P., Evans R. E., Lazorchak J. M. and Flick R. W., Collapse of a fish population after exposure to a synthetic estrogen, *Proc. Natl. Acad. Sci. U.S.A*, **2007**, *104,* 8897-8901.

96. Angus R. A., McNatt H. B., Howelt W. M. and Peoples S. D., Gonopodium development in normal male and 11-ketotestosterone-treated female mosquitofish (*Gambusia affinis)*: a quantitative study using computer image analysis, *Gen. Com. Endocrinol.*, **2001**, *123*, 222-234.

97. Stahl A., Lazar A. J., Muchemu V. N., Mau W. M., Ullrich M. S. and Hennig A., A fluorescent, supramolecular chemosensor to follow steroid depletion in bacterial cultures, *Anal. Bioanal. Chem.*, **2017**, *409*, 6485-6494.

98. You L., Zha D. and Anslyn E. V., Recent advances in supramolecular analytical chemistry using optical sensing, *Chem. Rev.*, **2015**, *115*, 7840-7892.

99. Màjer F., Salomon J. J., Sharma R., Etzbach S. V., Najid M. N. M., Keaveny R., Long A. Wang J., Ehrhardt C. and Gilmer J. F., New fluorescent bile acids: Synthesis, chemical characterization, and diastereoselective uptake by Caco-2 cells of 3-deoxy 3-NBD-amino deoxycholic acid and ursodeoxycholic acid, *Bioorg. Med. Chem.*, **2012**, *20*, 1767-1778.

100. Berstein C., Holubec H., Bhattacharyya A. K., Nguyen H., Payne C. M., Zaitlin B. and Berstein H, Carcinogenicity of deoxycholate, a secondary bile acid, *Arch. Toxicol.*, **2011**, *85*, 863-871.

101. Zhou Y., Doyen R. and Lichtenberger L. M., The role of membrane cholesterol in determining bile acid cytotoxicity and cytoprotection of ursodeoxycholic acid, *Biochim. Biophys. Acta.*, **2009**, *1788*, 507-513.

102. Amaral J. D., Viana R. J. S., Ramalho R. M., Steer C. J. and Rodrigues C. M. P., Bile acids: regulation of apoptosis by ursodeoxycholic acid, *J. Lipid. Res.*, **2009**, *50*, 1721-1734.

103. Byrne A.-M., Foran E., Sharma R., Davies A., Mahon C., O´Sullivan J., O´Donoghue D., Kelleher D. and Long A., Bile acids modulate the Golgi membrane fission process via a protein kinese Cη and protein kinase D-dependent pathway in colonic epithelic cells, *Carcinogenesis,* **2010**, *31*, 737-744.

104. Morzycki J. W., Recent advances in cholesterol chemistry, *Steroids*, **2014**, *83*, 62-79.

105. Motoyama K., Nishiyama R., Maeda Y., Higashi T., Ishitsuka Y., Kondo Y., Irie T., Era T. and Arima H., Synthesis of multi-lactose-appended β-cyclodextrin and its cholesterol-lowering effects in Niemann-Pick type C disease-like HepG2 cells, *Beilstein J. Org. Chem.*, **2017**, *13*, 10-18.

106. Ono Y., Kawase A., Watanabe H., Shiraiski A., Takeda S., Higurchi Y., Sato K., Yamauchi T., Mikami T., Kato M., Tsugawa N., Okamo T. and Kubodera N., Synthesis and preventive effects of analogues related to 1α,25-Dihydroxy-2β-(3-hydroxypropoxy)vitamin D_3 (ED-71) on bone mineral loss in ovariectomized rats, *Bioorg. Med. Chem.*, **1998**, *6*, 2517-2523.

107. Kolehmainen E., Tamminen J., Lappalainen K, Torkkel T. and Seppälä R., Substituted methyl 5β-Cholan-24-oates; Part III: Synthesis of novel cholaphane from ethylene glycol diester of lithocholic acid by cyclization with terephthalic acid, *Synthesis*, **1996**, 1082-1084.

108. Inanaga J., Hirata K., Saeki H., Katsuki T., and Yamaguchi M., A rapid esterification by means of mixed anhydride and its application to large-ring lactonization, *Bull. Chem. Soc. Jpn.*, **1979**, *52*, 1989-1993.

109. Virtanen E., Tamminen J., Linnanto J., Mänttäri P., Vainiotalo P. and Kolehmainen E., Synthesis, ^{1}H, ^{13}C, ^{15}N, and ^{113}Cd NMR, ESI-TOF MS, semiempirical MO (PM3), *ab inito/*HF and cation/anion binding studies of N-deoxycholyl-L-tryptophan, *J. Inclusion Phenom. Macrocyclic Chem.*, **2002**, *43*, 319-327.

110. Noponen V., Nonappa, Lahtinen M., Valkonen A., Salo H., Kolehmainen E. and Sievänen E., Bile acid-amino acid ester conjugates: gelation, structural properties, and thermoreversible solid to solid phase transition, *Soft Matter*, **2010**, *6*, 3789-3796.

111. Noponen V., Valkonen A., Lahtinen M., Salo H. and Sievänen E., Self-assembly properties of bile acid derivatives of l-cysteine, l-valine, and l-serine alkyl esters, *Supramol. Chem.*, **2012**, *25*, 133-145.

112. Pandey P. S., Rai R. and Sigh R. B., Synthesis of cholic acid-based molecular receptors: head-to-head cholaphanes, *J. Chem. Soc., Perkin Trans 1*, **2002**, 918-923.

113. Bonar-Law R. P., Davis A. P. and Sanders K. M., A rapid esterification by means of mixed anhydride and its application to large-ring lactonization, *J. Chem. Soc., Perkin Trans 1*, **1990**, 2245-2250.

114. Coupling reagents and additives offered by Bachem, http://documents.bachem.com/coupling_reagents.pdf (26.3.2019).

115. Funosos-Subiròs R., El-Faham A. and Albericio F., Low-epimerization Peptide Bond Formation with Oxyma Pure: Preparation of Z-*L*-Phg-Val-OMe, *Org. Synth.*, **2013**, *90*, 306-315.

116. Clayden J., Greevs N., Warren S., *Organic Chemistry*, 2. ed., OUP Oxford, 2012, 747.

117. Montalbetti C. A. G. N. and Falque V., Amide bond formation and peptide coupling, *Tetrahedron*, **2005**, *61*, 10827-10852.

APPENDIX

APPENDIX 1

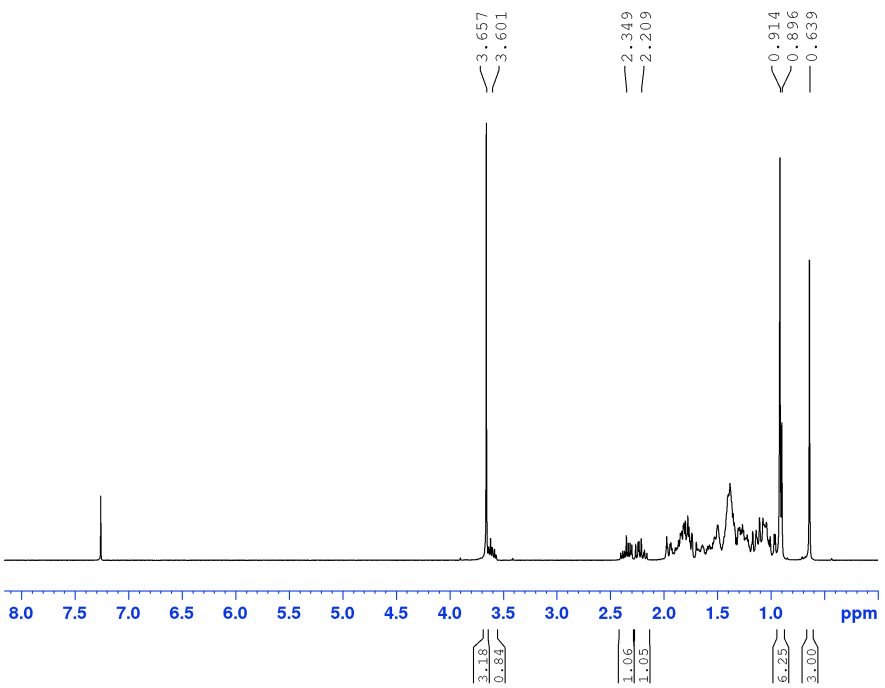


```
Current Data Parameters
NAME                  JA-005
EXPNO                      1
PROCNO                     1

F2 - Acquisition Parameters
Date_              20170504
Time                 15.25 h
INSTRUM              spect
PROBHD    Z104275_0269 (
PULPROG              zg30
TD                  32768
SOLVENT              CDCl3
NS                       8
DS                       0
SWH               3898.129 Hz
FIDRES            0.237923 Hz
AQ                4.2030420 sec
RG                   151.8
DW                 128.267 usec
DE                   6.50 usec
TE                  303.2 K
D1              2.00000000 sec
TD0                      1
SFO1           300.1516625 MHz
NUC1                    1H
P1                   14.00 usec
PLW1           7.90000010 W

F2 - Processing parameters
SI                  131072
SF             300.1500070 MHz
WDW                    EM
SSB       0
LB                   0.10 Hz
GB        0
PC                   1.00
```

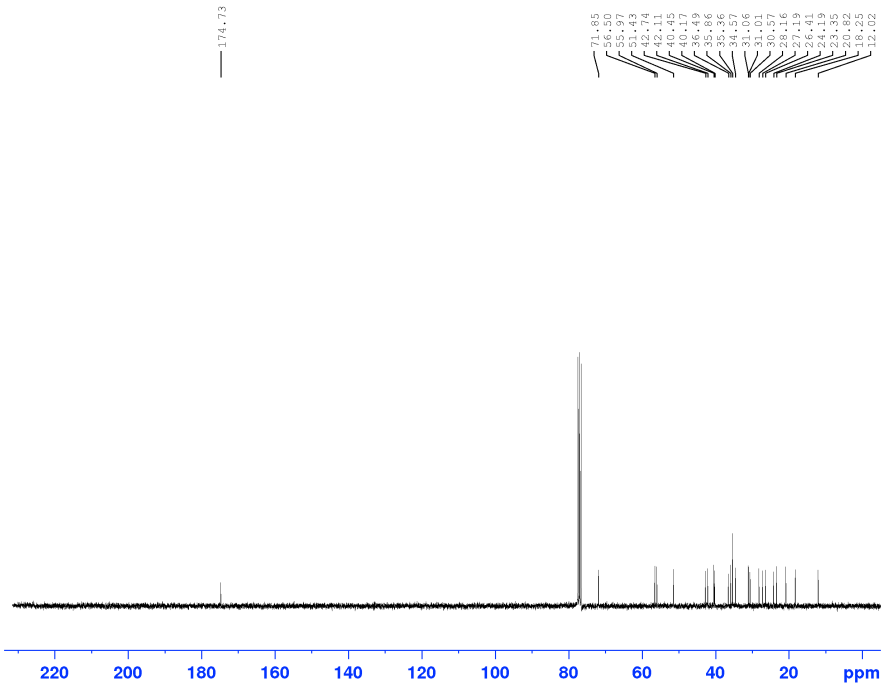


```
Cur
NAME                  JA-005
EXPNO                    101
PROCNO                     1

F2 - Acquisition Parameters
Date_              20170504
Time                 15.42 h
INSTRUM              spect
PROBHD    Z104275_0269 (
PULPROG           zgpg30
TD                  65536
SOLVENT              CDCl3
NS                     217
DS                       0
SWH              18028.846 Hz
FIDRES            0.550197 Hz
AQ                1.8175317 sec
RG                   210.25
DW                  27.733 usec
DE                   6.50 usec
TE                  303.3 K
D1              2.00000000 sec
D11             0.03000000 sec
TD0                   1024
SFO1           75.4812305 MHz
NUC1                   13C
P1                   10.00 usec
PLW1           31.98900032 W
SFO2          300.1530015 MHz
NUC2                    1H
CPDPRG[2          waltz16
PCPD2                90.00 usec
PLW2           7.90000010 W
PLW12          0.15706000 W
PLW13          0.07900000 W

F2 - Processing parameters
SI                  65536
SF             75.4727787 MHz
WDW                    EM
SSB       0
LB                   1.00 Hz
GB        0
PC                   1.40
```

APPENDIX 2

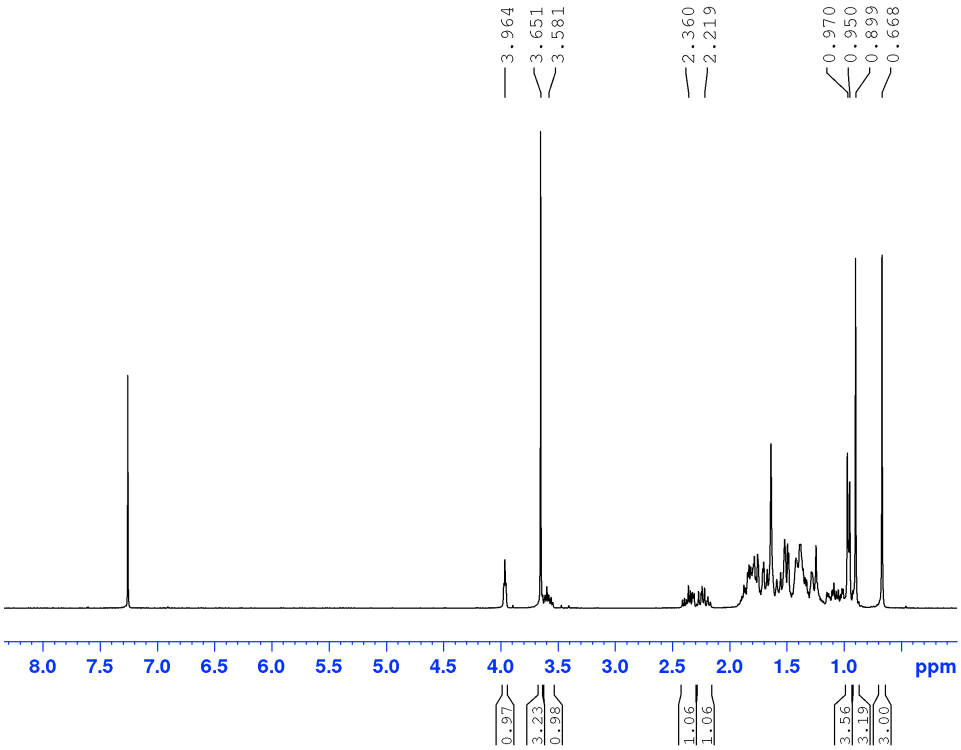


```
Current Data Parameters
NAME                  JA-007
EXPNO                      1
PROCNO                     1

F2 - Acquisition Parameters
Date_              20170523
Time                 15.39 h
INSTRUM                spect
PROBHD    Z104275_0269 (
PULPROG                zg30
TD                    32768
SOLVENT               CDCl3
NS                        8
DS                        0
SWH               3898.129 Hz
FIDRES           0.237923 Hz
AQ               4.2030420 sec
RG                   119.32
DW                  128.267 usec
DE                     6.50 usec
TE                    303.2 K
D1              2.00000000 sec
TD0                       1
SFO1           300.1516625 MHz
NUC1                     1H
P1                    14.00 usec
PLW1           7.90000010 W

F2 - Processing parameters
SI                   131072
SF           300.1500075 MHz
WDW                      EM
SSB       0
LB                    0.10 Hz
GB        0
PC                    1.00
```

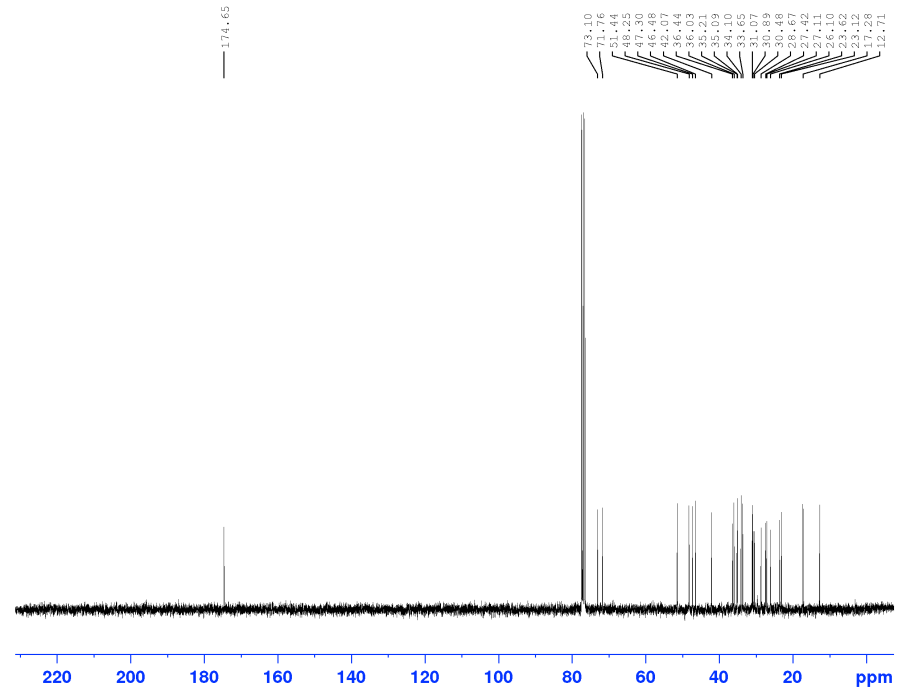


```
Current Data Parameters
NAME                  JA-007
EXPNO                    101
PROCNO                     1

F2 - Acquisition Parameters
Date_              20170523
Time                 15.55 h
INSTRUM                spect
PROBHD    Z104275_0269 (
PULPROG             zgpg30
TD                    65536
SOLVENT               CDCl3
NS                      201
DS                        0
SWH              18028.846 Hz
FIDRES           0.550197 Hz
AQ               1.8175317 sec
RG                   210.25
DW                   27.733 usec
DE                     6.50 usec
TE                    303.3 K
D1              2.00000000 sec
D11             0.03000000 sec
TD0                    1024
SFO1           75.4812305 MHz
NUC1                     13C
P1                    10.00 usec
PLW1           31.98900032 W
SFO2          300.1530015 MHz
NUC2                     1H
CPDPRG[2          waltz16
PCPD2                 90.00 usec
PLW2           7.90000010 W
PLW12          0.15706000 W
PLW13          0.07900000 W

F2 - Processing parameters
SI                    65536
SF           75.4727797 MHz
WDW                      EM
SSB       0
LB                    1.00 Hz
GB        0
PC                    1.40
```

APPENDIX 3

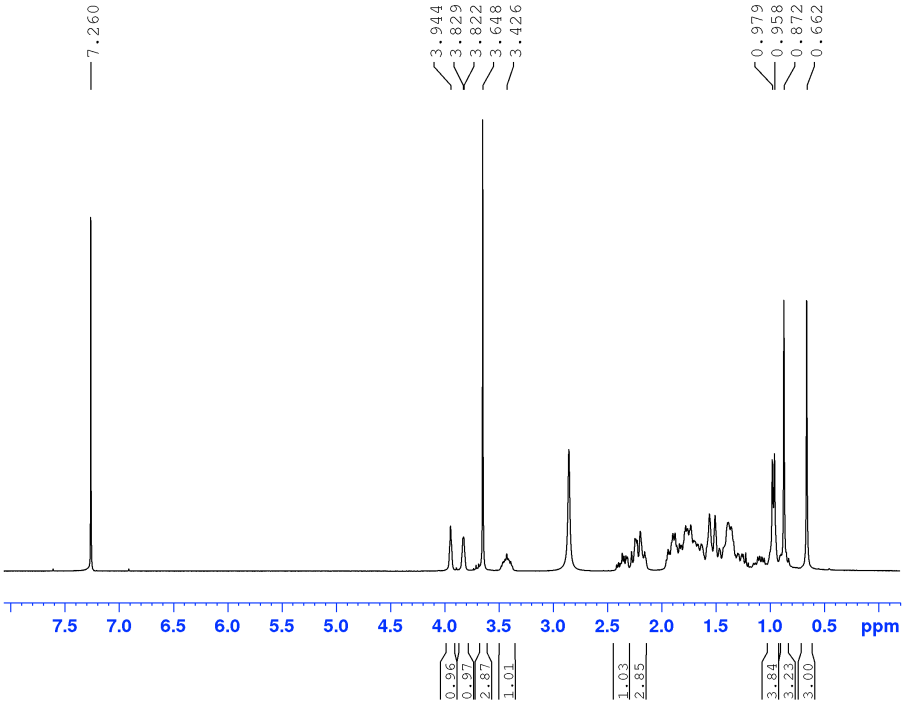

BRUKER

```
Current Data Parameters
NAME                 OGT-040
EXPNO                      4
PROCNO                     1

F2 - Acquisition Parameters
Date_               20180803
Time                   11.05 h
INSTRUM                spect
PROBHD    Z104275_0269 (
PULPROG                zg30
TD                    32768
SOLVENT               CDCl3
NS                         8
DS                         0
SWH                3898.129 Hz
FIDRES            0.237923 Hz
AQ                4.2030420 sec
RG                     92.42
DW                  128.267 usec
DE                    6.50 usec
TE                   303.2 K
D1              2.00000000 sec
TD0                        1
SFO1           300.1516625 MHz
NUC1                      1H
P1                    14.00 usec
PLW1            7.90000010 W

F2 - Processing parameters
SI                    131072
SF           300.1500078 MHz
WDW                       EM
SSB       0
LB                     0.10 Hz
GB        0
PC                     1.00
```

APPENDIX 4

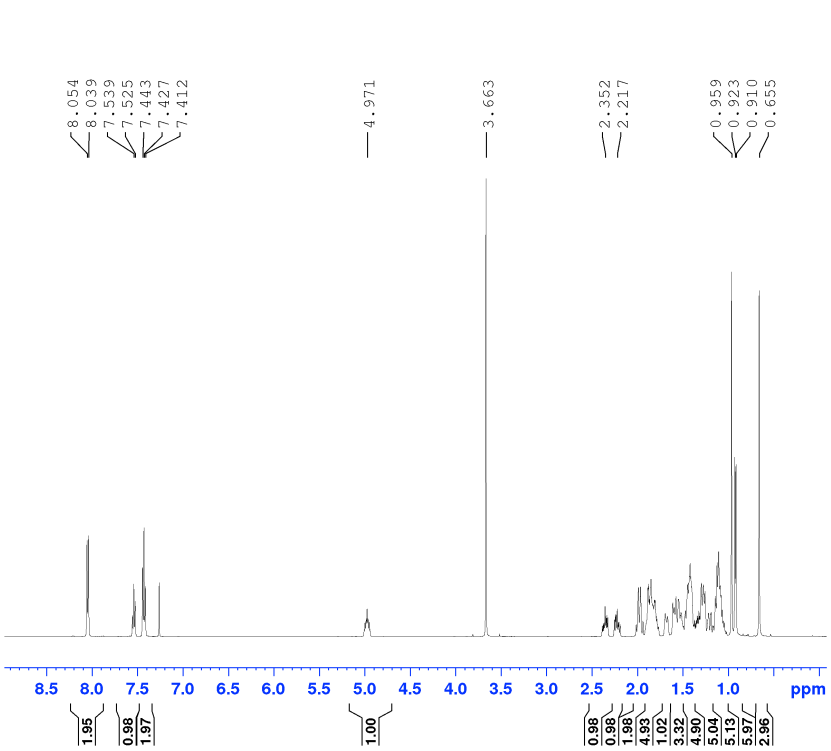

BRUKER

```
Current Data Parameters
NAME                 OGT-006-1
EXPNO                        1
PROCNO                       1

F2 - Acquisition Parameters
Date_               20171026
Time                    2.30 h
INSTRUM                spect
PROBHD     Z135420_0012 (
PULPROG                zg30
TD                    65536
SOLVENT               CDCl3
NS                       16
DS                        0
SWH                6009.615 Hz
FIDRES            0.183399 Hz
AQ                5.4525952 sec
RG                       16
DW                   83.200 usec
DE                    6.50 usec
TE                   298.1 K
D1                1.00000000 sec
TD0                       4
SFO1           500.1324006 MHz
NUC1                     1H
P1                    9.00 usec
PLW1          12.00000000 W

F2 - Processing parameters
SI                    65536
SF               500.1300122 MHz
WDW                      EM
SSB          0
LB                    0.30 Hz
GB           0
PC                    1.00
```

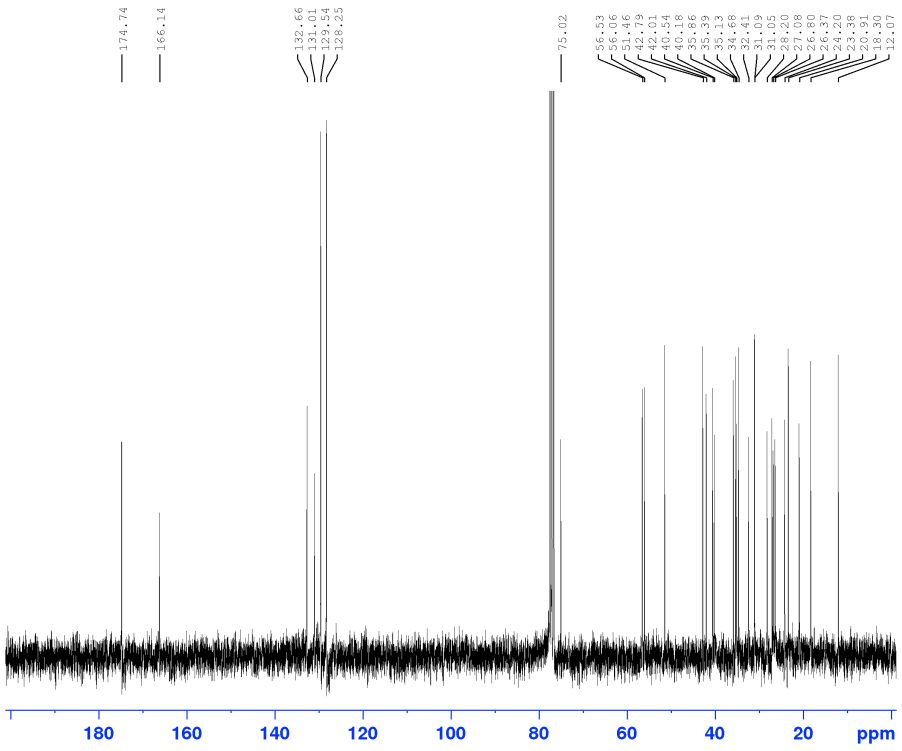

BRUKER

```
Current Data Parameters
NAME          OGT-006-kuivattu
EXPNO                      101
PROCNO                       1

F2 - Acquisition Parameters
Date_               20171005
Time                   12.07 h
INSTRUM                spect
PROBHD     Z104275_0269 (
PULPROG             zgpg30
TD                    65536
SOLVENT               CDCl3
NS                      353
DS                        0
SWH               18028.846 Hz
FIDRES            0.550197 Hz
AQ                1.8175317 sec
RG                   210.25
DW                   27.733 usec
DE                    6.50 usec
TE                   303.3 K
D1                2.00000000 sec
D11               0.03000000 sec
TD0                    1024
SFO1           75.4812305 MHz
NUC1                    13C
P1                   10.00 usec
PLW1          31.98900032 W
SFO2          300.1530015 MHz
NUC2                     1H
CPDPRG[2          waltz16
PCPD2                90.00 usec
PLW2           7.90000010 W
PLW12          0.15706000 W
PLW13          0.07900000 W

F2 - Processing parameters
SI                    65536
SF               75.4727769 MHz
WDW                      EM
SSB          0
LB                    1.00 Hz
GB           0
PC                    1.40
```

APPENDIX 5

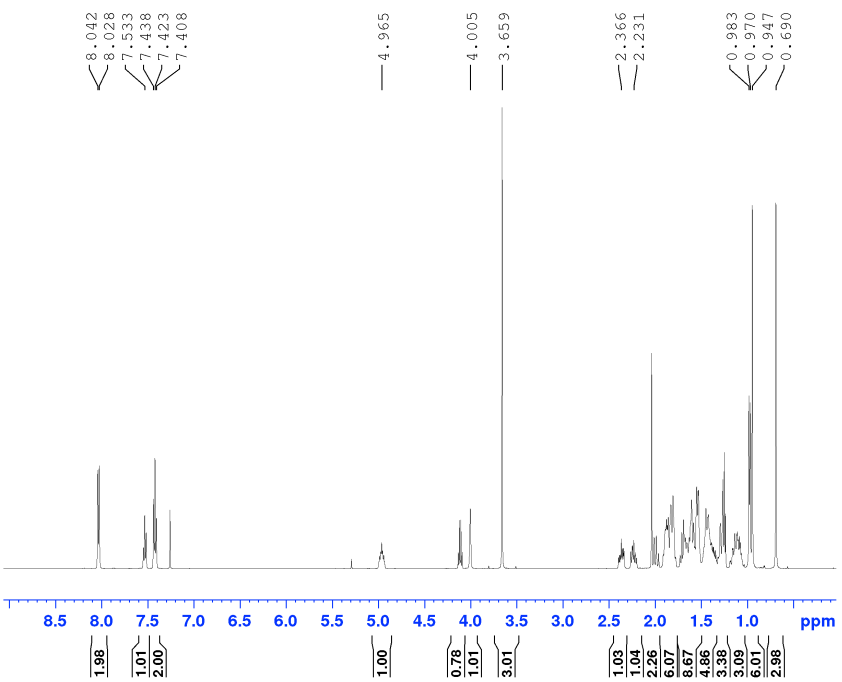


```
Current Data Parameters
NAME              OGT-008-1
EXPNO                     1
PROCNO                    1

F2 - Acquisition Parameters
Date_            20171026
Time                15.50 h
INSTRUM              spect
PROBHD    Z135420_0012 (
PULPROG              zg30
TD                  65536
SOLVENT             CDCl3
NS                     16
DS                      0
SWH              5482.456 Hz
FIDRES           0.167311 Hz
AQ               5.9768834 sec
RG                     18
DW                 91.200 usec
DE                  6.50 usec
TE                 298.1 K
D1              1.00000000 sec
TD0                     4
SFO1          500.1326035 MHz
NUC1                   1H
P1                  9.00 usec
PLW1         12.00000000 W

F2 - Processing parameters
SI                  65536
SF            500.1300117 MHz
WDW                    EM
SSB       0
LB                  0.30 Hz
GB        0
PC                  1.00
```

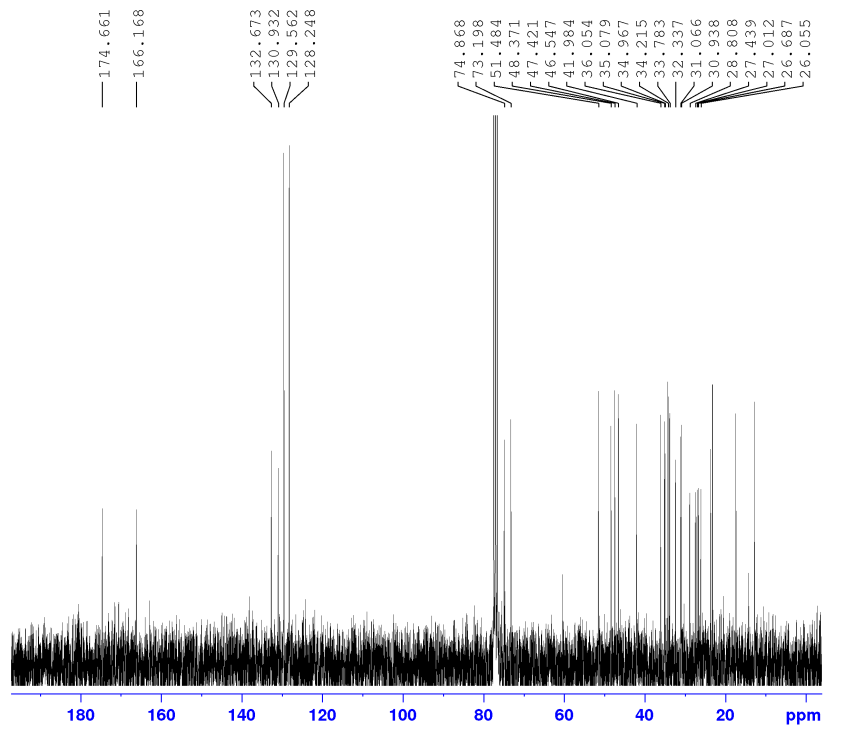


```
Current Data Parameters
NAME       OGT-008-kuivattu
EXPNO                   101
PROCNO                    1

F2 - Acquisition Parameters
Date_            20171005
Time                14.24 h
INSTRUM              spect
PROBHD    Z104275_0269 (
PULPROG            zgpg30
TD                  65536
SOLVENT             CDCl3
NS                    162
DS                      0
SWH             18028.846 Hz
FIDRES           0.550197 Hz
AQ               1.8175317 sec
RG                  210.25
DW                 27.733 usec
DE                  6.50 usec
TE                 303.3 K
D1              2.00000000 sec
D11             0.03000000 sec
TD0                  1024
SFO1          75.4812305 MHz
NUC1                  13C
P1                 10.00 usec
PLW1         31.98900032 W
SFO2         300.1530015 MHz
NUC2                   1H
CPDPRG[2          waltz16
PCPD2              90.00 usec
PLW2          7.90000010 W
PLW12         0.15706000 W
PLW13         0.07900000 W

F2 - Processing parameters
SI                  65536
SF            75.4727769 MHz
WDW                    EM
SSB       0
LB                  1.00 Hz
GB        0
PC                  1.40
```

APPENDIX 6

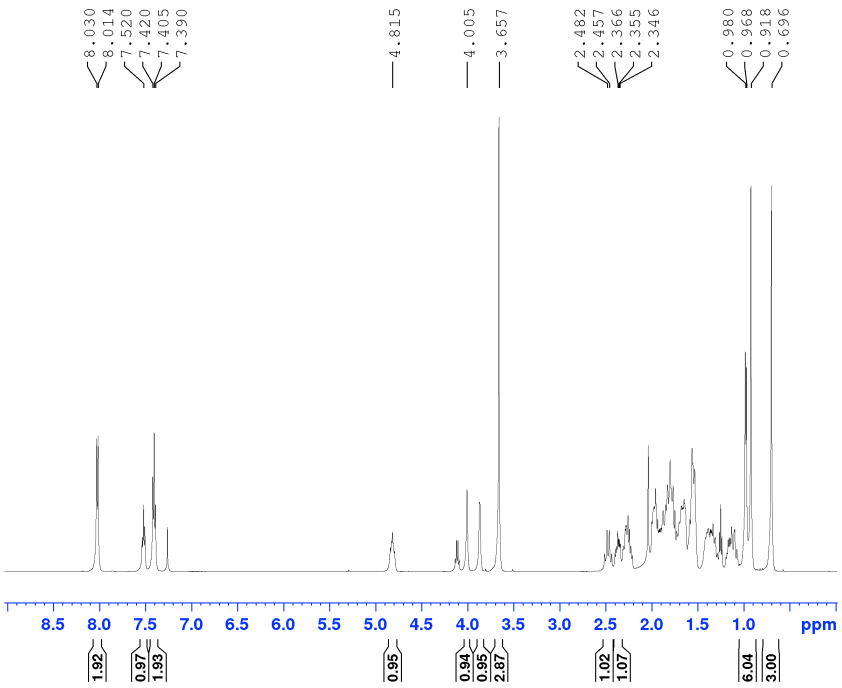


```
Current Data Parameters
NAME            OGT-010-1
EXPNO                   1
PROCNO                  1

F2 - Acquisition Parameters
Date_           20171108
Time                9.48
INSTRUM            spect
PROBHD    5 mm CPPTCI 1H
PULPROG             zg30
TD                 65536
SOLVENT            CDCl3
NS                    16
DS                     0
SWH             6270.903 Hz
FIDRES          0.095686 Hz
AQ              5.2254038 sec
RG                    18
DW                79.733 usec
DE                 6.50 usec
TE                298.1 K
D1             1.00000000 sec
TD0                    4

======== CHANNEL f1 ========
SFO1          500.1329821 MHz
NUC1                  1H
P1                 9.00 usec
PLW1          12.00000000 W

F2 - Processing parameters
SI                 65536
SF            500.1300131 MHz
WDW                   EM
SSB       0
LB                 0.30 Hz
GB        0
PC                 1.00
```

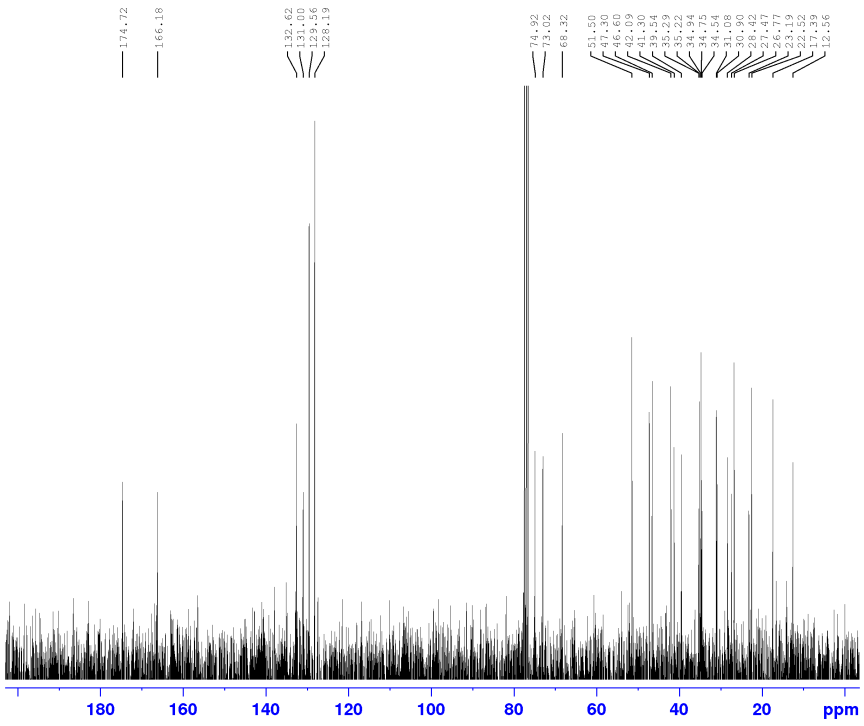


```
Current Data Parameters
NAME      OGT-010-kuivattu
EXPNO                  101
PROCNO                   1

F2 - Acquisition Parameters
Date_           20171005
Time              13.37 h
INSTRUM            spect
PROBHD   Z104275_0269 (
PULPROG           zgpg30
TD                 65536
SOLVENT            CDCl3
NS                    99
DS                     0
SWH            18028.846 Hz
FIDRES          0.550197 Hz
AQ              1.8175317 sec
RG                210.25
DW                27.733 usec
DE                 6.50 usec
TE                303.3 K
D1             2.00000000 sec
D11            0.03000000 sec
TD0                 1024
SFO1           75.4812305 MHz
NUC1                  13C
P1                10.00 usec
PLW1          31.98900032 W
SFO2          300.1530015 MHz
NUC2                  1H
CPDPRG[2          waltz16
PCPD2              90.00 usec
PLW2           7.90000010 W
PLW12          0.15706000 W
PLW13          0.07900000 W

F2 - Processing parameters
SI                 65536
SF            75.4727769 MHz
WDW                   EM
SSB       0
LB                 1.00 Hz
GB        0
PC                 1.40
```

APPENDIX 7

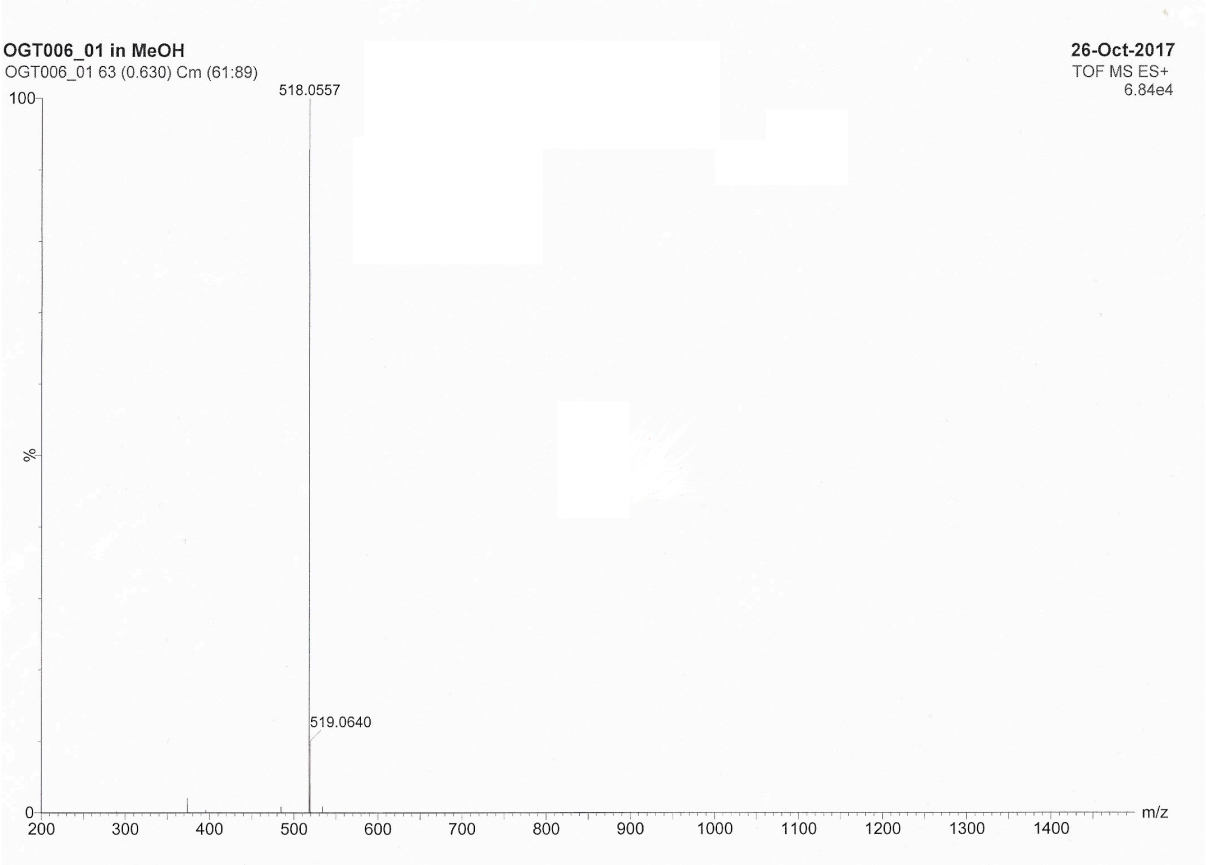
OGT006_01 in MeOH
OGT006_01 63 (0.630) Cm (61:89)
26-Oct-2017
TOF MS ES+
6.84e4
518.0557
519.0640
100
%
0
200
300
400
500
600
700
800
900
1000
1100
1200
1300
1400
m/z

APPENDIX 8

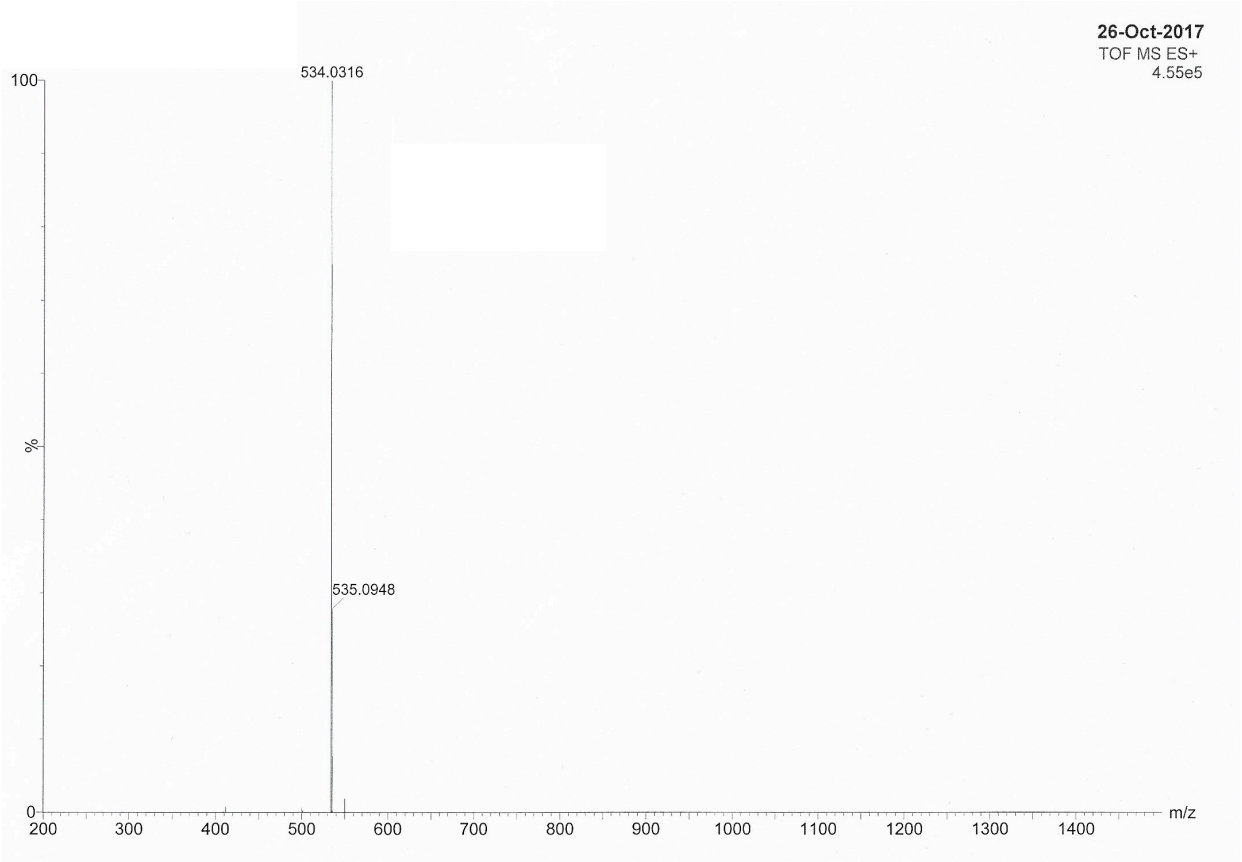
26-Oct-2017
TOF MS ES+
4.55e5
534.0316
535.0948
100
%
0
200
300
400
500
600
700
800
900
1000
1100
1200
1300
1400
m/z

APPENDIX 9

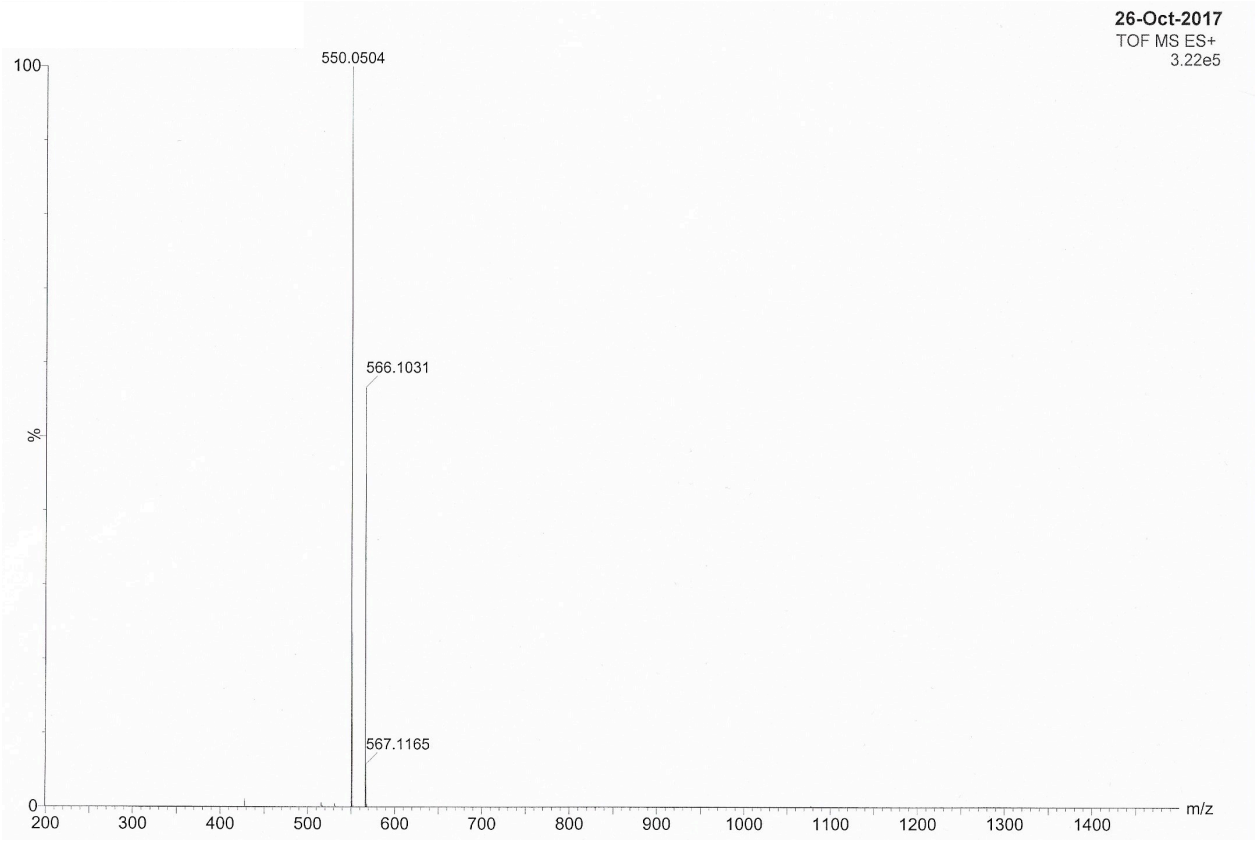
26-Oct-2017
TOF MS ES+
3.22e5
100
%
0
550.0504
566.1031
567.1165
200
300
400
500
600
700
800
900
1000
1100
1200
1300
1400
m/z

APPENDIX 10

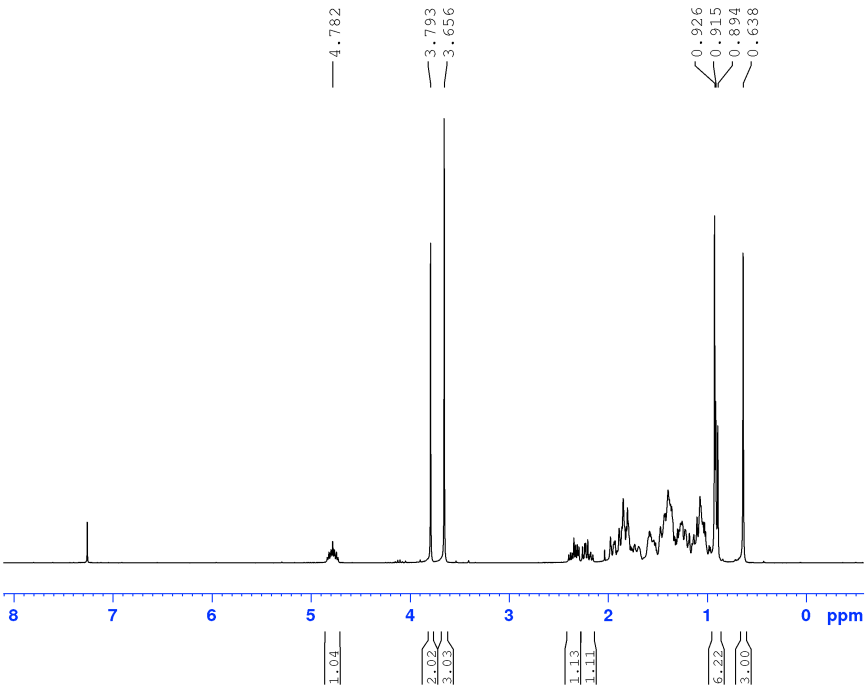


```
Current Data Parameters
NAME         OGT-038-fr1u
EXPNO                   1
PROCNO                  1

F2 - Acquisition Parameters
Date_             20180711
Time                12.14 h
INSTRUM              spect
PROBHD   Z104275_0269 (
PULPROG              zg30
TD                  32768
SOLVENT             CDCl3
NS                      8
DS                      0
SWH              3898.129 Hz
FIDRES           0.237923 Hz
AQ               4.2030420 sec
RG                 105.09
DW                 128.267 usec
DE                   6.50 usec
TE                 298.6 K
D1              2.00000000 sec
TD0                     1
SFO1          300.1516625 MHz
NUC1                   1H
P1                  14.00 usec
PLW1           7.90000010 W

F2 - Processing parameters
SI                 131072
SF            300.1500074 MHz
WDW                   EM
SSB       0
LB                 0.10 Hz
GB        0
PC                 1.00
```

APPENDIX 11

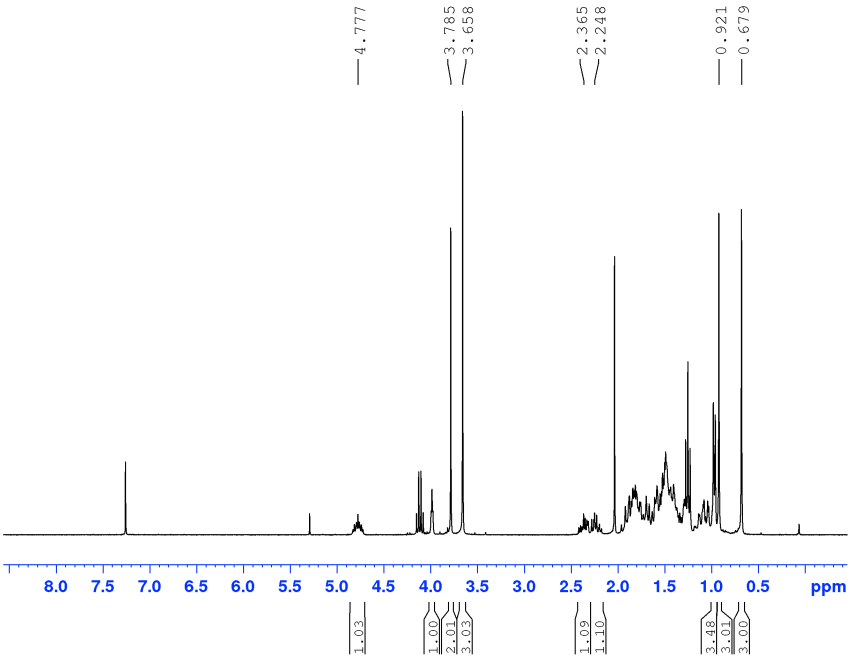


```
Current Data Parameters
NAME       OGT-033-fr2-u
EXPNO                 1
PROCNO                1

F2 - Acquisition Parameters
Date_           20180626
Time              16.09 h
INSTRUM             spect
PROBHD   Z104275_0269 (
PULPROG             zg30
TD                 32768
SOLVENT            CDCl3
NS                     8
DS                     0
SWH             3898.129 Hz
FIDRES          0.237923 Hz
AQ              4.2030420 sec
RG                185.47
DW               128.267 usec
DE                 6.50 usec
TE                303.1 K
D1             2.00000000 sec
TD0                    1
SFO1          300.1516625 MHz
NUC1                  1H
P1                 14.00 usec
PLW1           7.90000010 W

F2 - Processing parameters
SI                131072
SF            300.1500083 MHz
WDW                   EM
SSB       0
LB                 0.10 Hz
GB        0
PC                 1.00
```

APPENDIX 12

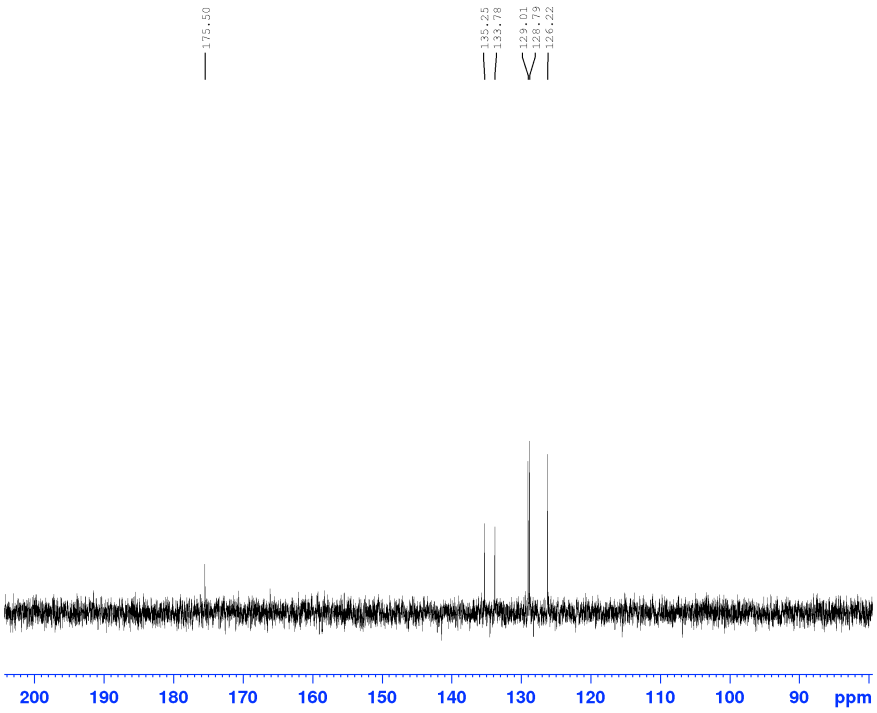

BRUKER

```
Current Data Parameters
NAME                  OGT-031
EXPNO                     101
PROCNO                      1

F2 - Acquisition Parameters
Date_              20180625
Time                  16.20 h
INSTRUM                spect
PROBHD    Z104275_0269 (
PULPROG              zgpg30
TD                    65536
SOLVENT                 D2O
NS                        825
DS                          0
SWH               18028.846 Hz
FIDRES             0.550197 Hz
AQ                1.8175317 sec
RG                   210.25
DW                   27.733 usec
DE                     6.50 usec
TE                   303.3 K
D1              2.00000000 sec
D11             0.03000000 sec
TD0                    1024
SFO1            75.4812305 MHz
NUC1                   13C
P1                    10.00 usec
PLW1           31.98900032 W
SFO2           300.1530015 MHz
NUC2                   1H
CPDPRG[2           waltz16
PCPD2                 90.00 usec
PLW2            7.90000010 W
PLW12           0.15706000 W
PLW13           0.07900000 W

F2 - Processing parameters
SI                    65536
SF              75.4727769 MHz
WDW                      EM
SSB       0
LB                     1.00 Hz
GB        0
PC                     1.40
```

APPENDIX 13

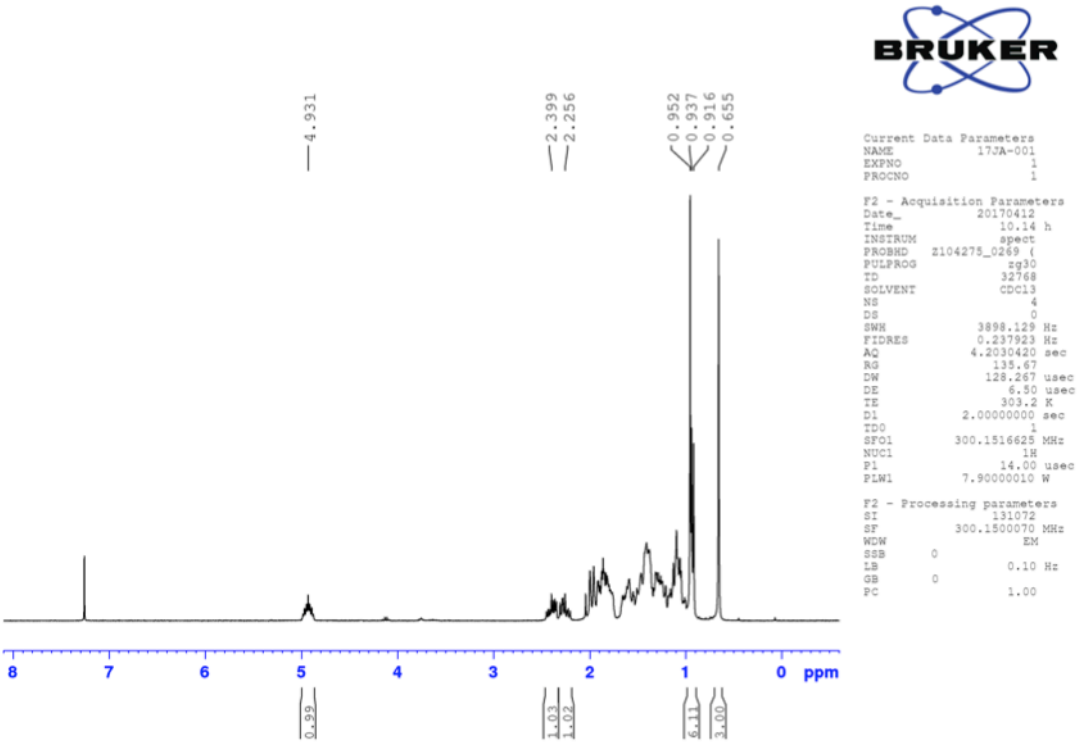
4.931
2.399
2.256
0.952
0.937
0.916
0.655
8
7
6
5
4
3
2
1
0
ppm
0.99
1.03
1.02
6.11
3.00
BRUKER
Current Data Parameters
NAME 17JA-001
EXPNO 1
PROCNO 1
F2 - Acquisition Parameters
Date_ 20170412
Time 10.14 h
INSTRUM spect
PROBHD Z104275_0269 (
PULPROG zg30
TD 32768
SOLVENT CDCl3
NS 4
DS 0
SWH 3898.129 Hz
FIDRES 0.237923 Hz
AQ 4.2030420 sec
RG 135.67
DW 128.267 usec
DE 6.50 usec
TE 303.2 K
D1 2.00000000 sec
TD0 1
SFO1 300.1516625 MHz
NUC1 1H
P1 14.00 usec
PLW1 7.90000010 W
F2 - Processing parameters
SI 131072
SF 300.1500070 MHz
WDW EM
SSB 0
LB 0.10 Hz
GB 0
PC 1.00

APPENDIX 14

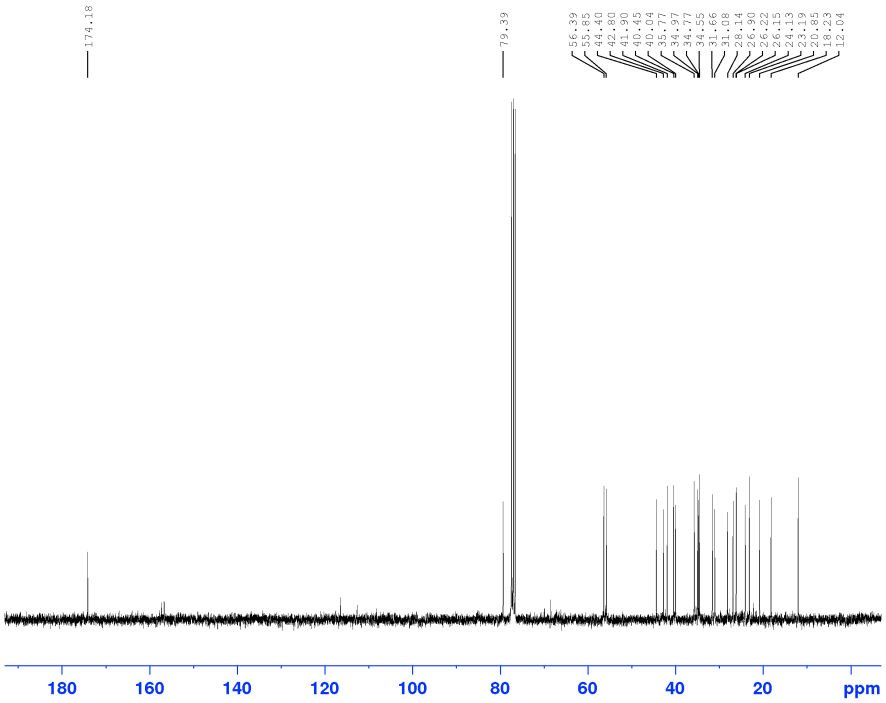

BRUKER

```
Current Data Parameters
NAME                  JA-013
EXPNO                    101
PROCNO                     1

F2 - Acquisition Parameters
Date_              20170626
Time                 14.19 h
INSTRUM                spect
PROBHD    Z104275_0269 (
PULPROG             zgpg30
TD                   65536
SOLVENT              CDCl3
NS                     169
DS                       0
SWH              18028.846 Hz
FIDRES            0.550197 Hz
AQ                1.8175317 sec
RG                   210.25
DW                   27.733 usec
DE                     6.50 usec
TE                   303.3 K
D1             2.00000000 sec
D11            0.03000000 sec
TD0                    1024
SFO1           75.4812305 MHz
NUC1                   13C
P1                    10.00 usec
PLW1          31.98900032 W
SFO2          300.1530015 MHz
NUC2                   1H
GPDPRG[2            waltz16
PCPD2                 90.00 usec
PLW2           7.90000010 W
PLW12          0.15706000 W
PLW13          0.07900000 W

F2 - Processing parameters
SI                   65536
SF             75.4727806 MHz
WDW                    EM
SSB       0
LB                    1.00 Hz
GB        0
PC                    1.40
```